Light-induced collisions of ultracold rubidium atoms

by

Dominikus Hoffmann

A dissertation submitted in partial fulfillment of the requirements for the degree of

Doctor of Philosophy

(Physics)

at the

University of Wisconsin - Madison

1996

Abstract

In this dissertation I present a variety of experiments on collisions between ultra-cold rubidium atoms. These collisions take place in light-force atom traps, where temperatures below 1 mK are reached. At these low temperatures weak, long-range interactions between the atoms are important, and collision times are long. Consequently, the absorption and spontaneous emission of photons plays an important role in determining the collision dynamics.

The collisions studied in this dissertation involve excitation of the atoms to a state where the relatively strong dipole-dipole interaction with another atom results in attraction (or repulsion) after which spontaneous emission may take place. The resulting energy transfer in such a collision can eject the atoms from the trap.

We have observed such collisions in both stable isotopes of rubidium. If the $P_{3/2}$ excited-state is involved, the two isotopes behave quite differently. This makes clear the importance of hyperfine interactions in the collision dynamics. In contrast, for the $P_{1/2}$ excited-state such differences disappeare, because the hyperfine interaction is strong enough to eliminate hyperfine mixing of the potentials.

Another collision process involved collisions with a repulsive dipole-dipole interaction. This experiment gives strong support for a Landau-Zener treatment of the excitation process. These collisions enabled the measurement of the trap depth.

Finally, collisions between rubidium atoms that have undergone a two-step excitation by two near-infrared photons produce violet fluorescence as a signature of the collision. We have observed this effect. The data shows unexpected features, which warrant further investigation.

Table of contents

1 Introduction

Atom traps produce samples of atoms at temperatures below a few hundred microkelvin with densities in excess of $10^{10}/\mathrm{cm}^3$. These samples are of great interest for a variety of experiments. Under these conditions, collisions between trapped atoms often have cross sections on the order of 10^{-11} cm^2, as compared to 10^{-14} cm^2 or less for room temperature atoms. This is a consequence of the atoms' small kinetic energy, such that even weak, long-range interactions, such as the dipole-dipole interaction between the atoms, are important. Excited-state collisions provide a loss mechanism in atom traps, which limits the number of atoms an atom trap can hold.[1,2] There is also considerable interest in ground-state collisions, since they play an important role in cooling a sample of atoms to the phase-space densities where Bose-Einstein condensation occurs.[3] In atomic fountain clocks collisions between the ultra-cold atoms produce phase shifts of the atomic coherence, which limit the clock's accuracy.[4]

In addition to their practical importance, ultra-cold collisions are of interest in their own right. Collision times and distances are in a completely new regime as compared to collisions at high temperatures and pressures. Under certain circumstances, because the colliding atoms are so slow, the nature of the collisions may be quantum mechanical where only small relative angular momenta are important. The weak, long-range interaction of the atoms leads to long collision times in the range of microseconds. Thus the collision dynamics can be strongly modified by the presence of light fields. Excited-state collisions can be terminated by spontaneous emission, since the lifetime of the excited state is short compared to the duration of the collision.

In this dissertation I describe experiments on ultra-cold collisions between rubidium atoms in optical traps, in the presence of a laser that excites the colliding atom pairs. The collisions studied are inelastic, and the energy transfer permits the atoms to overcome the confinement of the trap. These collisions are studied by observing the loss of atoms from the trap.

As this field and sophistication has progressed, theories of increasing complexity have been proposed. It has been the purpose of this research to devise and carry out experiments that lend themselves to comparison with these theories.

In this dissertation I describe a series of ultra-cold collisions experiments. Much has been learned through studying both stable rubidium isotopes, ^{85}Rb and ^{87}Rb. Studying collisions using light tuned near the Rb $5^2P_{3/2}$ excited-state, the isotopic comparison revealed substantial differences. This pointed toward the excited-state hyperfine interaction playing an important role in the dynamics of these collisions (see Sec. 4.1).[5,6] Because of the larger hyperfine interaction, collisions involving the $5^2P_{1/2}$ excited-state proved to show no isotopic dependence (Sec. 4.2).[7] In that case the dipole-dipole interaction is weaker than the hyperfine-interaction and does not produce a noticeable difference in the two isotopes. This experiment illustrated how a collision experiment may be devised that avoids the problems associated with a dipole-dipole interaction strongly modified by hyperfine interaction. This far all collisions had involved excitation to attractive potentials. An experiment with repulsive collisions gave evidence for a Landau-Zener description of the excitation process (Ch. 5).[8] These types of collisions also provided us with the first direct measurement of the depth of a trap (Sec. 5.5).[9] Finally, collisions modified by the absorption of two sequential photons[10] to a double-excited state restrict the collisional dynamics between the two excitations to a regime, where a reliable theoretical treatment should be possible with simple means (Ch. 6). As an additional benefit, this experiment provided the first direct detection of photons emitted during ultra-cold collisions.

1.1 The Gallagher-Pritchard model

Ultra-cold collisions can be described using molecular states that consist of appropriately symmetrized atomic states of two individual atoms with a ground and an excited state. Excited-state collisions take place in the presence of light in resonance with a transition from the ground state to the excited molecular state. The atom pair is prepared in the excited-state through the absorption of a photon. During the process of the collision the atoms may change states to a lower energy level or make a transition to the ground state through spontaneous emission. If in either case the kinetic energy that the atoms gained due to their mutual attraction in the excited state is larger than allowed by the finite trap depth (typically 1 K), they are ejected from the trap. Thus the collisions induce a *loss rate* that counteracts the loading of the trap, which takes place at a constant rate in the case of a background-vapor-loaded MOT (see

Sec. 2.1). Thus higher loss rates shift the equilibrium between loading and losses resulting in smaller numbers of trapped atoms.

The first and simplest model of ultra-cold collisions is the Gallagher-Pritchard model.[11] It is an attempt to break down the collision process into a sequence of steps, that can each be treated with relative ease. It consists of excitation at large interatomic separation, followed by motion on the excited state, characterized by survival if no spontaneous emission occurs, and energy transfer at small separations.

In detail, this sequence is as follows (see Fig. 1.1): Thermal motion on the ground-state potential ($5^2S_{1/2} + 5^2S_{1/2}$ for rubidium) at trap temperatures (~100 – 200 μK) brings an atom pair to within the distance of each other (step 1), where their dipole-dipole interaction makes them resonant with the excitation of light from a "catalysis laser." Excitation may then take place (step 2). After excitation the excited-state potential ($5^2S_{1/2} + 5^2P_{3/2}$) accelerates the atoms toward each other (step 3). While the atoms are moving on the excited-state potential curve spontaneous emission may occur (step 4). If they have gained more kinetic energy than confinement allows, they leave the trap on the ground-state potential (step 5). If spontaneous emission occurs earlier, they remain in the trap, and the collision remains undetected, because they do not contribute to trap-loss, which is the signature of these collisions.

In its simplest form, the Gallagher-Pritchard model makes a few assumptions and approximations. It neglects the thermal motion of the atoms in step 1. Excitation in step 2 is treated quasi-statically, that is, as though the atoms were at rest both before and after the excitation. The model for excitation is that of an isolated atom whose excited-state energy level has been shifted by the perturbation of the dipole-dipole interaction of the two atoms. The acceleration and motion in the excited-state in step 3 is treated classically. In the model, the survival probability simply depends on the duration of the collision and on the excited-state lifetime, which is assumed to be unaffected by the dipole-dipole interaction.

In the following derivation of the model several convenient and meaningful definitions are made. Fig. 1.2 illustrates them.

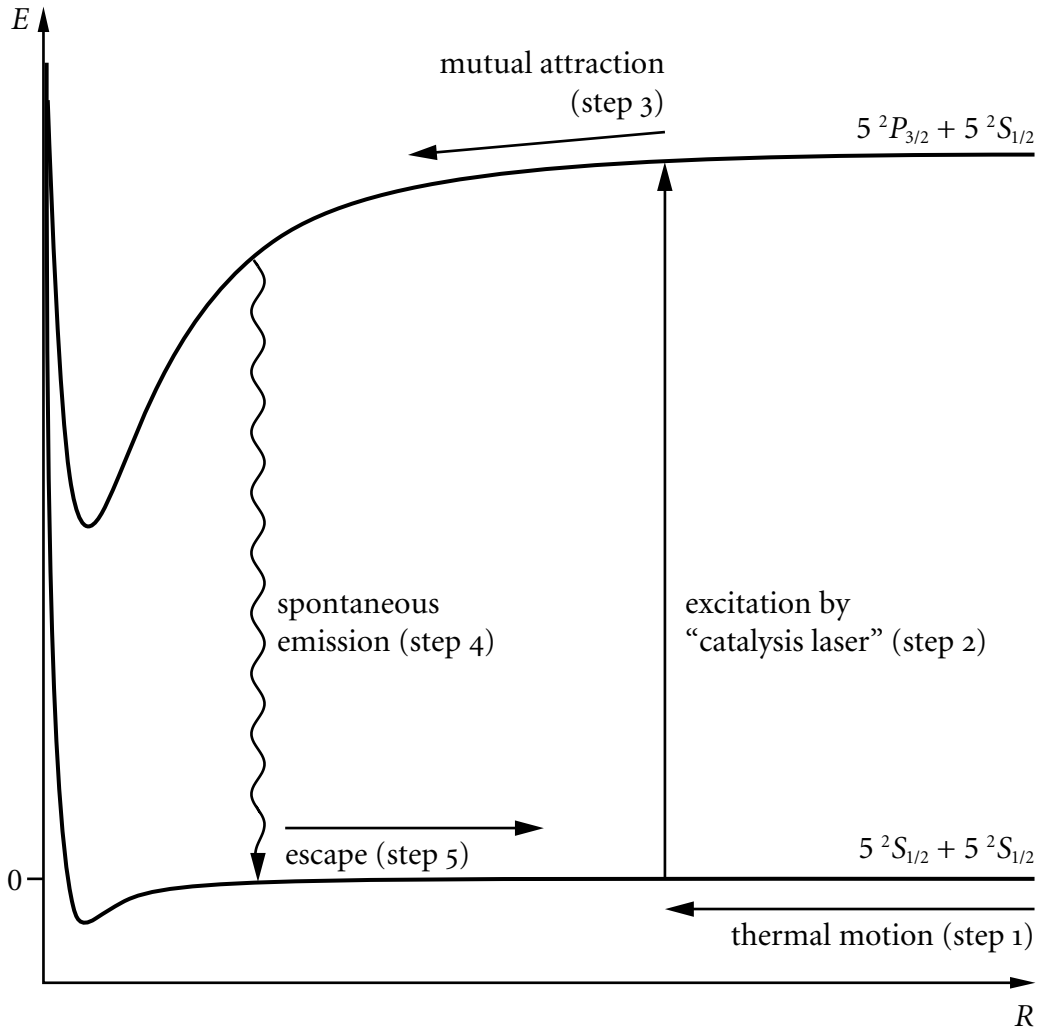

Figure 1.1: Anatomy of an attractive ultra-cold collision. Two atoms approach each other with thermal velocities (step 1). Excitation to an excited-state potential curve may occur in the presence of resonant light (step 2). Acceleration toward each other follows (step 3). Spontaneous emission (step 4) after picking up sufficient kinetic energy may lead to escape from the trap (step 5).

The resonance dipole-dipole interaction between two identical atoms has the form

$$V(R) = \pm\frac{C_3}{R^3}, \tag{1.1.1}$$

if one of the atoms is in the excited state. This simple form neglects fine- and hyperfine structure, but is still used in many models. The plus sign represents repulsive interaction, the minus

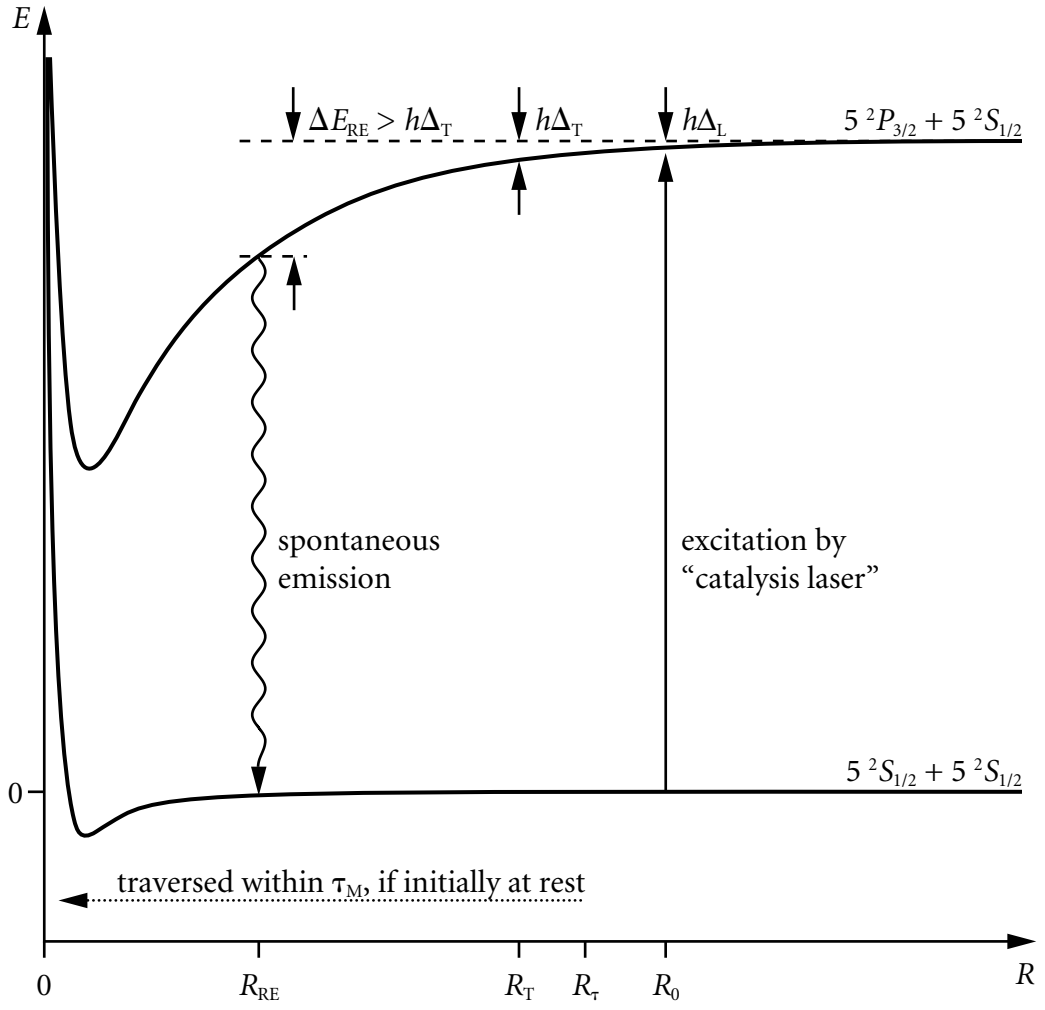

Figure 1.2: Important quantities in the Gallagher-Pritchard model. The atom is resonant with a transition from the ground-state potential curve to the excited-state at R_0 if the laser has a detuning Δ_L. The atom travels from R_τ to $R = 0$ within one natural lifetime. If spontaneous emission occurs at a position R_{RE}, after the atoms have passed R_T, they have more kinetic energy than the trap depth $h\Delta_T$ and escape the trap. The energy picked up in radiative escape is ΔE_{RE}.

sign attractive ones. C_3 is a coefficient specific to the species of atoms and excited state involved. In the ground state the dependence of the atom-atom interaction on the interatomic separation is much weaker (R^{-6}). Thus, at large separations, where the collision process involves the ground-state potential, it is a good approximation to neglect the ground-state potential.

If a pair of atoms a distance R_0 apart is excited out of the $5^2S_{1/2} + 5^2S_{1/2}$ into the $5^2S_{1/2} + 5^2P_{3/2}$ state, it has a total energy of $-C_3/R_0^3$, assuming it was at rest before being excited. When the two atoms have accelerated toward each other and have reached a separation R, energy conservation gives the relation

$$\frac{1}{2}\mu v^2 - \frac{C_3}{R^3} = -\frac{C_3}{R_0^3}, \tag{1.1.2}$$

where $\mu = m/2$ is the reduced mass of the atom pair and v is the relative velocity of the atoms. This differential equation can be solved for the time it takes the atom pair to reach a separation $R = 0$ after being excited. It is

$$t(R_0) = \sqrt{\frac{\mu}{2}}\int_{R_0}^{0} \frac{dR}{\sqrt{C_3/R^3 - C_3/R_0^3}}. \tag{1.1.3}$$

With the substitution $z = (R/R_0)^3$ and using the Beta-function,

$$B(x, y) = \int_0^1 t^{x-1}(1-t)^{y-1}dt = \frac{\Gamma(x)\Gamma(y)}{\Gamma(x+y)}, \tag{1.1.4}$$

this can be solved to yield

$$t(R_0) = \frac{\Gamma(5/6)\Gamma(1/2)}{3\Gamma(4/3)}\sqrt{\frac{\mu R_0^5}{2C_3}} = 0.747\sqrt{\frac{\mu R_0^5}{2C_3}}. \tag{1.1.5}$$

Rewriting this in terms of $h\Delta = -C_3/R_0^3$ and $h\Delta_\tau = -C_3/R_\tau^3$, where R_τ is defined through

$$t(R_\tau) \equiv \tau_M, \tag{1.1.6}$$

and τ_M is the lifetime of the associative excited state of the two atoms, gives

$$t(\Delta) = \tau_M\left(\frac{\Delta_\tau}{\Delta}\right)^{5/6}. \tag{1.1.7}$$

The number of atoms remaining in the excited state after having been excited at an interatomic separation $R = R_0$ decreases exponentially due to spontaneous emission. The number of

atoms reaching small interatomic separation where energy transfer can occur is decreased by $\exp[-t(R_0)/\tau_M]$.

The rate at which collisions lead to trap loss is the integral over all initial interatomic separations R_0 of the trap loss probability per unit time. The integrand is proportional to the density of trapped atoms n, as well as, given one atom, to the number of atoms $4\pi R_0^2 dR_0 n/2$, which might serve as potential collision partners because they are within a spherical shell of radius R_0 and thickness dR_0. Furthermore, the rate $\Re(R_0, \Delta_L)$, at which atoms are produced in the excited state, enters, as well as the fraction $\exp(-t(R_0)/\tau_M)$ of atoms remaining in the excited state and the probability of an energy transfer $P_{\Delta E}$. Δ_L is measured from the atomic resonance ($5^2S_{1/2} \rightarrow 5^2P_{3/2}$ transition). Also, in every such event two atoms are lost from the trap. Thus the collision rate is

$$\beta n = 2\int_0^\infty \frac{4\pi R_0^2 dR_0 n}{2} \Re(R_0, \Delta_L) \exp(-t(R_0)/\tau_M) P_{\Delta E} \quad , \tag{1.1.8}$$

where the proportionality to the density is made explicit by defining a trap-loss coefficient β. The excitation rate is assumed to be a Lorentzian involving the molecular linewidth $\Delta_M = (2\pi\tau_M)^{-1}$, the shift of the molecular level due to the atom-atom interaction $h\Delta = -C_3/R_0^3$, the intensity of the light I and the wavelength of the transition λ,

$$\Re(R_0, \Delta_L) = \frac{I}{hc/\lambda} \frac{\lambda^2/2\pi}{1 + 4(\Delta - \Delta_L)^2/\Delta_M^2} \, , \tag{1.1.9}$$

where a separate detuning for the laser Δ_L indicates that R_0 is not necessarily the separation at which the atom pair is resonant with the laser. $P_{\Delta E}$ is the total probability of energy transfer that leads to trap loss. The contributing factors to $P_{\Delta E}$ include radiative escape, where a photon is spontaneously emitted that has sufficiently less energy than the photon absorbed from the laser, and, less importantly, fine-structure changes, where a transition to a lower-lying fine-structure potential takes place, if there is one. If a fine-structure change occurs when the atoms are close to each other, $P_{\Delta E}$ has to be modified to include this effect. It is difficult to predict $P_{\Delta E}$ as pointed out by Dulieu *et al.*[12]

Over most of the range of laser detunings, Δ_L is large compared to the molecular line width Δ_M, such that the excitation rate of (1.1.9) can be approximated according to

$$\lim_{\Delta_L/\Delta_M \to \infty} \frac{I}{hc/\lambda} \frac{\lambda^2/2\pi}{1 + 4(\Delta - \Delta_L)^2/\Delta_M^2} = \frac{I}{hc/\lambda} \frac{\lambda^2}{2\pi} \frac{\Delta_M}{2} \pi\delta(\Delta - \Delta_L) \qquad (1.1.10)$$

This allows us to easily evaluate the integral of equation (1.1.8). With the substitutions $h\Delta = -C_3/R_0^3$ and $\Delta_L \to \Delta$, and assuming that n = const. throughout the trap this becomes[13]

$$\beta = \frac{I\lambda^3 P_{\Delta E} C_3 \Delta_M}{12\pi\hbar^2 c\Delta^2} \exp[-(\Delta_\tau/\Delta)^{5/6}] \qquad (1.1.11)$$

Fig. 1.3 is a plot of β as a function of Δ for rubidium. In that case, C_3 = 71.3 eV Å^3, from a calculation that neglects fine- and hyperfine structure.[13]

Eq. (1.1.11) also nicely separates the two regimes of trap loss rates evident from the plot. At laser detunings $0 < \Delta < \Delta_\tau$ the exponential term dominates and provides the onset near zero. At detunings where $\Delta \gg \Delta_\tau$ the exponential approaches one, and the Δ^{-2} dependence takes over, which arises from the distribution of atoms pairs available for excitation at the separation determined by Δ.

The model also predicts linearity in the dependence of collision rates upon the laser intensity. See Sec. 4.1.3 for our measurement of this property.

1.2 Modifications to the model

Since publication of the Gallagher-Pritchard model[11] several modifications have been offered. They all retain the separation of the collision process into initial excitation, dynamics and, finally, energy transfer, which leads to trap loss. The goal of these modifications has been to improve quantitative agreement of the models with data described in this dissertation and elsewhere. Some of the newer models include attempts to take into account the temperatures that the atoms have when they are excited. In contrast, the original Gallagher-Pritchard model assumes $T = 0$ and approaches the excitation process as quasistatic.

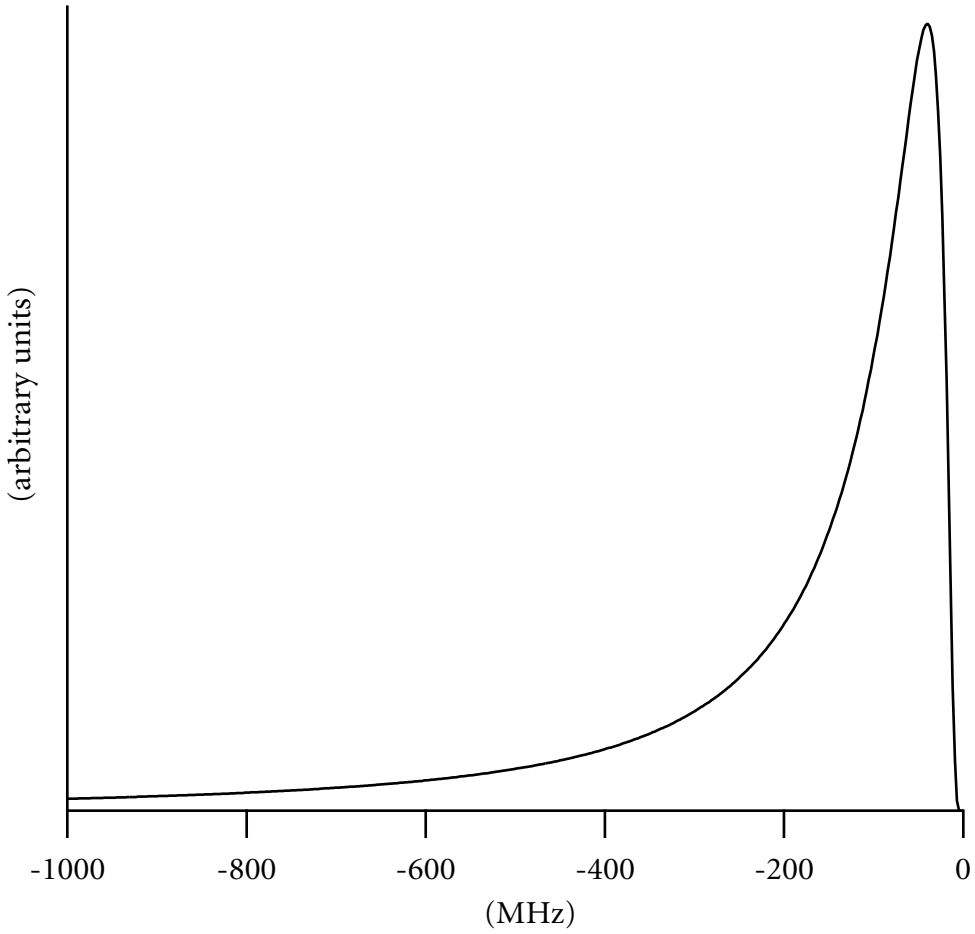

Figure 1.3: Spectrum of the trap loss coefficient β as predicted by the standard Gallagher-Pritchard model The onset at small detunings Δ results from spontaneous emission interrupting collision when excitation occurs at very large separations. At larger detunings, beyond the maximum, the trap loss rate decreases like Δ^{-2}, because the number of atoms available for excitation at a given detuning decreases as R^2.

Julienne and Vigué[14] included the conventional quantum mechanical analysis of the phase of the collision at close range, to properly account for fine-structure changes. Effects of retardation in the excited-state potential were also considered for states for which absorption and emission are dipole-forbidden. In the case of rubidium the dipole-dipole interaction of the excited state is so strong that our relatively large catalysis laser detunings excite atoms at small enough separations so that retardation plays no role. The purpose of these improvements was intended to bring the theory into quantitative agreement with measurements of the trap loss

rate resulting from a laser with detunings of only a few megahertz such as the trap laser in a MOT (see Sec. 2.1 for the description of the atom trap of the MOT type). Julienne and Vigué's calculations quantitatively agree with the measurements made in cesium.[15] However, measurements for rubidium in this dissertation showed that the Julienne-Vigué theory does not work for rubidium (Ch. 4.1).

Another approach, by Band and Julienne, uses an optical-Bloch-equation method.[16] It improves on the Gallagher-Pritchard model and Julienne and Vigué's theory in a couple of ways, but the optical-Bloch-equation method naturally takes into account the slow thermal motion of the atoms in the ground state as they are excited. It does not make a quasi-static approximation. This is especially important at smaller detunings, where the acceleration by the excited-state potential is small, such that any initial velocity is non-negligible. It also properly treats saturation at high intensities of the laser exciting the atom pair. The method incorporates the dynamics into the optical-Bloch-equation formalism, which emphasizes the collision being a continuous process, without, however, introducing new physics. Its results compare well with the cesium data mentioned above[15] that were measured at a detuning corresponding to one natural linewidth. With this theory, agreement with our rubidium data still was not achieved.

A simple Landau-Zener formulation of the excitation mechanism in contrast to the quasi-static approach of the Gallagher-Pritchard model, was shown to give analogous results to those of a fully quantum mechanical model treatment of the motion of the atoms.[17,18] If accurate, the Landau-Zener model would naturally allow the effects of high intensity to be taken into account, and predicts that the excitation probability depends on the relative velocities of the atoms. We have conducted an experiment that gives evidence for the validity of the Landau-Zener formulation (see Ch. 5).[8] However, to this date no theory has given a general quantitative description of ultra-cold collisions.

As a result of the interaction between theory and experiment, ultra-cold collisions can now be understood as sequence consisting of excitation at large interatomic separation, described by the Landau-Zener model, semiclassical dynamics in the excited-state, and subsequent spontaneous emission that may lead to escape from the trap. Previous attempts at improving the

ability to predict the absolute values of collision rates have shown this to be a very difficult task. The ability to do so depends on a good understanding of the processes at small interatomic separations, a regime that is not unique to ultra-cold collisions. Therefore, our interest is directed at understanding the shape of detuning dependences of trap loss rates, which result from the dynamics and excitation at large to intermediate separations. Because initial motion is slow, it is in those regimes where spontaneous emission can modify the collision in a detuning-dependent way.

Consequently, considering the excited-state hyperfine interaction and its coupling with the atoms' dipole-dipole interaction is very important. To date no calculation has fully taken the hyperfine interaction into account, even though the potential curves of dipole-dipole interaction in rubidium have been calculated.[19]

The remainder of this thesis is devoted to describing experiments that on the one hand give new insights into details of excited-state collisions and on the other are tailored to a simple theoretical approach.

2 The apparatus

The previous chapter layed down the theoretical foundation for this dissertation. In this chapter I describe the apparatus used to cool and trap the atoms, whose collisions we study. This involves the magneto-optical trap (MOT), the lasers that we use in the MOT, as well as for manipulating the atoms' collisions, and the detectors with which we observe the trapped atoms. The following chapter then describes the details of the method which we employ to study ultra-cold collisions.

The apparatus used in these experiments has a MOT[20] at its heart. Figure 2.1 is a schematic diagram of the apparatus. A MOT traps neutral atoms and cools them to temperatures where Doppler broadening is smaller than the natural line width of the atomic levels. A MOT manipulates the trapped atoms' external degrees of freedom, specifically, position and velocity. It does so by having resonant light scatter off the atoms to exert a slowing, as well as confining force on the atoms (Sec. 2.1).

We use diode lasers to provide the light that trap the atoms. With grating feedback the lasers possess linewidths smaller than the atomic linewidth (Sec. 2.3).Trapping takes place in an ultra-high vacuum chamber. Pressures below 10^{-9} torr are needed so that there is little interference of background-vapor atoms with those in the trap (Sec. 2.2).

Besides for collisions MOTs can be and have been used for a variety of experiments. These include atom interferometry,[21] quantum optics,[22] and the recent observations of Bose-Einstein condensation.[23] An application to more traditional atomic physics is the recent use of a laser trap for making reliable absolute measurements of electron-atom cross sections.[24]

2.1 The operation of the magneto-optical trap

When atoms scatter light, the photons transfer momentum to the atoms, exerting a force on them. In the simplified picture of an atom interacting with a single laser beam, this scattering process consists of multiple cycles involving absorption, stimulated and spontaneous emission. A sequence of absorption and stimulated emission does not change the atom's momentum, because the emitted photon has the same momentum and direction as the one absorbed. If, however, the absorption of a photon is followed by spontaneous emission, which can occur

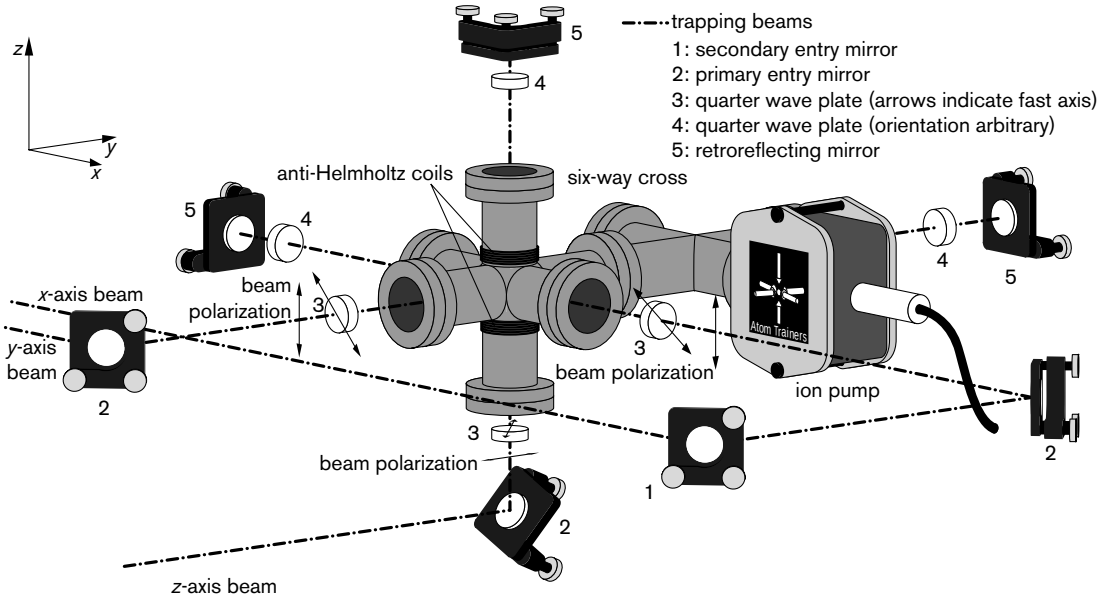

Figure 2.1: Magneto-optical trap. The illustration shows the six-way cross with viewports for access by the trapping laser beams, the polarization of the beams for MOT operation, and the ion pump that maintains the vacuum.

in a random direction, the atom is imparted the momentum difference between that of the absorbed and that of the emitted photon. When averaged over many cycles spontaneous emission does not contribute to the momentum transfer, because it occurs isotropically. The resultant force (F) acts along the propagation direction of the laser beam and is proportional to the absorption rate $\Re$ and the photon momentum p_γ. For the model of a two-level atom starting at rest, it takes the form

$$F = p_\gamma \Re = \frac{\hbar k \Gamma}{2} \frac{I/I_s}{1 + 4\Delta^2/\Gamma^2 + I/I_s}, \tag{2.1.1}$$

where $\hbar k$ is the photon momentum, Γ the natural line width of the transition in s^{-1}, I the laser beam intensity, I_s the saturation intensity, which for rubidium is 3.1 $\mathrm{mW/cm^2}$, averaged over Zeeman levels, and $\Delta = \omega - \omega_0$ the detuning of a laser with angular frequency ω from line center at ω_0.

In a MOT the arrangement of laser beams is designed such that these forces cool, as well as confine the atoms. In our system the beams are arranged in the standard configuration[1] con-

sisting of three pairs of counterpropagating beams whose axes are along the Cartesian axes of space and intersect at the center of our vacuum chamber.

To provide cooling the beams have to be tuned slightly (1 – 3 line widths) below center of the resonance of the transition used with the atoms (Fig. 2.2). In the atom's frame of reference the beams whose propagation direction are opposite to the atom's velocity components along the beam axes are always Doppler-shifted toward the blue—closer to resonance. Conversely, the atom recedes from the corresponding counterpropagating beams, which in the atom's frame of reference are red-detuned—farther from resonance. Thus it scatters photons with greater probability from the blue-detuned beams than from the red-detuned ones. The frequency of each beam from the perspective of the atom is Doppler-shifted by $-\mathbf{k}_i \cdot \mathbf{v}$, where $\mathbf{k}_i$ is the wave vector of the ith beam and $\mathbf{v}$ the atom's momentary velocity vector. Thus, the detuning in Eq. (2.1.1) has to be replaced with $\Delta - \mathbf{k}_i \cdot \mathbf{v}$. Combining the effects of all three pairs of beams, in the limit of $\mathbf{k}_i \cdot \mathbf{v} \ll \Gamma, |\Delta|$, which is the case in atom traps, this results in a net force $\mathbf{F}_{\text{cool}}$ proportional and opposite to $\mathbf{v}$:

$$\mathbf{F}_{\text{cool}} = \frac{8\hbar k^2 \Delta}{\Gamma} \frac{I/I_s}{(1 + 4\Delta^2/\Gamma^2 + I/I_s)^2} \mathbf{v} . \tag{2.1.2}$$

In order to spatially confine the atoms, a position-dependent force is needed. A pair of anti-Helmholtz coils coaxial with one of the pairs of laser beams, in our case the vertical, $\hat{z}$-axis, produces a magnetic quadrupole field with $B = 0$ at the intersection point of the laser beams and a gradient of $\partial B/\partial z = -2(\partial B/\partial x) = -2(\partial B/\partial y) \approx 25$ G/cm. Thus the magnetic field in the vicinity of the center of the trap ($\mathbf{r} = 0$) has a magnitude

$$\mathbf{B}(\mathbf{r}) = \frac{1}{2}\frac{\partial B}{\partial z}(\hat{x} + \hat{y} - 2\hat{z}) . \tag{2.1.3}$$

In the presence of such a magnetic field gradient due to the Zeeman-effect the atoms prefer to absorb photons whose spin is opposite to the magnetic field vector (see example for an atom with an $J = 0 \rightarrow J = 1$ trapping transition in Fig. 2.3). The Zeeman effect shifts the ground- as well as the excited-state magnetic hyperfine sublevels. This makes it more difficult to calculate the MOT force. However, in the case of low intensity, for an atom in a standing wave made up of

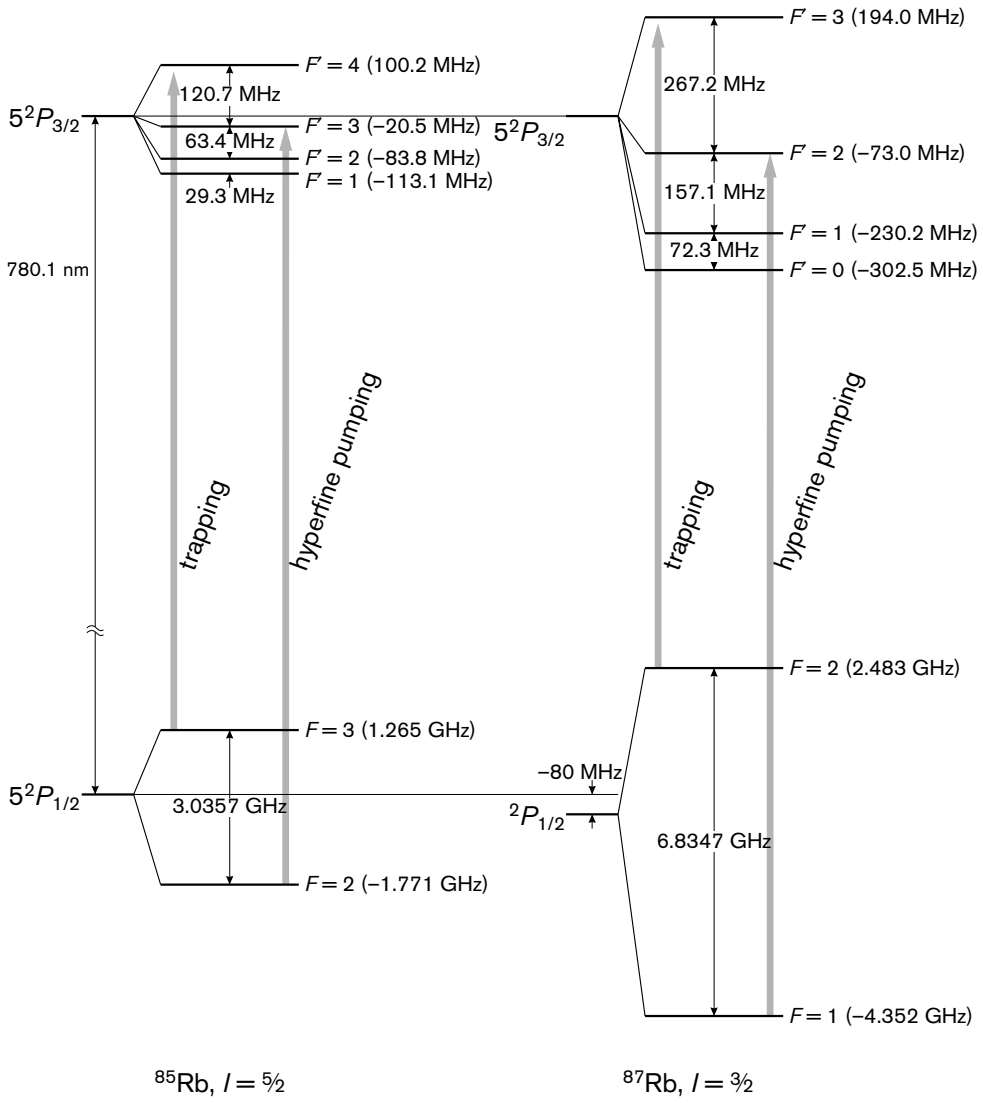

Figure 2.2: Trapping and hyperfine pumping transitions in ^{85}Rb and ^{87}Rb. The trap laser makes the atoms cycle between $5^2S_{1/2}(F = I + ½)$ and $5^2P_{1/2}(F = I + ⅜)$. The hyperfine pumping laser pumps the atoms out of the $5^2S_{1/2}(F = I - ½)$ state, if an off-resonant excitation to the $5^2P_{1/2}(F = I + ½)$ state resulting in spontaneous emission to the $5^2S_{1/2}(F = I - ½)$ ground state has taken place.

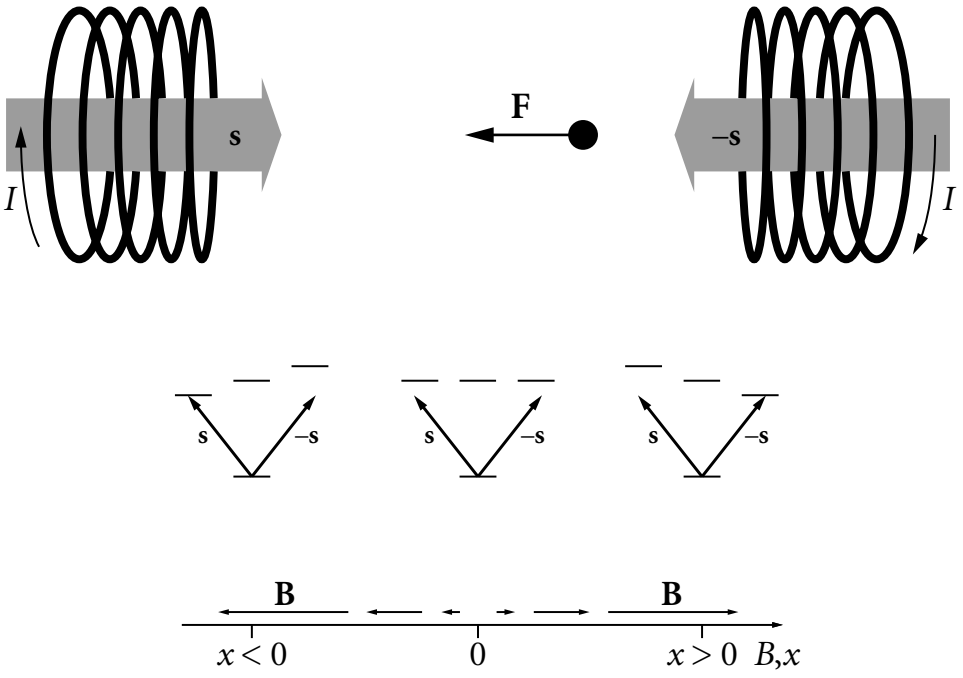

Figure 2.3: Zeeman force for an atom with $J = 0 \rightarrow J = 1$ in a standing wave detuned to the red from resonance. An atom in an inhomogeneous magnetic field, such as is generated by a pair of anti-Helmholtz coils, will preferentially absorb a photon from that red-detuned beam whose photons possess a spin $\mathbf{s}$ opposite to the local magnetic field $\mathbf{B}$. The result is a net scattering force toward $x = 0$.

two counterpropagating beams with equal intensity and opposite circular polarization the result can be expressed in simple terms. If the pair of beams is along the z-axis, the force is

$$\mathbf{F}_{\mathrm{MOT}} = -\frac{g_j \mu_{\mathrm{B}}}{\hbar c}\mathrm{Re}[\sigma_1(\Delta, \varepsilon^2)]B(z)\hat{z}\,, \tag{2.1.4}$$

where $\mu_{\mathrm{B}} = e\hbar/2m_{\mathrm{e}}$ is the Bohr magneton, g_J is the gyromagnetic ratio of the excited state, and

$$\sigma_1(\Delta, \varepsilon^2) = \frac{3\lambda^2\Gamma}{4\pi}\frac{-\Delta\Gamma - i(\Delta^2 - \Gamma^2/4 + \varepsilon^4/\Gamma^2)}{(\Delta^2 + \Gamma^2/4 + 2\varepsilon^2)(\Delta^2 + (\Gamma/2 + \varepsilon^2/\Gamma)^2)} \tag{2.1.5}$$

can be interpreted as a photon scattering cross-section per unit Larmor frequency.[19] To obtain the fully three-dimensional force, we have to take into account the magnetic field dependence of Eq. (2.1.3), as well as that $I_x = I_y = 2I_z$.

The trap loads from the background rubidium vapor in the vacuum chamber.[1] As room temperature atoms from the low-velocity tail of the Maxwell-Boltzmann distribution drift through the intersection region of the laser beams, they mainly experience the cooling force. It slows them enough for them to be captured and be driven toward $B = 0$. We have measured the capture velocity of the atoms to be on the order of $10\ \mathrm{m/s}$.[9] This means that for a room-temperature vapor of rubidium atoms a fraction of about 5×10^{-5} of the atoms are resonant with the trap laser and can therefore be trapped.

Loading occurs at a rate L. However, a steady state number of atoms N is reached in an equilibrium between the loading and loss rates. Loss processes are the collision of a room-temperature atom from the background vapor colliding with a trapped atom at a rate γN, or the type of inelastic collisions between trapped atoms that are the subject of this work, which occur at a rate $\langle \beta n \rangle N$, where n is the local density of the atoms and the brackets denote the average over the trap volume. The number of atoms N_∞ then reaches equilibrium at

$$N_\infty = \frac{L}{\gamma + \langle \beta n \rangle}. \tag{2.1.6}$$

The loading rate can be affected by a number of parameters. Greater trap laser detunings result in higher capture velocities. The loading rate depends linearly on the detuning up to about three natural linewidths,[10] beyond which the detuning becomes too large for the slow atoms in the trap to be affected by the light. The intensity of the trapping light affects the loading rate linearly, as well.

The capture volume of the trap is given by the trap laser beam diameter. The loading rate goes up linearly with the trap diameter, even when the total power in the cross section of the beams is kept constant.[10] The practical limit in our case is given by the one-inch dielectric mirrors used to steer the trap laser beam.

An increase in the partial pressure of the rubidium background vapor also leads to a higher loading rate. However, it at the same time increases the loss rate γ. By increasing the vapor pressure, one can therefore maximize the number of trapped atoms at the expense of a large γ. The trade-off is that this makes small collisional loss rates $\langle \beta n \rangle$ difficult to observe. We

choose vapor pressures low enough for a discernible $\langle \beta n \rangle$, yet large neough to provide us with enough atoms to be able to observe the effect of collisions.

2.2 Vacuum chamber

Trapping occurs in a vacuum chamber that was constructed from standard 1.5 inch stainless steel UHV vacuum components, with the MOT being constructed at the center of a six-way cross. Viewports allow for optical access. All of the windows for the trapping beams were anti-reflection coated for 780 nm. Later, for the experiment described in Sec. 4.2, the six-way cross was replaced with the custom-made chamber shown in Fig. 2.4. This allowed us to observe the fluorescence from the trapped atoms off-axis from the trapping beams, greatly reducing the contribution of scattered light to the signal. Of the four additional windows two remained uncoated, a necessity for observing the blue photons detected in the experiment described in Ch. 6.

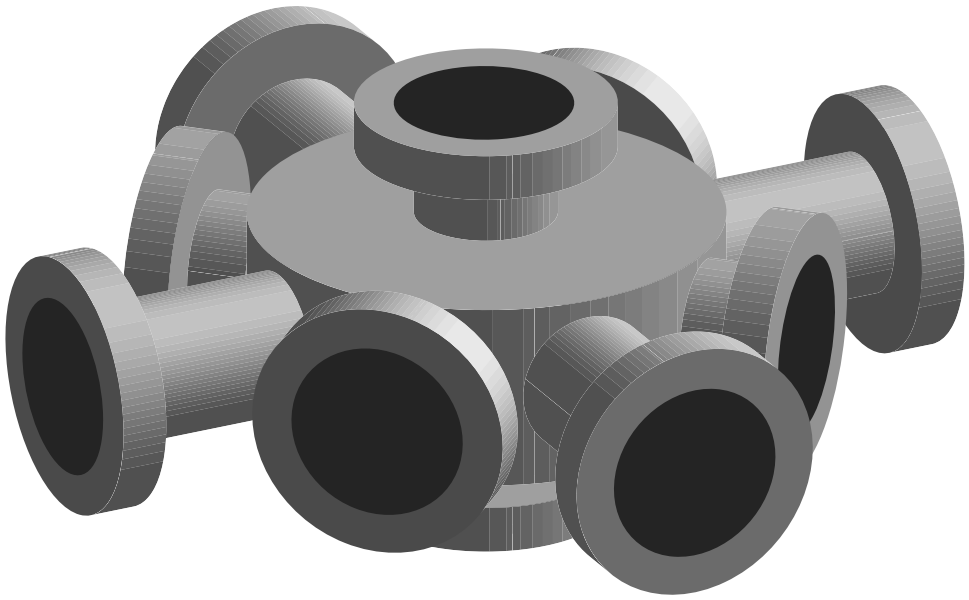

Figure 2.4: Second generation vacuum chamber. The vacuum chamber has viewports that allow access along the cartesian axes of space, as well as from four off-axis sides.

An 8 l/s ion pump provided a base pressure of 10^{-10} Torr. This value is derived from the ion pump current.

A reservoir containing rubidium metal was connected through a valve to the vacuum chamber. A base rubidium vapor pressure of $\sim 10^{-9}$ Torr was obtained in the chamber by opening the valve, heating the reservoir until the vapor pressure in the chamber reached the desired value, and then closing the valve. With the valve closed the Rb vapor pressure would slowly decrease over a time-scale of several months. The reason for that is that the rubidium gets adsorbed by the stainless-steel walls of the vacuum chamber and because some of it gets pumped into the ion pump. The rubidium vapor pressure was measured by sending on-resonant light from the trap laser through the chamber and measuring the column density in an absorption experiment. The magnetic-field coils are wound in opposite directions directly on the vertical tubing of the vacuum chamber.

2.3 Lasers

The lasers used for the experiment are diode lasers (Sharp LT024MD0 or Spectra Physics Labs SDL-5411-G1 for higher power) that are stabilized with optical feedback from a grating.[26] The grating narrows the linewidth of the laser to below 1 MHz and allows the laser to be tuned by adjusting the grating's alignment (Fig. 2.5). A piezo-electric crystal between the grating and its mount lets us electronically tune the laser continuously over a range of typically a few gigahertz. With the help of an saturated absorption spectrometer and an electronic circuit providing negative feedback to the piezo, we lock the laser to the spectral features of rubidium contained in a small glass cell that is part of the spectrometer. Since laser diodes put out light beams with an elliptical cross section, each laser beam passes through an anamorphic prism pair that stretches the beam profile along the minor axis, such that the output is circular.

2.3.1 Trapping and hyperfine pumping lasers

The "trap laser" is locked 5 – 10 MHz to the red of the $5^2S_{1/2}(F = I + ½) \rightarrow 5^2P_{3/2}(F' = I + ⅜)$ resonance line of rubidium ($I = ⅝$ for ^{85}Rb and $I = ⅜$ for ^{87}Rb), whose natural linewidth is 5.9 MHz (Fig. 2.2). The detuning of the trap laser is determined to ±1 MHz by linear interpolation referenced to the line centers of the above resonances and the nearest crossover resonances in the saturated absorption spectrum. The output beam is sent through an optical isolator and a spatial filter/telescope to produce a 1.5 cm diameter beam, which is then passed through a $\lambda/2$ plate, a polarizing beamsplitter, and a non-polarizing

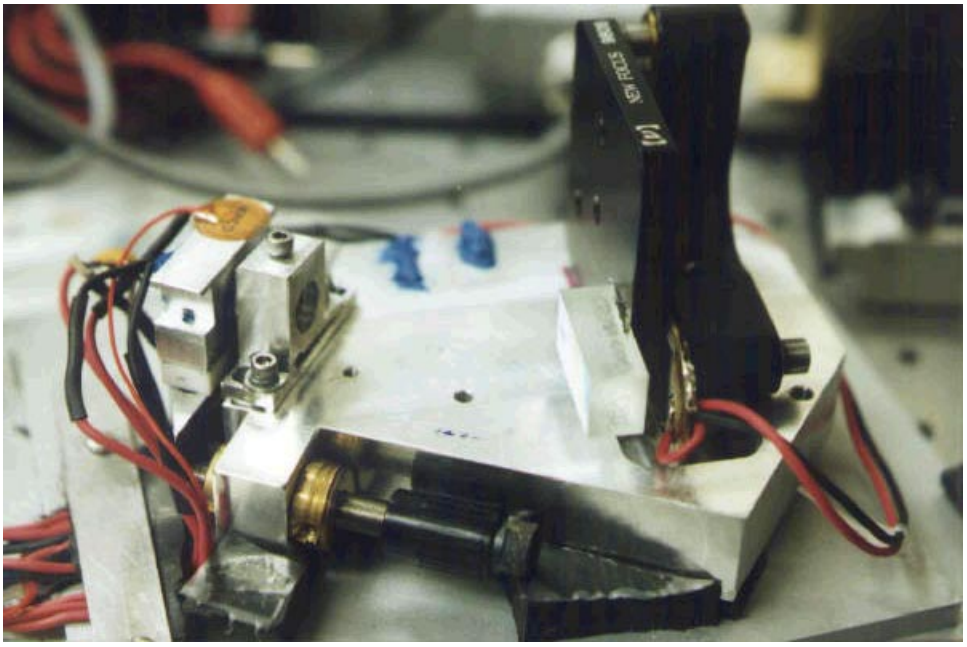

Figure 2.5: Diode laser. On the left the laser diode is held in a block temperature stabilized with the help of a heater. A lens collimates the laser diode's output. The grating that is attached to the mirror mount on the right serves for optical feedback and output coupling. A piezo mounted behind the grating allows electronic tuning.

beamsplitter, producing three beams that are used for trapping along the $\pm\hat{x}$, $\hat{y}$ and $\hat{z}$ directions. The $\lambda/2$ plate is adjusted to make the intensity of the $\pm\hat{z}$ beam ½ that of the others, thus compensating for the stronger magnetic field gradient along the $\hat{z}$ direction and giving a roughly isotropic confining force for the atoms. The three beams are aligned to intersect at the center of the vacuum chamber, and are passed through $\lambda/4$ plates to give the appropriate circular polarizations, some of which are shown in Fig. 2.1, for producing the standard MOT.[1] The total spatially-averaged intensity of the trap laser light at the position of the trapped atoms is typically 5.0 $\mathrm{mW/cm^2}$.

As the trap laser cycles the atoms between the $F = I + ½$ ground state and the $F' = I + ⅜$ excited state, occasional optical pumping into the untrapped hyperfine ground state $F = I - ½$ may occur, when the trap laser off-resonantly excites the the Lorentzian wing of the $5^2S_{1/2}(F = I + ½) \rightarrow 5^2P_{3/2}(F' = I + ½)$ transition. To counteract this effect we employ a second laser, a "hyperfine-pumping" laser,[1] that is locked to the $5^2S_{1/2}(F = I - ½) \rightarrow$

$5^2P_{3/2}(F' = I + ½)$ resonance. Later in the experiment described in Ch. 5 we switched to hyperfine pumping on the $5^2S_{1/2}(F = I - ½) \rightarrow 5^2P_{1/2}(F' = I + ½)$ transition. The 1.5 cm diameter beam from this laser is combined with the trap laser beam in one of the beamsplitters and produces an average intensity of 1.8 $\mathrm{mW/cm^2}$ at the position of the trapped atoms.

2.3.2 Catalysis laser

The purpose of the "catalysis laser" is to induce collisions between the trapped atoms. Since it contributes to β in Eq. (2.1.6), the trap laser, too, has this effect. However, its detuning can be adjusted only within a narrow range without loosing its ability to cool and trap the atoms. Even when adjusted within this range the trap laser drastically changes trap characteristics like number of trapped atoms, trap density, trap depth (see Sec. 5.5, Fig. 5.7). Thus it is difficult to make systematic collision measurements by varying the trap laser parameters.

The catalysis laser being a separate laser does not impose these limitations. Apart from about ±50 MHz around an atomic transition, its tuning range is only limited by the technical specifications of the laser. In this way, the catalysis laser can be swept over several gigahertz of frequency range, and its intensity can be varied without affecting the trapped atoms. In the vicinity of an atomic transition, it exerts forces on the trapped atoms, which alter the density distribution such that no reliable measurements can be made. Also, it can contribute to optical pumping, which renders the fluorescence from the trapped (see Sec. 2.4) atoms a useless diagnostic. We check for absence of these effects by rapidly blocking and unblocking the catalysis laser. Where this results in instantaneous changes in the fluorescence we reject the data. In addition, using a separate laser as a catalysis laser opens the regime of blue detunings for investigation (see Ch. 5).

More details on the operation of the catalysis laser and how it is used to observe ultra-cold collisions is described in detail in Ch. 3.

The catalysis laser is tuned to a specified frequency near the $5^2S_{1/2}(F = I + ½) \rightarrow 5^2P_{3/2}(F' = I + ⅜)$ or the $5^2S_{1/2}(F = I + ½) \rightarrow 5^2P_{1/2}(F' = I + ½)$ resonances using an optical spectrum analyzer (finesse ~150, free-spectral-range 300 MHz) as a frequency reference. To correct for slow drifts in the spectrum analyzer, a small fraction of the trap laser output is simultaneously measured as a stable reference frequency. The catalysis laser beam, after

passing through an optical isolator and an electro-optic intensity modulator, progresses through a telescope to produce a beam with a diameter of 3.0 mm. The beam entered the cell through one of the windows for the trapping beams at a slight angle to them and overlaps the cloud of trapped atoms. In our second-generation vacuum chamber we had it enter through one of the off-axis windows, instead. Optimum alignment of the catalysis laser through the trapped-atom cloud is obtained by tuning the catalysis laser near one of the atomic resonances to put a force on the trapped atom cloud. Adjustments are made to the catalysis laser beam alignment to maximize the displacement of the cloud. For the experiment, retroreflection of the catalysis laser reduces its mechanical influence on the trapped atoms. Ch. 3 describes the method we employ to make measurements of trap loss spectra in detail.

2.4 Detection

A CCD video camera is focussed on the cloud of trapped atoms in order to observe its shape. The position and shape of the cloud can be adjusted by slightly changing the alignments of the trapping beams as well as by adding a trimming magnetic field using extra coils or a small permanent magnet. In this way the shape of the cloud of atoms can be made to be nearly spherical, and the growth of the cloud as atoms are added is observed to be symmetric. For quantitative measurements of the spatial distribution of the atoms, a single horizontal line of the video output is selected for analysis.

In the fluorescence setup a fraction of the trapped atoms' total fluorescence is collected and imaged onto a photo diode. With our first-generation vacuum chamber, a part of the fluorescence emitted through one of the windows for the trap laser beams was picked off with a mirror and imaged though a bi-convex lens ($f = 5$ cm, $\varnothing = 1"$) onto a Hamamatsu photodiode (S2387-1010R, spectral response of 0.5 mA/mW at 780 nm). This lacked a well defined geometry, which made estimating the solid angle subtended by the system difficult. We therefore used the absorption of an on-resonant probe beam for an absolute measurement of the number of trapped atoms. This setup did allow us to observe the transient behavior of the trap fluorescence, which is of significance for making absolute trap loss rate measurements (see Sec. 3.2).

Our second-generation vacuum chamber is a major improvement. In it, the fluorescence detection setup collects the light from the fluorescence of the trapped atoms that passes through one of the off-axis viewports. Thus light is emitted into a solid angle fraction of around 1% is emitted. A combination of two identical plano-convex lenses ($f = 15\,\mathrm{cm}$, $\varnothing = 2''$) images the fluorescing cloud of trapped atoms onto a photodiode at 1:1 magnification. With the improved determination of the solid angle this allows us to accurately deduce the number of trapped atoms (see below).

In both cases an iris is placed in the image plane and opened just enough to transmit the light from the image of the trapped atoms. The photodiode is placed immediately behind the iris. This is to increase the rejection of scattered light from within the chamber, as well as of room lights.

The photocurrent from the photodiode is fed into a current-to-voltage converter (IVC). In it, the signal is connected to the inverting input of a JFET op-amp (LF 356). The non-inverting input of this op-amp can be biased to make up for any undesired dc offsets in the signal. Resistors in the range of $10^5 - 10^8$ produce a current-to-voltage conversion gain between 10^5 and 10^8 V/A. The signal of the IVC's output is typically displayed on an oscilloscope for measurement and monitoring.

Knowing the scattering rate R of the trapped atoms at the given trap laser detuning and power, the number of atoms is given by

$$N = \frac{V_{\mathrm{fl}}}{G_{\mathrm{IVC}}\eta_{\mathrm{p.d.}}(\Delta\Omega/\Omega)} \times \frac{6.2\times10^{15}\ \mathrm{eV}/s}{\mathrm{mW}} \times \frac{1\ \mathrm{photon}}{1.6\ \mathrm{eV}} \times \frac{1}{R}, \qquad (2.4.1)$$

where V_{fl} is the voltage at the output of the IVC, G_{IVC} is the gain of the IVC, $\eta_{\mathrm{p.d.}}$ is the spectral response of the photodiode and $\Delta\Omega/\Omega$ the solid angle fraction. The other factors serve the conversion of units from milliwatts to the number of photons per second emitted by the atoms. $R = \sigma I/\hbar\omega$, where σ is the absorption cross section of light from the trap laser beams whose intensity is I and which are at a frequency ω.

For measurements of the density of the trapped atoms, a small fraction of the trap laser is split off and focussed to a waist smaller than the size of the atom cloud through the atoms in

order to probe the absorption. The alignment is optimized by maximizing the absorption of the light in the beam. Its intensity is reduced with neutral density filters to the point where the fractional absorption is independent of the intensity of the probe beam.

The absorption A of the beam is given by

$$A = 1 - \exp[-\int n(l)\sigma(\Delta, I)\,dl]\,, \tag{2.4.2}$$

where $n(l)$ is the density of atoms along the absorption beam and σ the same absorption cross section as in Eq. (2.4.1). This can be solved for the average density $\langle n \rangle$ in the following way:

$$\langle n \rangle \equiv \frac{n_{\max}}{2r_c}\int \frac{n(l)}{n_{\max}}\,dl = \frac{\ln(1-A)}{2\sigma r_c}\,, \tag{2.4.3}$$

where Sec. 3.2 describes how to obtain r_c from trap fluorescence profiles taken with the CCD camera. In lieu of a reliable absolute fluorescence measurement we can use this to get the number of trapped atoms by multiplying $\langle n \rangle$ by the volume $4\pi r_c^3/3$.

3 The catalysis laser method

The last chapter described the apparatus used for investigating ultra-cold collisions. It also described the laser that we employ as a "catalysis" laser. In this chapter I go into the details of how it affects the trapped atoms as an ensemble and of how we extract information about the process of an individual collision from observing this ensemble. The next chapter presents measurements and their interpretations.

The most straightforward means of observing ultra-cold collisions is to measure the rate at which atoms are ejected from the trap. The relevant parameter is the loss rate coefficient β (see Ch. 1). Its frequency dependence gives information about the behavior of collisions with different initial interatomic separations.

However, in measuring β, we face the problem that in traps variables like the number of atoms, the density distribution and the trap depth are highly coupled with each other and with the trap laser parameters such as intensity, detuning, polarization and intersection volume. Many workers in this field have ignored these effects, but they must be accounted for, if reliable measurements are to be made. Thus, in measuring the frequency dependence of β we devised a method that affects the trapped atoms in a well-controlled way. The most important feature of our method is that we employ a separate laser, a "catalysis" laser, to induce the ultra-cold collisions we observe. That way the trap laser may provide constant trapping while all changes in the collisional loss rate are due to changes in the catalysis laser's intensity or detuning. While the catalysis laser thus leaves the loading rate unaffected, its effect on the loss rate and thereby on the density distribution of the atoms has to be given special consideration.

Our procedure consists of measuring the frequency dependence on a relative scale first. Then the absolute value of one particular β in the trap loss spectrum is determined. This scales and calibrates the whole spectrum. How this is done in detail is described in the following.

3.1 Frequency dependence

The frequency dependence of β can be measured in a very reliable way, as long as no absolute scale is required. At each detuning β is determined relative to its value at a specific reference detuning. The resulting shape contains most of the information about the collisions, that

is it is directly related to the collision dynamics. As explained in Sec. 1.1, the difficulties inherent in calculating absolute trap-loss rates make absolute measurements less interesting. The following describes how we make these measurements and what the underlying physics is.

As described in Sec. 2.3.1 collisional loss rates are related to the loading and capacity of traps. The balance between loading and losses determines the number of trapped atoms. This is expressed in (2.1.6). N_∞ is the equilibrium number of trapped atoms, which is the steady state solution of the differential equation in the number of atoms

$$\frac{dN}{dt} = L - \gamma N - \beta \int n^2(\mathbf{r};N)\, d^3 r \,. \tag{3.1.1}$$

The terms contributing to the change of N are the loading rate L, the rate at which hot background atoms eject trapped atoms, γN, and the rate $\beta \int n^2(\mathbf{r};N)\, d^3 r$ at which inelastic collisions between trapped atoms contribute to trap loss. The integral in the last term takes into account that the atoms' density distribution $n(\mathbf{r};N)$ is not uniform. In the presence of a catalysis laser there are two contributions to β. One, denoted β_t, is that of the trap laser, whose excitation to the ${}^2P_{3/2}(F' = I + 3/2)$ level can lead to collisional trap loss in the presence of another distant atom. The other, which we call β_c, is due to the loss rate induced by the catalysis laser.

Because we make our measurements by keeping everything, except the catalysis laser parameters, constant, the steady-state solution to Eq. (3.1.1) is important. It is

$$N_\infty = \frac{L}{\gamma + \beta N_\infty^{-1} \int n^2(\mathbf{r};N_\infty)\, d^3 r} \,. \tag{3.1.2}$$

The objective of maintaining a constant N_∞ arises from difficulty in making a measurement of β as a function of an independent parameter, like catalysis laser detuning Δ. This is because a change in β affects N_∞, which also changes $\int n^2(\mathbf{r};N)\, d^3 r$. The density of a sample of trapped atoms is strongly affected by radiation trapping, which produces mutual repulsion between the atoms. As the number of atoms changes, the influence of radiation trapping involving atoms on the edge of the distribution, which do not experience uniform radiation trapping, affects the overall distribution. Because $n(\mathbf{r};N)$ is inherently difficult to measure, it is advantageous

to devise a method that avoids measuring it for every different β. For a further discussion see the following section.

However, we can make use of the linearity of β_c with respect to the catalysis laser intensity I_c (see Sec. 4.1.3), that is

$$\beta_c(\Delta, I_c) = \beta_c(\Delta, I_{ref}) I_c(\Delta) / I_{ref} , \tag{3.1.3}$$

with an arbitrary parameter I_{ref}. We simply adjust I_c to keep β_c constant over the range of detunings at which a measurement is made. That way, we can keep N_∞ constant, because neither β nor, as a consequence, $\int n^2(\mathbf{r};N)\, d^3r$ change. With this method, the collisional trap loss coefficient is

$$\beta_c(\Delta, I_{ref}) = \beta_c(\Delta_{ref}, I_{ref}) I_{ref} / I_c(\Delta) . \tag{3.1.4}$$

If absolute values are desired we measure $\beta_c(\Delta_{ref}, I_{ref})$ as a reference value, typically at $\Delta_{ref} = 300$ MHz and $I_{ref} = 10$ mW/cm^2 (see following section on how this is done). Otherwise, like for the measurements described in Sec. 4.2, we leave $\beta_c(\Delta_{ref}, I_{ref}) I_{ref}$ unspecified and Eq. (3.1.4) becomes

$$\beta_c(\Delta, I_{ref}) \propto 1 / I_c(\Delta) \tag{3.1.5}$$

Alternatively, if the intensity is not an independent or linear parameter we can vary the duty cycle of the catalysis laser, in order to keep β_c constant, as we have done in the case of our intensity dependence of repulsive collisions.

There are two advantages to this method of measuring trap loss spectra. First, as already mentioned, the knowledge of the atoms' density distribution, which is difficult to measure, is required at most for one value of β_c. Second, since the measurement of $\beta \int n^2(\mathbf{r};N)\, d^3r$ is inherently inaccurate, it is advantageous to avoid making it. The scatter in the data is mainly determined by how well we can maintain the constancy of the number of atoms and by the stability of the catalysis laser parameters, detuning and intensity. We estimate the typical point-to-point error of the relative measurements to be around 20%.

3.2 Absolute calibration

The previous section described how we obtain frequency-dependent trap loss spectra. The method of making relative measurements of the trap loss rate coefficient at various detunings is quite robust. Determining an absolute scale for the data is more elaborate and is the subject of this section.

According to Eq. (3.1.1), the loss rate affects the time dependence of the number of atoms in the trap. from measuring these loading transients, combined a knowledge of the density distribution of the atoms in the trap we can determine the absolute magnitude of the loss-rate coefficient β. The measurement of such loading transients is shown in Figure 3.1 for two different collisional loss rates. In the presence of a catalysis laser equilibrium is reached faster because of a larger β. Because our data is taken in a regime ($N > 10^6$) where radiation trapping is nonneglible, this changes the density distribution $n(\mathbf{r};N)$. To avoid this, for determining relative values of β, the data can be taken in such a way that N remains constant (see previous section).

An absolute measurement of β requires knowledge of the density distribution $n(\mathbf{r};N)$. The analysis of the observed profiles of the density distribution, which we derive from a trap image taken by a CCD camera (see Sec. 2.4), is based on the model developed by Sesko *et al.*[27] for the relationship between radiation trapping and trap densities.

When the number of atoms in an optical trap is small, the atoms move independently of each other, and the spatial distribution of the atoms is determined by the shape of the trapping force field and the temperature. For a force proportional to displacement, $\mathbf{F} = -k\mathbf{r}$, the distribution is $n(\mathbf{r}) = n(0)\exp(-kr^2/2T)$, where T is the temperature, and $\mathbf{F}$ and k are expressed in terms of temperature units, in which the Boltzmann constant $k_B = 1$. When the number of atoms confined by the trap is very large, the density distribution is dominated by radiation trapping, and the finite temperature may be neglected, and $n(\mathbf{r})$ is given by

$$n(\mathbf{r}) = \begin{cases} n_{\max} & r < \left(\dfrac{3N}{4\pi n_{\max}}\right)^{1/3} \\ 0 & \text{otherwise} \end{cases} \tag{3.2.1}$$

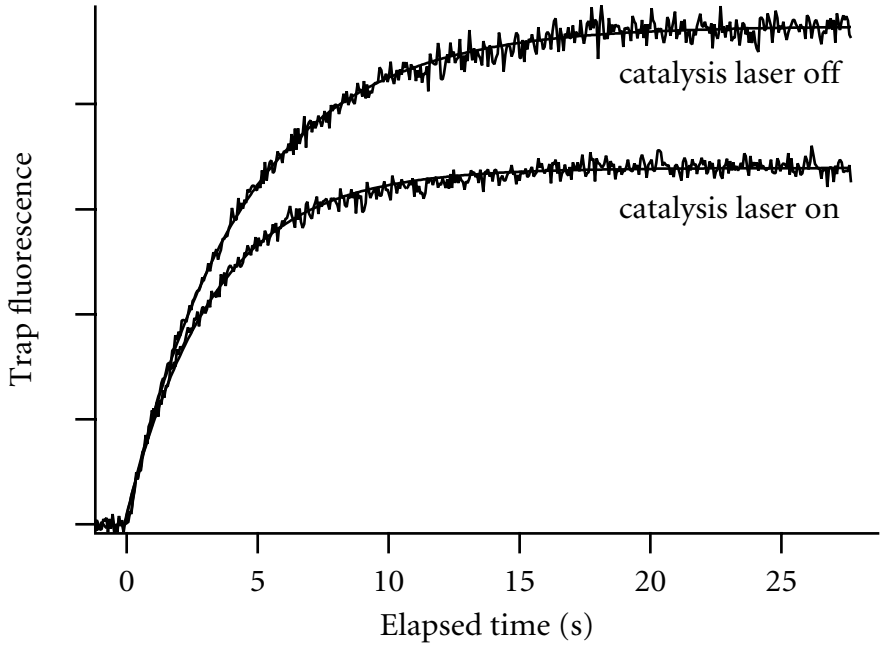

Figure 3.1: Two trap loading transients. They show the fluorescence as a function of time after unblocking the trap laser, which begins loading. The top loading transient is taken with the catalysis laser blocked. The bottom transient has the catalysis laser induce trap loss collisions in the trap. There the loss rate is higher and the equilibrium number of atoms is reached faster.

In general, neither limiting case is appropriate and it is necessary to consider the intermediate regime where both non-zero temperature and radiation trapping are important. Fig. 3.2 shows density distributions in the intermediate regime. They were generated by numerically integrating

$$T\nabla^2 \ln[n(\mathbf{r})] = 3k(n/n_{\max} - 1), \tag{3.2.2}$$

which represents hydrostatic equilibrium between the radiation pressure gradient and the trapping forces.[27] A convenient parameter is $N_{\rm rt} = 4\pi n_{\max}(T/k)^{3/2}$ which is very nearly the number of atoms contained in a uniform sphere of radius $\sqrt{2T/k}$. As shown in Fig. 3.2, for $N/N_{\rm rt} = 0.10$ or more the density is limited to the value $n_{\max}$, so we can write $n(\mathbf{r};N) = n_{\max}g(r;N)$, with $g(0;N) = 1$. A typical value for $n_{\max}$ is 2×10^{10} cm^{-3}, and $\sqrt{2T/k}$ is typically about 150 μm, giving $N_{\rm rt} = 3\times10^5$. For our experiment $N/N_{\rm rt}$ is typically 20.

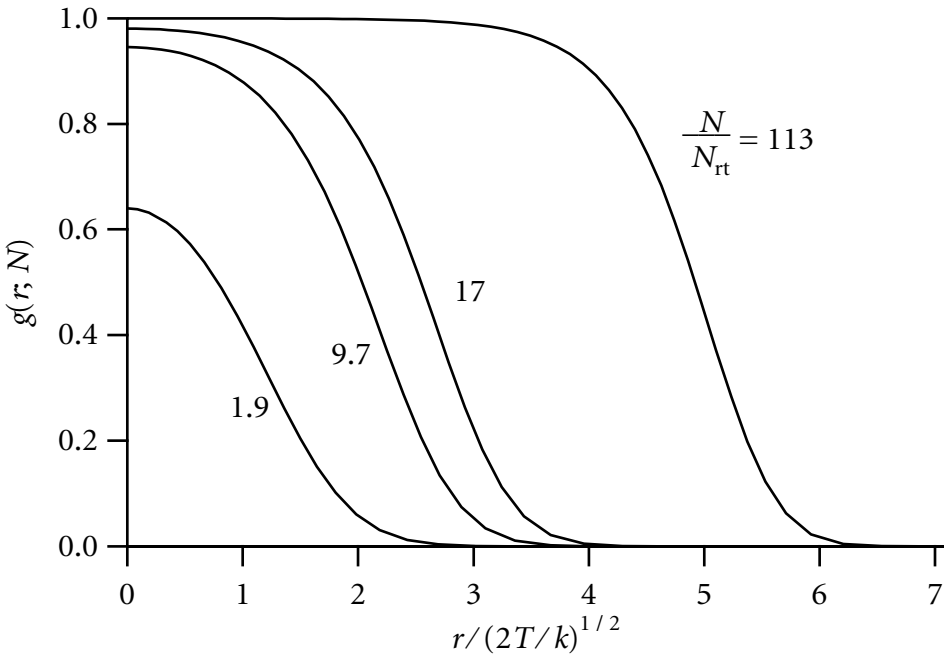

Figure 3.2: Theoretical density distributions of optically trapped atom clouds for nonzero temperatures at various numbers of trapped atoms. n_{max} is the ratidation trapping limited density, T is the temperature of the atom cloud, and k is the spring constant of the Zeeman trapping force; $(2T/k)^{1/2}$ is roughly the radius of the atom distribution when radiation trapping is not present. The number of atoms in the trap required for radiation trapping to begin to affect the atomic density distribution is approximately $N_{rt} = 4\pi n_{max}(T/k)^{3/2}$.

Even though the density of the atoms is limited by radiation trapping to the value $n_{\max}$, it is necessary to consider the effect of temperature on the density-distribution near the edge of the cloud. This is very important because the collision rate $\beta\int n^2(\mathbf{r};N)\,d^3r$ preferentially weights large r, where the non-zero temperature reduces the density below $n_{\max}$. To include this effect, we rewrite Eq. (3.1.1) as

$$\frac{dN}{dt} = L - \gamma N - \beta n_{\max}\left(\frac{\int g^2(\mathbf{r};N)\,d^3r}{\int g(\mathbf{r};N)\,d^3r}\right)N. \tag{3.2.3}$$

The factor in parentheses,

$$f = \frac{\int g^2(\mathbf{r};N)\,d^3r}{\int g(\mathbf{r};N)\,d^3r}, \tag{3.2.4}$$

is a measure of the reduction of the collision rate due to the non-uniform density distribution that arises from non-zero temperature. For $T = 0$, $f = 1$.

In Fig. 3.3 we present model calculations of $f(N)$ for a range of N/N_{rt}. The dependence of f on N is very weak, slower than logarithmic, approaching 1 only for $N/N_{rt} \gg 1000$. Since the dependence is so weak, we can approximate $f[N(t)]$ as being independent of time and rewrite Eq. (3.2.3) as

$$\frac{dN}{dt} = L - [\gamma + \beta n_{\max} f(N_\infty)]N \tag{3.2.5}$$

This has transient solutions

$$N(t) = N_\infty[1 - \exp(-\gamma_t t)], \tag{3.2.6}$$

where $\gamma_t = \gamma + \beta n_{\max} f(N_\infty)$ is the total collisional loss rate and the initial condition is assumed to be $N(0) = 0$. As Fig. 3.1 shows, Eq. (3.2.6) indeed fits the observed time dependence. Because γ and $\beta n_{\max} f(N_\infty)$ are not independently determined by a fit to Eq. (3.2.6),

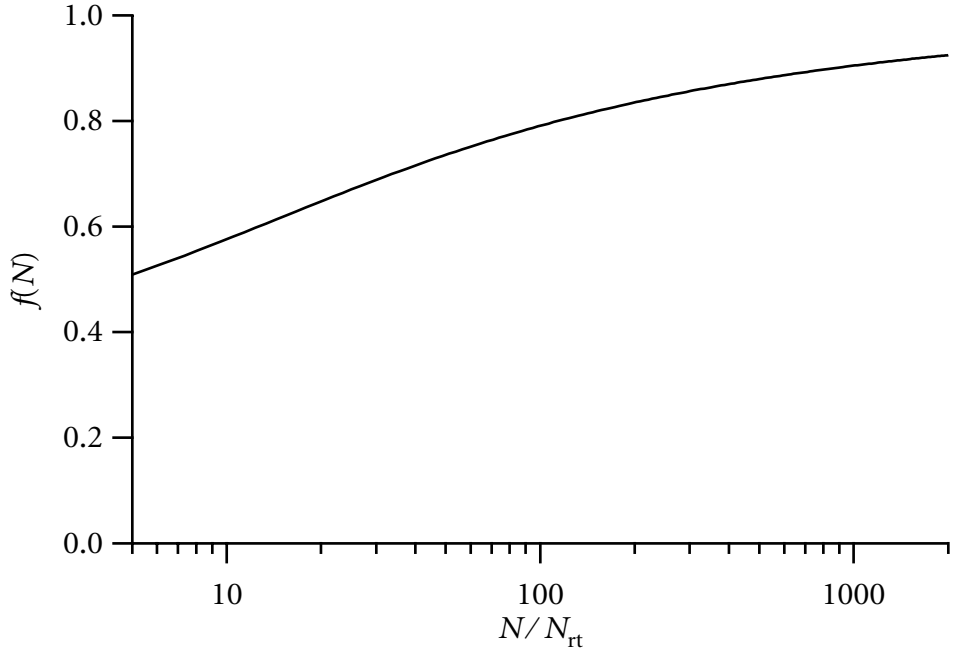

Figure 3.3: Plot of the parameter $f(N)$, which specifies the decrease of the binary collision rate for an optically thick cloud at finite temperature from the rate for zero temperature.

we use the catalysis laser technique to isolate the contribution of β. To do this we collect two transients, one with the catalysis laser and one without, and the catalysis laser contribution $\beta_c n_{max} f(N_\infty)$ is the difference between the two measured values of γ_t.

The approximation $f(N) = f(N_\infty)$ is even better than suggested by Fig. 3.3 for two reasons. First, for small t the transients depend only on the loading rate, $N = Lt$, so the collision rate does not affect the transients at small t. Second, the curvature of the transients, which determines γ_t, is determined mainly by $\frac{1}{2}L/\gamma_t < N < L/\gamma_t$, and in this regime f varies by at most 10%. As an additional test of this we have also measured transients where the trap was allowed to fill without the catalysis laser present, then the catalysis laser was added and the resulting transient was observed. The time constants measured in this way agreed to better than 10% with those obtained in the way described above. Alternatively, one can consider the fitting of the exponential function in Eq. (3.2.6) as a convenient approximation that obeys the rigorous limits $N = Lt$ for small t and $N = L/\gamma_t$ for large t.

To determine the trap loss rate coefficient β_c from the value of $\beta_c n_{max} f(N_\infty)$ as deduced from the transients, an absolute measurement of the density distribution $n(\mathbf{r})$ is necessary. The distribution is deduced from the CCD camera output, with an absolute scale set by an absorption measurement (see following section). In analyzing the data we have found a convenient parameterization for the density distribution to be

$$n(\mathbf{r}) = \frac{n_{max}}{1 + \exp[(r - r_c)/r_T]}, \tag{3.2.7}$$

where r_c is the radius at which the density falls to half its maximum value, and r_T corresponds to the range of distances over which the density deviates from n_{max}. This functional form fits the calculated distributions of Fig. 3.2 and the observed distributions quite well.

The procedure to determine $n(r)$ was to first determine r_c and r_T by fitting the output of the CCD camera to the integral of Eq. (3.2.7) along the line of sight. Then we used the absorption measurement with a calculated absorption cross-section to determine n_{max}. Typical measured densities were in the range of $(1-3)\times10^{10}$ cm^{-3}. Using the distribution, we calculated $f(N_\infty)$ from Eq. (3.2.4). This procedure was checked to be internally consistent by taking data

at various trap laser detunings and intensities and background rubidium vapor pressures. The variation in our results was found to be ±30%, and the results were reproducible over several months.

Since the absorption measurement is performed with the trap on, a possible concern are the effect of Raman wave-mixing processes[28,29] on the absorption signals. These effects are prominent when the probe laser and the trap laser frequencies differ ~1 MHz. However, since our probe used for absorption is split off from the trap laser, it has precisely the same frequency and so we do not expect the Raman processes to be important. As a check, we also measured the density using fluorescence (which is insensitive to these effects) and the results agreed to within 50%, the estimated uncertainty of the fluorescence measurement.

The measurement of the frequency dependence (Ch. 4) assumed a linear dependence of β on the catalysis laser intensity. The assumed linearity was checked in two ways. First, the trap-loss rate was measured from transients as described above at several catalysis laser intensities for a single detuning of –300 MHz for ^{85}Rb, as shown in Fig. 4.4. Second, the spectra were measured using different catalysis laser intensities, and the shape was found to be the same within experimental scatter. Since the method for obtaining the spectra relies on a linear intensity dependence, finding that the shapes of the spectra are independent of intensity is equivalent to doing an intensity dependence over the whole range of detunings.

4 Excited-state attractive collisions

This chapter presents results of measurements we made applying the method described in the previous chapter. The comparison of $P_{3/2}$ collisions of the two rubidium isotopes shows that the hyperfine interaction plays an important role in the dynamics of these collisions. At the same time, $P_{1/2}$ collisions are insensitive to isotopic effects because the much larger hyperfine interaction decouples the interaction between the various potential curves.

In each of these experiments the frequency of the catalysis laser (Sec. 2.3.2, previous chapter) is adjusted over a spectrum of negative detunings, such that it excites predominantly attractive interaction potentials. To characterize these collisions we observe the increase in the rate at which atoms are lost from the trap at each detuning.

We gain considerable information about these collisions by making comparisons between the two stable rubidium isotopes, ^{85}Rb and ^{87}Rb. Their different hyperfine interaction modifies the colliding atoms' dipole-dipole interaction in a isotope-dependent way. An additional parameter is the choice between the $5^2P_{1/2}$ and $5^2P_{3/2}$ excited states. We use the Gallagher-Pritchard model (Sec. 1.1) to qualitatively, as well as in some cases, to quantitatively describe the underlying physics of these collisions.

4.1 Isotopic differences in rubidium using $P_{3/2}$ collisions

The two rubidium isotopes have different nuclear spins and moments (I = 5/2 for ^{85}Rb and I = 3/2 for ^{87}Rb) and therefore different hyperfine structure. This allows us to make comparisons between the collisions of ^{85}Rb and ^{87}Rb. This comparison will experimentally show under what conditions the hyperfine interaction is important for excited-state collisions. The results are in contrast to popular theories that neglect such interactions.

4.1.1 Detuning dependence

Fig. 4.1 shows measurements of the trap-loss spectra for the two stable isotopes of rubidium, ^{85}Rb and ^{87}Rb. The detunings of the catalysis laser are measured from the $5^2S_{1/2}(F = I + 1/2) \rightarrow 5^2P_{3/2}(F' = I + 3/2)$ atomic transition. Thus zero-detuning corresponds to infinite separation. There are two regimes in the trap loss spectra. Where the detuning is within the range of the hyperfine structure (184.1 MHz for ^{85}Rb and 424.3 MHz for ^{87}Rb) the

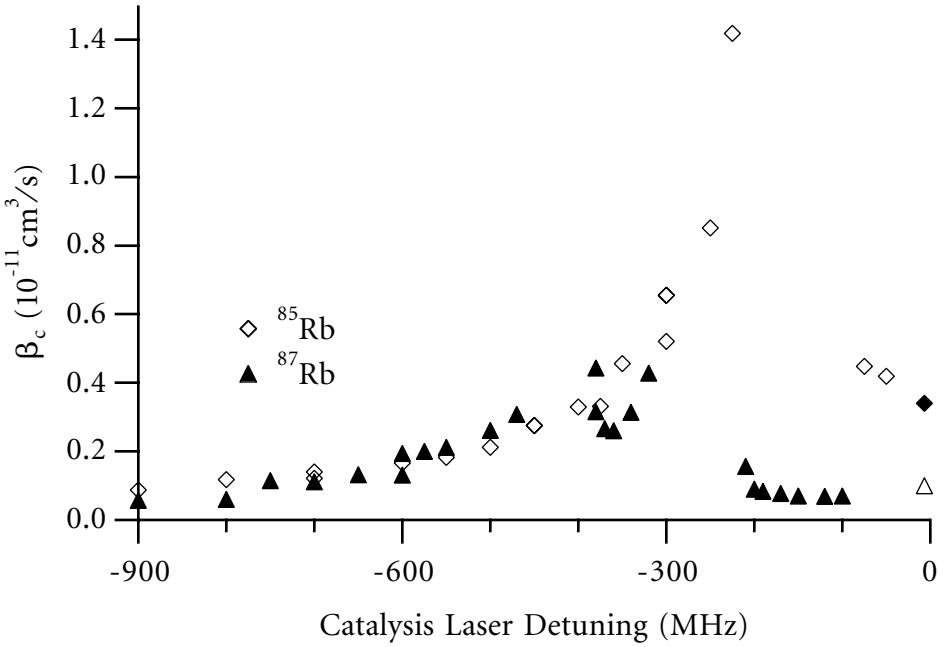

Figure 4.1: Trap loss rates for ^{85}Rb and ^{87}Rb.[5,6] β_c is the coefficient of the catalysis laser contribution to the trap loss rate. The catalysis laser detunings are measured from the $5^2S_{1/2}(F = I + ½) \rightarrow 5^2P_{3/2}(F = I + ⅜)$ transition. The gaps in these trap loss spectra result from our inability to make measurements where the catalysis laser interacts with the atomic excited hyperfine states and thereby perturbs the operation of the trap. The data points at –7 MHz were measured by Wallace *et al.*[32] and are in good agreement with our trap loss spectrum.

spectra are quite different for the two isotopes. For both the maxima in the spectra occur at the position of the lowest frequency component of the atomic hyperfine structure, just as for cesium in the data reported by Sesko *et al.*,[15] for which the first such trap-loss spectrum was measured. Furthermore, for ^{87}Rb another maximum occurs very near the next atomic hyperfine resonance, and for small detunings the rate coefficients for the two isotopes differ greatly. For large detunings, no experimentally significant isotopic dependence is observed. There the loss rate falls off at the expected $1/\Delta^2$ rate.

It is clear from these results that the excited-state hyperfine interaction has a profound effect on the trap-loss spectra. Based on the ideas behind the Gallagher-Pritchard model,[11] there are several natural reasons why this should be so.[6] First, it is clear that the modification of the potential curves by the hyperfine interaction will change the excitation function $\Re(R, \Delta)$ in

Eq. (1.1.8). For a given detuning there will be in general a number of different potential curves that can be resonantly excited by the catalysis laser. Second, the hyperfine interaction will affect the survival probability both through $t(R)$ and the spontaneous emission time τ (see Sec. 1.1). Third, curve crossings and avoided crossings that arise from the interplay of the hyperfine interaction with the dipole-dipole interaction will affect the acceleration process once the atoms have been excited. To illustrate this, Fig. 4.2 shows selected potential curves[19] for ^{87}Rb. For the catalysis laser tuned as shown, an acceleration of the atoms toward each other that leads to trap loss can happen only if a non-adiabatic transition occurs at the avoided crossing of the potentials. This could explain the observed isotopic difference for detunings within the excited-state hyperfine structure since it is within that detuning region that most of the avoided crossings occur, as shown in Fig. 4.2. For large detunings the ^{85}Rb and ^{87}Rb curves are similar and so the isotopic difference is small.

An interesting feature of the ^{87}Rb data (and possibly in the older cesium data[15]) is a minimum in the region between the lower two atomic hyperfine resonances, which has since been reported for ^{85}Rb by P.D. Lett *et al.*[30] as well. This is somewhat surprising, since one might expect multiple peaks to arise to the red side of the atomic resonances, if the effect of hyperfine structure is simply to make the spectrum a sum of contributions similar to Fig. 1.3 but shifted by the atomic hyperfine splittings. In this case the minimum would be very close to the lower hyperfine resonance, in contrast to our results that find the minimum at roughly halfway between the two atomic hyperfine resonances. No simple explanation for the position of the minimum has been made, yet, but it is possible that it may arise from modification of the excitation rates in the region of avoided crossings of the molecular potentials.[31]

Besides the shapes of the spectra, the absolute rates are also of interest. Since the absolute rates depend both on the dynamical factors (excitation and survival in the excited state) as well as the energy transfer probabilities, successful comparison of theory and experiment requires accurate calculations of both the dynamics and the energy transfer probabilities. Despite the neglect of hyperfine effects on the dynamics by the models, there is quantitative agreement between theory and experiment[15] for the case of cesium at very small[14] and very large[16] detunings. These calculations predict that Rb trap-loss collisions should occur at a rate about

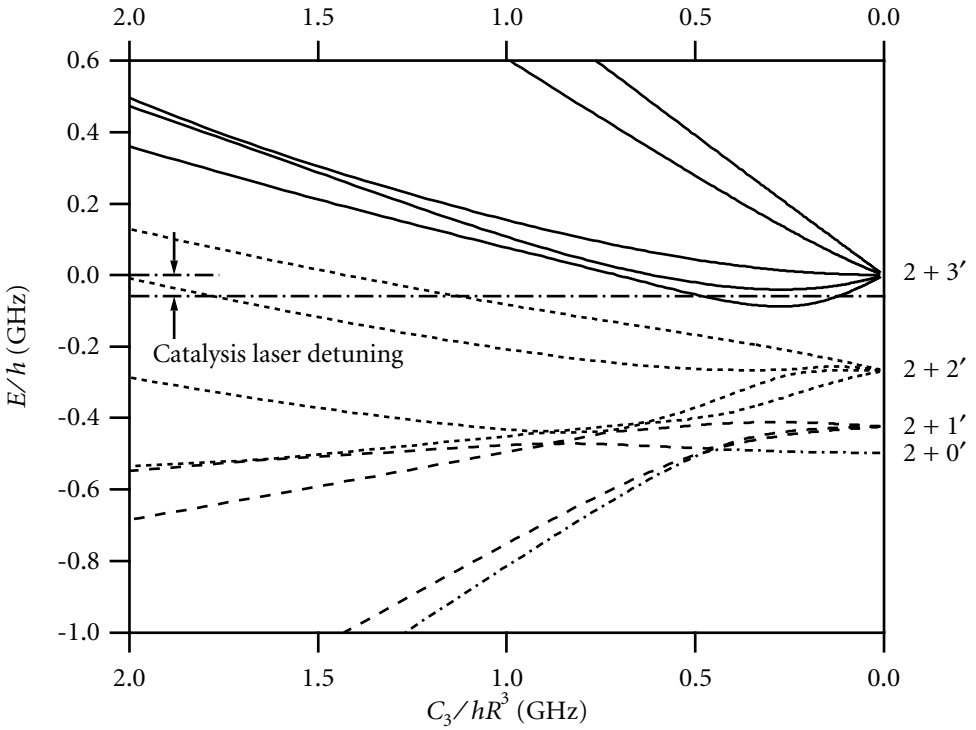

Figure 4.2: Avoided curve crossings in potential curves with energy E of the same symmetry. The curves belong to the 1^g manifold of ^{87}Rb. The numbers on the right are the hyperfine quantum numbers of the asymptotically dissociated atoms. Primes indicate the excited state. It is convenient to express the internuclear separation in terms of C_3/hR^3, where C_3 is the coefficient of the dipole-dipole interaction unperturbed by hyperfine effects. Correspondingly, smaller interatomic separations are on the left and larger ones on the right. The states that connect to the same asymptote have identical dashing patterns.

twice that of cesium collisions.[14] Thus, our observation of a factor of five or more smaller rate than expected at small detunings for rubidium, confirmed by Wallace *et al.*[32] (included in Fig. 4.1), suggests inaccuracies in the calculated energy transfer probabilities. Further calculations have been made that indeed show a strong sensitivity to the precise knowledge of the potential curves,[12] due to interference effects. It is unclear whether this sensitivity can explain some of the isotopic difference in the trap-loss rates at very small detunings.

4.1.2 Hyperfine structure

The comparison between the two rubidium isotopes' trap-loss spectra suggests that their hyperfine structure is responsible for any differences. At larger detunings potential curves with

larger dipole-dipole interaction are excited, so that the isotope-dependent hyperfine interaction is increasingly decoupled. A more detailed knowledge of the potential curves gains us increased insight into the dynamics, as well, and allows a more meaningful interpretation of the data.

The electron spins of the individual colliding atoms interact with each other during the collision. At small detunings around a few 100 MHz up to about 10 GHz this interaction is much stronger than the dipole-dipole interaction.

This dipole-dipole interaction is given by the interaction Hamiltonian

$$V(R) = \frac{e^2}{R^3}(x_1 x_2 + y_1 y_2 - 2 z_1 z_2)\,, \tag{4.1.1}$$

where R is the internuclear separation of the atoms and x_i,y_i,z_i are the operators of the coordinates of the two colliding atoms' valence electrons relative to the corresponding nuclei.

In order to calculate the potential curves we have to diagonalize the Hamiltonian

$$H = H_1(F_1, m_{1F}) + H_2(F_2, m_{2F}) + V(R)\,, \tag{4.1.2}$$

where H_1 and H_2 are the Hamiltonians of the isolated atoms and F and m_F are the quantum numbers of the hyperfine states the atoms are in. This is best done using the basis consisting of linear superpositions of the two atoms, such that for $R = \infty$ we get the atomic energy levels[19]. Given the rotational symmetry about the axis connecting the two atoms the angular projection of the molecule's angular momentum $\phi = m_{1F} + m_{2F}$ on that axis is conserved. The other conserved quantum numbers is the symmetry parameter *ungerade* (u) and *gerade* (g), which determine whether the state changes sign or not, respectively, under the operation that exchanges the two atoms. In the limit of $R = \infty$ the well-defined quantum numbers also include the individual atoms' hyperfine level quantum numbers. Thus in that limit the molecular states can be written as

$$|\phi ½ F_1 J_2 F_2 m_{2F}\rangle^{g/u} = (|(J_1 = ½) F_1 m_{1F} J_2 F_2 m_{2F}\rangle \pm |J_2 F_2 m_{2F} (J_2 = ½) F_1 m_{1F}\rangle)/\sqrt{2}\,, \tag{4.1.3}$$

where one component state is obtained from the other by exchanging the two atoms. J_2 is the electronic angular momentum of the valence electron of the excited atoms. In alkali atoms it can take the value ½ or ³⁄₂. The ground state atoms have $J_1 = ½$. With these basis states, H_1 and H_2 are already diagonal.

The energies at any given R can be found by numerically diagonalizing the matrix with elements

$$\langle \phi ½ F_1 J'_2 F_2 m'_{2F} |^{g/u} V(R) | \phi ½ F_1 J_2 F_2 m_{2F} \rangle^{g/u} . \qquad (4.1.4)$$

Figure 4.3 shows the results of these calculations for molecular states with the 3^u symmetry. These curves are taken from reference [19].

Looking at these potentials a couple of qualitative statements can be made. Because of avoided curve crossings none of the potential curves starting from the $3 + 4'$ asymptotic state remain attractive. Thus, an atom pair excited with a catalysis laser detuning less than the $F' = 4 - F' = 3$ splitting can only survive to small internuclear separations if it undergoes a diabatic transition to a different, attractive potential curve. If they do not undergo such a transition, the interaction will become repulsive and the atoms will quickly turn around without ever having picked up enough energy to cause trap loss.

Walker and Pritchard[19] estimate the probabilities of diabatic transfer between potential curves according to the Landau-Zener picture. They conclude that rotational coupling of potential curves with different spin quantum number as well as magnetic coupling is negligible. The dominant diabatic transfer should be due to radial coupling with a Landau-Zener transfer probability[33] of

$$p = \exp\left(-\frac{2\pi V_{12}^2}{v\hbar \left| (d/dR)(\varepsilon_2 - \varepsilon_1) \right|_{R = R_x}} \right), \qquad (4.1.5)$$

where V_{12} is have the smallest separation between the potential curves occurring at $R = R_x$, ε_1 and ε_2 are the potentials of the two curves and v is the velocity at which the closest approach is traversed. Radial coupling occurs between potentials of like symmetry. A high

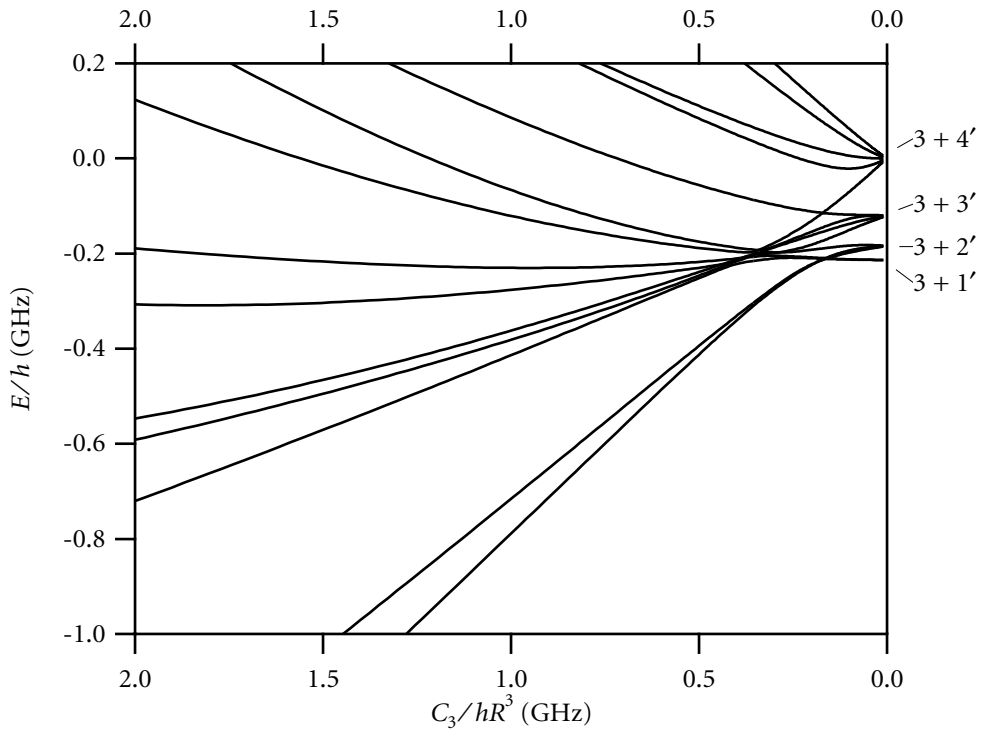

Figure 4.3: Calculated hyperfine potential curves for ^{85}Rb. The numbers on the right are the asymptotic hyperfine quantum numbers of the two atoms. Primes denote the excited state ($5^2P_{3/2}$; the ground state is $5^2S_{1/2}$).

velocity as well as a small separation of potential curves favors a transfer. This would be the case, if the atoms were excited sufficiently far to the red of the avoided crossing.

A full quantitative analysis would have to take into account the potential transfer to the multitude of all the other curves of the same symmetry. We can avoid this difficulty by designing our experiments in such a way that the collisional dynamics does not involve avoided potential curve crossings (see Sec. 4.2, as well as Ch. 6).

If the detuning is sufficiently large, that is, near the lowest-lying excited-state hyperfine state, potential curves that are attractive outnumber those that are not. This may explain[19] why the spectrum is peaked there both in ^{85}Rb, ^{87}Rb and in Cs.[15] The atom pair then proceed along a potential curve that is purely attractive until the dipole-dipole interaction becomes roughly half of the ground-state hyperfine splitting.

4.1.3 Intensity dependence

The measurement of the frequency dependence (Sec. 4.1) assumes a linear dependence of β on the catalysis laser intensity. This is predicted by the Gallagher-Pritchard model (see Eq. (1.1.11)). We checked the assumed linearity in two ways. First, we measured the trap-loss rate from transients as described above at several catalysis laser intensities for a single detuning of –300 MHz for ^{85}Rb, as shown in Fig. 4.4. Second, the spectra were measured using different catalysis laser intensities, and the shape was found up to an overall factor to be the same within experimental scatter. Since the method for obtaining the spectra relies on a linear intensity dependence, finding that the shapes of the spectra are independent of intensity is equivalent to doing an intensity dependence over the whole range of detunings.

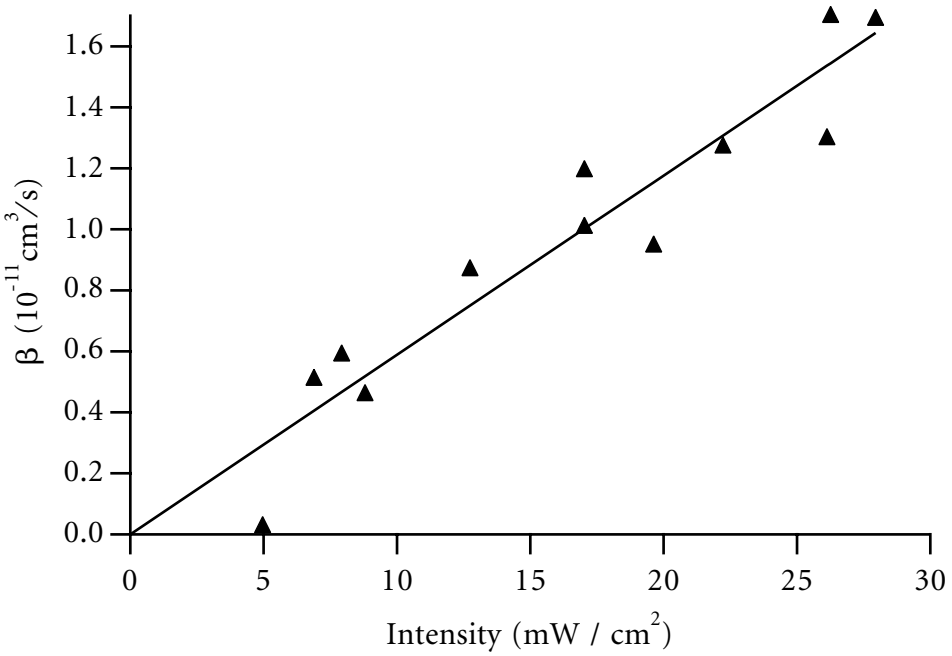

Figure 4.4: Intensity dependence of trap loss collisions. This data was taken with ^{85}Rb at a catalysis laser detuning of –300 MHz. The solid line is a linear fit to the data.

4.2 Collisions independent of hyperfine structure in $P_{1/2}$ collisions

There are two features of $P_{1/2}$ collisions that make them more accessible to theoretical studies than $P_{3/2}$ collisions. First, trap loss through fine-structure changes is not possible, since there are no lower-lying excited-state fine-structure potential curves. The only mechanism of

energy transfer leading to trap loss is spontaneous emission during the collision process. This spontaneous emission has to occur at an internuclear separation where the difference between the energy of the photon absorbed from the catalysis laser and that of the emitted photon exceeds the trap depth.

Second, the hyperfine structure is much larger in the $P_{1/2}$ state, compared to the $P_{3/2}$ state, for both rubidium isotopes. Also, the excited atom's spin can only be $I \pm ½$, as opposed to $I \pm 3/2$, $I \pm ½$ for $P_{3/2}$. Thus the dipole-dipole potential curves are greatly simplified, because they are farther apart and there is a smaller number of them.

We conducted trap-loss experiments in rubidium involving the $P_{1/2}$ excited-state.[7] To this end the catalysis laser was tuned below the $5^2S_{1/2}(F = I + ½) \rightarrow 5^2P_{1/2}(F' = I - ½)$ transition. With this choice of catalysis laser detunings the excited-state energies are beneath the region where the excited-state hyperfine interaction mixes the various attractive and repulsive potential curves that extend to the two $5^2P_{1/2}(F' = I \pm ½)$ asymptotes (see Fig. 4.5).

The trap loss rates due to the catalysis laser as a function of its detuning are shown in Fig. 4.1 for both isotopes, ^{85}Rb and ^{87}Rb. They show no isotopic effect, indicating the insensitivity of the collision dynamics to hyperfine interactions. Our experimental results are quantitatively consistent with the Gallagher-Pritchard model[11] for the role of spontaneous emission (see Sec. 1.1), modified in a simple way to account for hyperfine interactions. The data supports multiple traversals of the potential wells by the colliding atoms.

This effect of multiple traversals, or ultra-cold vibrations, can be described by the Gallagher-Pritchard model. Fig. 4.6 depicts the collision process. The atom pair is excited at R_0. Only if the atom has come closer to each other than R_T will spontaneous emission to the ground state result in trap loss. At R_T each atom has picked up a kinetic energy corresponding to the trap depth. If the kinetic energy exceeds that value the trap cannot continue to hold the atoms.

Thus there are two distinct phases in an atom pair's trajectory (Fig. 4.6). Phase 1 is the motion between R_0 and R_T. Integrating a simplified excited-state potential, which does not

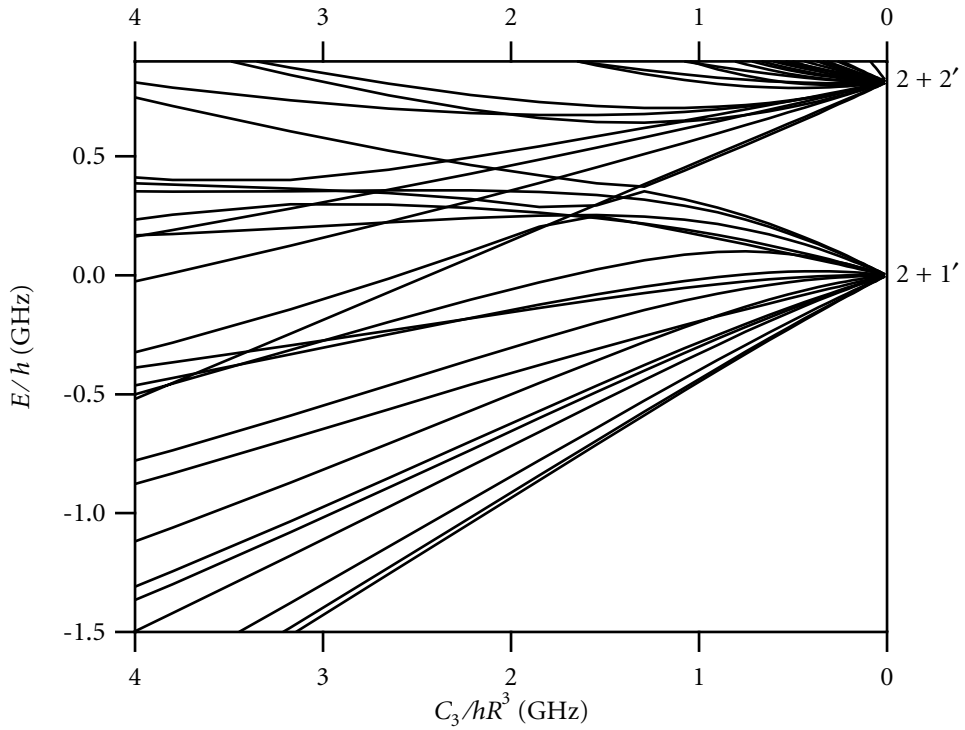

Figure 4.5: Calculated potential curves for the relevant $P_{1/2}$ state of ^{87}Rb. The curves shown correlate at large separations to the $S_{1/2}(F = 2) + P_{1/2}(F = 1', 2')$ atomic states. In the region on the low energy side of the $(2 + 1')$ state the potential curves closely follow an R-3 dependence, facilitating a relatively straightforward comparison with simple models. In between the $(2 + 1')$ and $(2 + 2')$ states the curves and resulting hyperfine dynamics are more complicated.

take hyperfine interaction into account, $V(R) = h\Delta = -C_3/R^3$ ($C_3 = 71$ eV Å^3), the duration of phase 1 is, according to Eq. (1.1.5),

$$t_1 = t(R_0) - t(R_T) = \tau_M\left[\left(\frac{\Delta_\tau}{\Delta}\right)^{5/6} - \left(\frac{\Delta_\tau}{\Delta_T}\right)^{5/6}\right], \tag{4.2.1}$$

where R_T and, correspondingly, $\Delta_T \equiv C_3/hR_T^3$ depend on Δ.

Phase 2 lasts for maximum duration of twice

$$t_2 = t(R_T) = \tau_M\left(\frac{\Delta_\tau}{\Delta_T}\right)^{5/6} \tag{4.2.2}$$

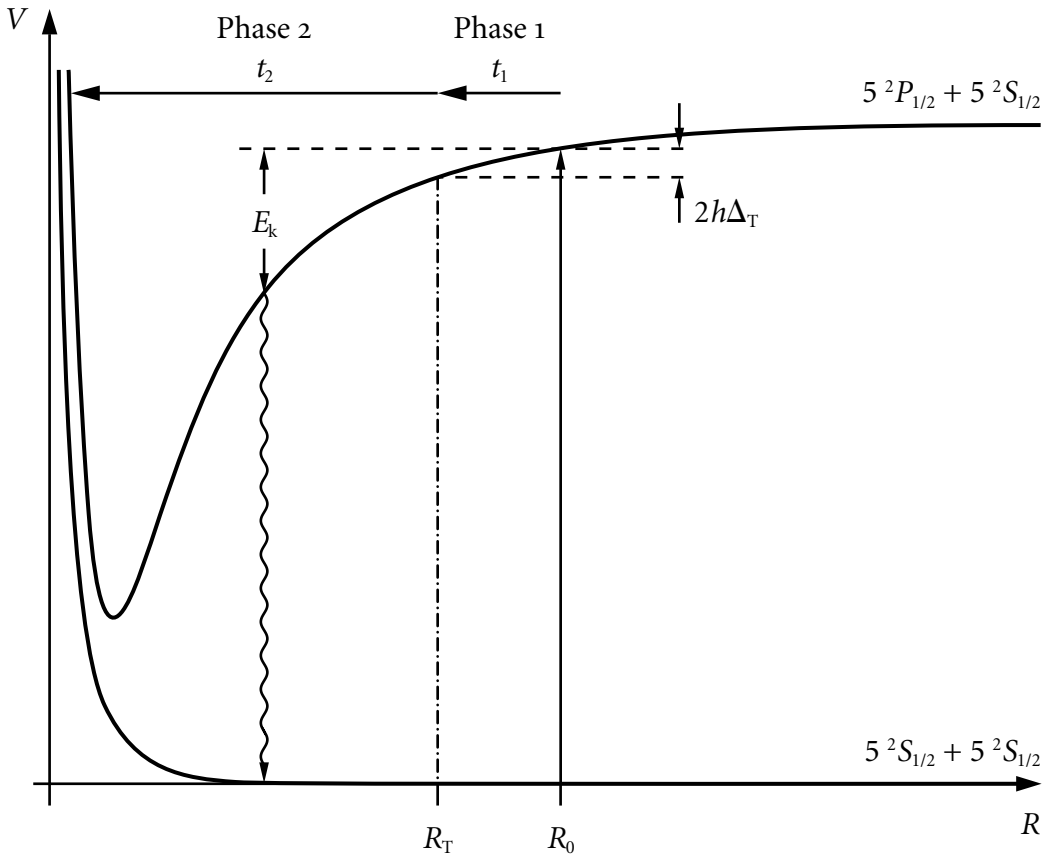

Figure 4.6: Gallagher-Pritchard model of trap-loss collisions. The laser of detuning Δ excites atom pairs at interatomic separation R_0. The atoms are accelerated toward each other by the attractive excited-state potential curve. If the atoms radiate while separated by $R < R_T$, where $h\Delta - V(R_T) = 2h\Delta_T$ and $h\Delta_T$ is the trap depth, the outgoing atoms have kinetic energy $E_k > h\Delta_T$ and escape the trap.

as the atoms continue to approach each other until they rebound at $R = 0$, returning to R_T. Trap loss occurs only if the atom pair fails to undergo spontaneous emission during phase 1 and does during phase 2. Thus the probability of trap loss during one orbit is

$$p_1 = \exp(-\Gamma t_1)[1 - \exp(-2\Gamma t_2)], \tag{4.2.3}$$

where $\Gamma = \tau_M$ is the spontaneous emission rate. Subsequent orbits have the property that spontaneous emission occurs only on the last traversal of the region between $R = 0$ and R_T. Thus the trap-loss probabilities are

$$\begin{aligned} p_2 &= \exp[-\Gamma(3t_1 + 2t_2)][1 - \exp(-2\Gamma t_2)] \\ p_3 &= \exp[-\Gamma(5t_1 + 4t_2)][1 - \exp(-2\Gamma t_2)] \\ &\cdots \end{aligned} \tag{4.2.4}$$

Summing over repeated orbits we get a total trap loss probability

$$P = [1 - \exp(-2\Gamma t_2)]\exp(-\Gamma t_1)\sum_{n=0}^{\infty}\exp[-2n\Gamma(t_1 + t_2)]. \tag{4.2.5}$$

The series is geometric and evaluates to

$$\sum_{n=0}^{\infty}\exp[-2n\Gamma(t_1 + t_2)] = \frac{1}{1 - \exp[-2\Gamma(t_1 + t_2)]}. \tag{4.2.6}$$

Thus the total trap loss probability is

$$P = \frac{\sinh(\Gamma t_1)}{\sinh[\Gamma(t_1 + t_2)]}. \tag{4.2.7}$$

Our data fits a detuning dependence of the trap-loss rate coefficient

$$\beta \propto \{\Delta^2 \sinh[(\Delta_\tau/\Delta)^{5/6}]\}^{-1} \quad . \tag{4.2.8}$$

This reflects that the loss rate is proportional to P, as well as to Δ^{-2} (see Eq. (1.1.11)). In addition, the approximation is found to hold that for the range of detunings in our experiment $R_0^3 \gg R_T^3$, which means that $t_1 \gg t_2$ and, therefore, that t_1 is independent of detuning. For detunings large enough that $\Delta \gg \Delta_\tau$, the argument of the hyperbolic sine in Eq. (4.2.8) becomes small, such that $\beta \propto \Delta^{-7/6}$. This is verified in our data to be valid over the entire range of catalysis laser detunings.

Our data does indeed exhibit such a detuning dependence (see Fig. 4.7). The dashed line has a simple Δ^{-2} dependence and shows the detuning dependence expected if no multiple orbits

occurred. With the detuning range of $-1200\ \text{MHz} < \Delta/(2\pi) < -50\ \text{MHz}$ accessible in this experiment we expect no resonant trap loss due to vibrations. There are two reasons for this. First, the discrete vibrational states are the highest-lying ones of the dipole-dipole interaction well and are thus lying together closer than $\Gamma/2\pi$. Second, there is a multitude of potential curves as shown in Fig. 4.5 to which the catalysis laser can excite. These effects wash out any discrete structure in the trap-loss spectrum. Going to very large detunings of a few nanometers, discrete trap-loss peaks become visible as R. A. Cline *et al.* observed in rubidium.[34] The experiment of R.A. Cline *et al.* greatly benefits from the weak $\Delta^{-7/6}$ detuning dependence of the loss rate. At detunings of a few nanometers this makes a big difference compared to a Δ^{-2} dependence, which does not take vibrations into account.

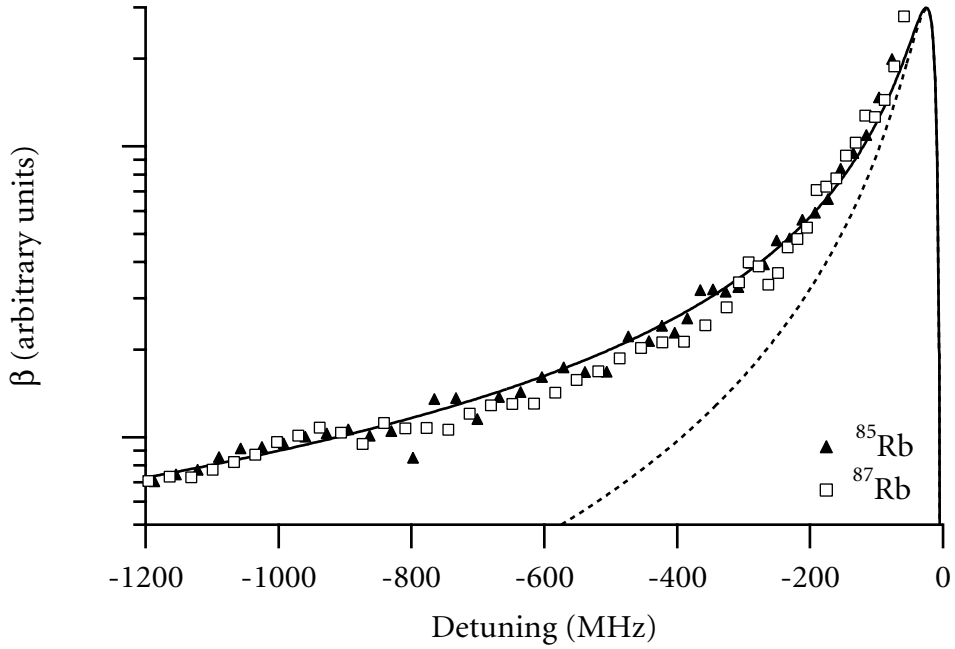

Figure 4.7: Measurements of trap-loss spectra for ^{85}Rb and ^{87}Rb for detunings to the red of the lowest atomic $P_{1/2}$ hyperfine states. The lack of isotopic effect in the shapes of the trap-loss spectra indicates the relative unimportance of hyperfine dynamics for this data. The data is scaled to allow comparison of the shapes. Two model calculations are shown, the solid line including effects of multiple orbits of the atoms and the dashed line assuming a single orbit.

In addition, despite the simplicity of the potentials in the detuning region $-1200\ \text{MHz} < \Delta/2\pi < -0\ \text{MHz}$, there are curve crossings and avoided crossings that will change the values of t_1 and t_2 at distances where the dipole-dipole interaction is comparable to the ground-state hyperfine splitting. Although this effect is important for t_1, it changes t_2 by only $\sim 10\%$ and therefore changes the absolute scale of the spectrum but not its predicted shape.

It is important to address the issue of whether there is a maximum at $|\Delta/2\pi| < 50\ \text{MHz}$, as Eq. (4.2.8) predicts for $\Delta = 0.36\Delta_\tau = 41\ \text{MHz}$. Distortion of the atom cloud and optical pumping effects render the catalysis laser technique unreliable in this range. We have probed the physics of the $|\Delta/2\pi| < 50\ \text{MHz}$ region in a two-color $P_{1/2}$ experiment (see Sec. 6) similar to the $P_{3/2}$ photo-associative ionization experiment recently reported by Bagnato *et al.*[35]. In this type of experiment, both lasers can be tuned far from atomic resonances and the spontaneous emission effects show up in the collision rate as a function of the relative detuning of the two lasers. Since both lasers are off resonance with the isolated atoms, the distortion and optical pumping effects would not be a problem.

Finally, it is important to recognize which features of the model are really tested by our data. In particular, it is surprising that a quasistatic calculation of the excitation rate should be valid because of motion on both the ground and excited-state potential curves. However, Julienne *et al.*[36] have shown that the same detuning dependence of the excitation rate results from a stationery phase calculation where the atoms are moving but spontaneous decay is neglected. Thus two very different approaches to calculating the excitation rate give the same result. Based on this we suggest that the trap-loss probability [Eq. (4.2.5)] is what is principally being tested by our experiment.

So far we have concentrated on the spectra to the red of the $F = I + ½ \rightarrow F' = I - ½$ states. To the blue of these states, the trap-loss rate is smaller and increases for increasing blue detunings, as expected. However, in this region the distortions of the potential curves that are evident in Fig. 4.5 decrease the prospects for simple interpretation of the data.

Our trap loss experiments involving the $5^2P_{1/2}$ excited state of both stable rubidium isotopes has brought us closer to understanding the excited-state ultra-cold collisions. First,

because the hyperfine splitting is larger than in the $5^2P_{3/2}$ state, isotopic differences in the loss rate spectra have vanished. This further points to the hyperfine interaction being an important factor if the collisions involve regions where it is comparable to the dipole-dipole interaction. Second, because in this experiment this is not the case, a description of the dynamics in terms of classical mechanics, in the way the Gallagher-Pritchard model does it, is quite successful.Therefore, we have applied these insights to the following experiments.

5 Repulsive excited-state collisions

This far we have considered experiments using attractive potential curves. However, the dipole-dipole interaction between two colliding atoms can be repulsive, as well as attractive. The repulsive collisions experiments presented in this chapter are a test of the Landau-Zener model for the excitation process, especially at high intensity. The trap-depth plays an important part in these collisions, such that they can be used to measure it.

One of the problems with attractive collisions is the complicated dynamics of the interaction as the atoms get to within a couple of atomic radii of each other. Detailed analysis is hampered by the requirement of a precise knowledge of the shape of the potential barrier at $R = 0$.[12]

When excited by a blue-detuned catalysis laser to a repulsive potential curve, a pair of atoms, as they are repelling each other, will pick up kinetic energy proportional to the blue detuning. If this energy is large enough, this will result in trap loss. With the small thermal energies with which the atoms approach each other in the ground state, they are quickly turned around on the excited-state potential. Thus they never reach close range, where the complications mentioned above arise. Also, after being turned around they pass through the resonance with the catalysis laser a second time, which can lead to stimulated deexcitation. This results in the interesting intensity dependence in Sec. 5.3. In addition, we have used repulsive collisions to measure the trap-depth of our trap.[9]

5.1 Apparatus

To perform this experiment we made several changes to the apparatus described in Ch. 2. The catalysis light came from a Ti:Sapphire laser and was sent to the setup by way of a single-mode optical fiber whose output was collimated and sent through a $\lambda/2$ plate and linear polarizer to allow adjustment of intensity (see Fig. 5.1). A beamsplitter picked off a small fraction of the light and sent it to a calibrated photodiode to measure the catalysis laser power. Using the Ti:Sapphire laser afforded us with two major advantages over the diode lasers we had used previously for manipulating the atoms' collisions. First, we were able to tune it over a far larger range, up to 200 GHz. The diode laser would mode hop in an unpredictable fashion at the ends of a maximally 4 GHz wide tuning range. Second, we had much more power (1 – 15

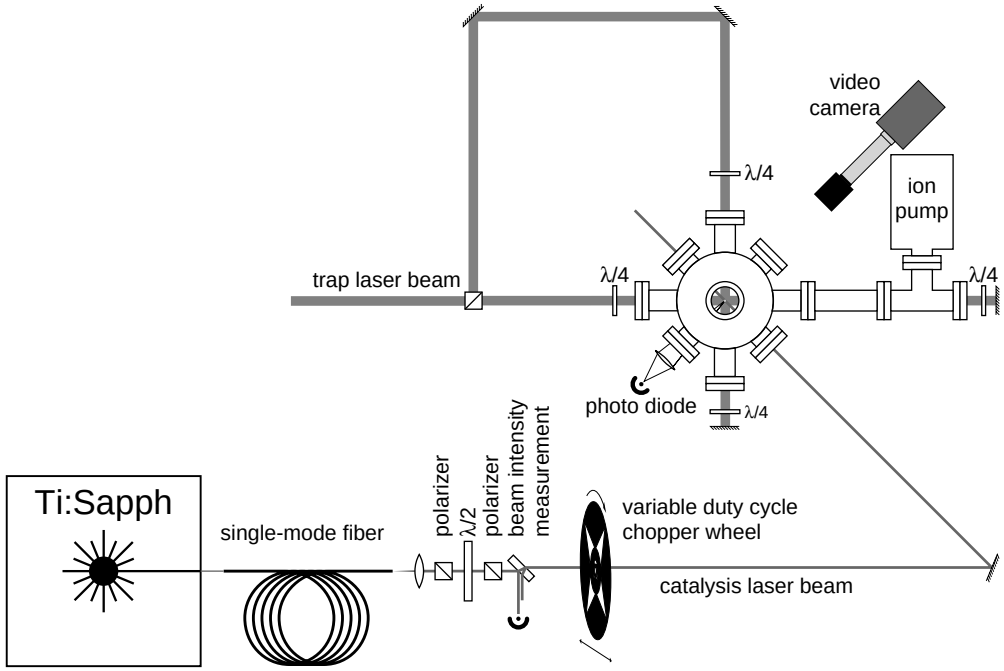

Figure 5.1: Apparatus for repulsive collisions. The collisions are induced by light from a Ti:Sapphire laser, which provides up to 15 W/cm² of intensity. It can be chopped at variable duty cycle with a chopper wheel. The fluorescence is measured by imaging the trap onto a photo diode. The spatial distribution of the trap is monitored with a video camera.

W/cm^2) at our disposal. At the large detunings used in this experiment, correspondingly higher catalysis power was necessary to achieve appreciable trap loss. The Ti:Sapphire laser was detuned relative to the $5^2S_{1/2}(F = 3) \rightarrow 5^2P_{3/2}$ transition. It was measured by sending a small amount of light from its output beam into an optical spectrum analyzer, whose zero was determined by the frequency at which the laser blew away the atoms, that is, was on resonance.

The catalysis laser beam was chopped mechanically at around 1 kHz. By making a chopper wheel with two triangular cutouts with their tips near the wheel's hub, we could adjust the duty cycle of the beam between 0 and 45% by sliding the wheel across the beam. Since we used the fluorescence as a measure of the trap loss rate coefficient, an increase in loss rate could be made up for by a decrease in catalysis duty cycle. That way, from data point to data point a constant number of trapped atoms was maintained. This ensured consistency of the data across a whole data set.

At the large powers used for catalysis the laser produced considerable AC-Stark shifts. These decrease only inversely with detuning, unlike mechanical effects on the distribution of atoms in the trap which go like Δ^{-2}. This led to changes in the level of fluorescence. Therefore we observed the trap fluorescence during the phase of the chopping cycle in which the catalysis laser beam was off. By chopping the beam at a rate faster than 500 Hz, AC-Stark-shift-induced forces that perturbed the atoms' density distribution were reduced to a negligible level.

For reasons to be explained later, the parameters of the trap were chosen to reproduce those reported by Wallace *et al.*[32] The detuning of the trapping light was $\Delta_t = -4.9$ MHz from the $5^2S_{1/2}(F = I + ½) \rightarrow 5^2P_{3/2}(F' = I + ⅜)$ transition. Like in the previous experiments, a hyperfine-pumping laser repumped the atoms to the upper hyperfine ground state. The MOT intensity was 2 $\mathrm{mW/cm^2}$. The Gaussian beam diameter was 6.3 mm. The magnetic-field gradient was 20 G/cm. Under these conditions Wallace *et al.* were barely able to capture ^{87}Rb atoms which had undergone a ground-state hyperfine changing collision. Therefore the trap depth of such a trap must be on the order of 6.8 GHz, the ground-state hyperfine splitting. With these parameters our trap loaded around 3×10^6 atoms at a density of 3×10^{10} $\mathrm{cm^{-3}}$. We were able to quickly switch between trapping ^{85}Rb and ^{87}Rb by switching the locking of the trap and hyperfine-pumping laser between the relevant transitions.

In addition, the trap laser locking method was modified. For this experiment we applied a 20 kHz current dither to the laser diode and fed the saturated-absorption signal into a lock-in amplifier which was synchronized with the dither frequency. In this case, the output of the lock-in amplifier provides the first derivative of the saturated absorption spectrum, enabling us to lock the laser to the center of the absorption feature, where the derivative changes most rapidly with frequency. The beam that was used to operate the saturated absorption setup was passed through an acousto-optic modulator (AOM). For ^{85}Rb it was driven at a frequency $\nu_{AOM} = \Delta(F' = 3, F' = 4) - \Delta_t = 115.8$ MHz, where $\Delta(F' = 3, F' = 4)$ means the splitting between the $F' = 3$ and $F' = 4$ levels in the $5^2P_{3/2}$ term. Using the minus-first-order output beam of the AOM for the saturated-absorption setup and locking the laser to the $5^2S_{1/2}(F = 3) \rightarrow 5^2P_{3/2}(F' = 3)$ transition in the saturated-absorption spectrum provides trapping light at a detuning Δ_t. In ^{87}Rb the AOM frequency is

$\nu_{\mathrm{AOM}} = \Delta(F' = 2, F' = 3)/2 - \Delta_t = 128.7$ MHz. The trap laser was therefore locked to the saturated-absorption crossover between the $5^2S_{1/2}(F = 2) \rightarrow 5^2P_{3/2}(F' = 2)$ and $5^2S_{1/2}(F = 2) \rightarrow 5^2P_{3/2}(F' = 3)$ transitions. Locking the laser to these non-trapping transitions in this way makes up for the shift in the light passing through the AOM. This method provided us with more precise control over the trap laser detuning, as well as with a more stable lock.

5.2 Landau-Zener excitations

As laid out in Sec. 1.1, the Gallagher-Pritchard model[11] treats ultra-cold collisions as a sequence consisting of a quasi-static resonant excitation to an excited-state potential, followed by motion on the excited-state potential and energy transfer at smaller separations, which leads to trap loss. More recent models abandon the quasi-static excitation in this model and substitute a Landau-Zener excitation treatment.[17,18,37,38]

It is convenient to use a dressed state approach to treat the excitation process. In this picture, the relevant eigenstates are the ground ("g") state is $|\mathrm{g};N\rangle$ and the excited ("e") state is $|\mathrm{e};N-1\rangle$, where N denotes the number of photons in the field. Since the energy of the photon that is to be absorbed is included in the ground state, for blue detunings it lies above the excited-state asymptote (see Fig. 5.2). Ground-state and exited-state potential curves intersect at the resonant internuclear separation $R = (C_3/h\Delta)^{1/3}$. The Landau-Zener transition probability[33] for the adiabatic transition is

$$P = 1 - \exp\left(-\frac{8\pi\varepsilon C_3^{1/3}}{3v_r(h\Delta)^{4/3}}\right), \tag{5.2.1}$$

where ε is the Rabi frequency, and $v_r = v\sqrt{1 - b^2/R^2}$ the radial velocity component of the relative motion of the two atoms, if their collision has an impact parameter b.

Fig. 5.2 illustrates the excitation process. In the ground state ($|\mathrm{g};N\rangle$) atoms have only small thermal kinetic energies. When atom pairs are excited to a repulsive potential curve as they are passing through the resonant internuclear separation, they are quickly turned around by the strong repulsive interaction. Thus they pass through the resonant internuclear separation a second time, remaining on the excited-state potential with a probability $1 - P$. Only then does

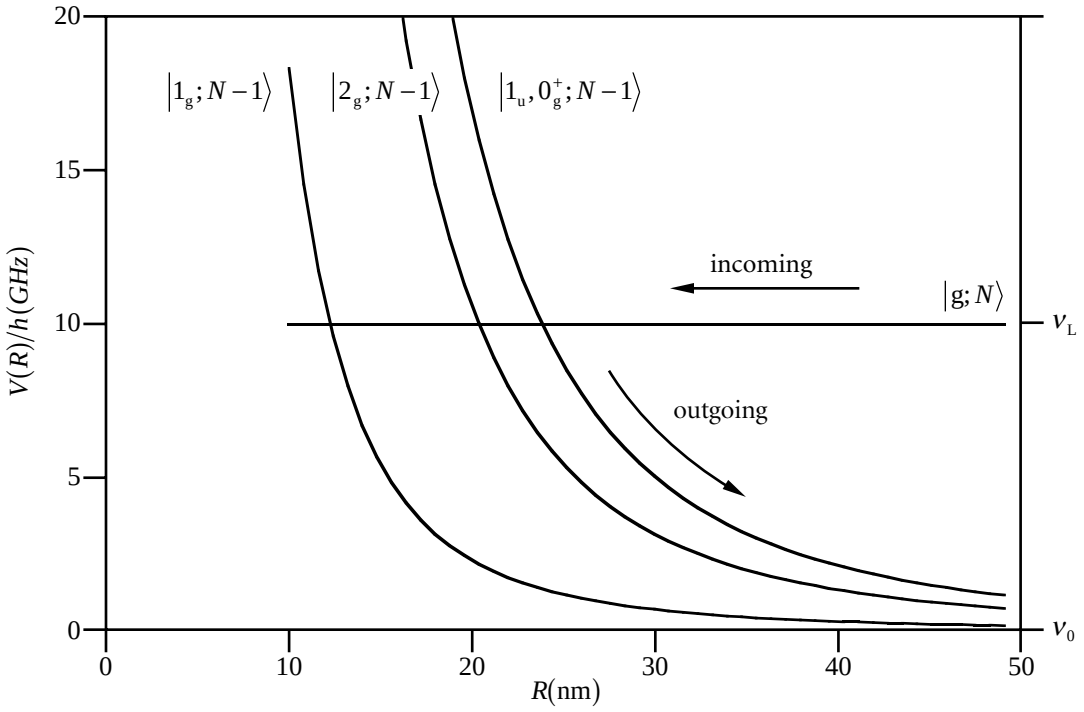

Figure 5.2: Repulsive potential curves in the dressed-state picture. An atom pair approaches each other in the ground state $|g;N\rangle$. Where the ground state curve intersects the excited-state potentials, a transition may take place, which results in a quick turn-around and in the pick-up of kinetic energy corresponding to $\nu_L - \nu_0$, as the atoms repel each other.

trap loss occur. In that case, the probability of trap loss is $P(1-P)$. If they are not excited in the first place (probability $1-P$), there is a second opportunity of being excited with a probability P after being reflected off the centrifugal barrier. The total probability P_t of trap loss occurring in one approach is thus

$$P_t = 2P(1-P). \tag{5.2.2}$$

This theory can be tested most directly by measuring the intensity dependence of the excited-state collisions. As the intensity varies between 0 and ∞, P goes from 1 to 0. As P depends monotonically on the intensity, that is, on ε, the intensity dependence should have a peak corresponding to $P = ½$.

5.3 Intensity dependence

We measured repulsive trap loss as a function of intensity (Fig. 5.3).[8] The detuning of the

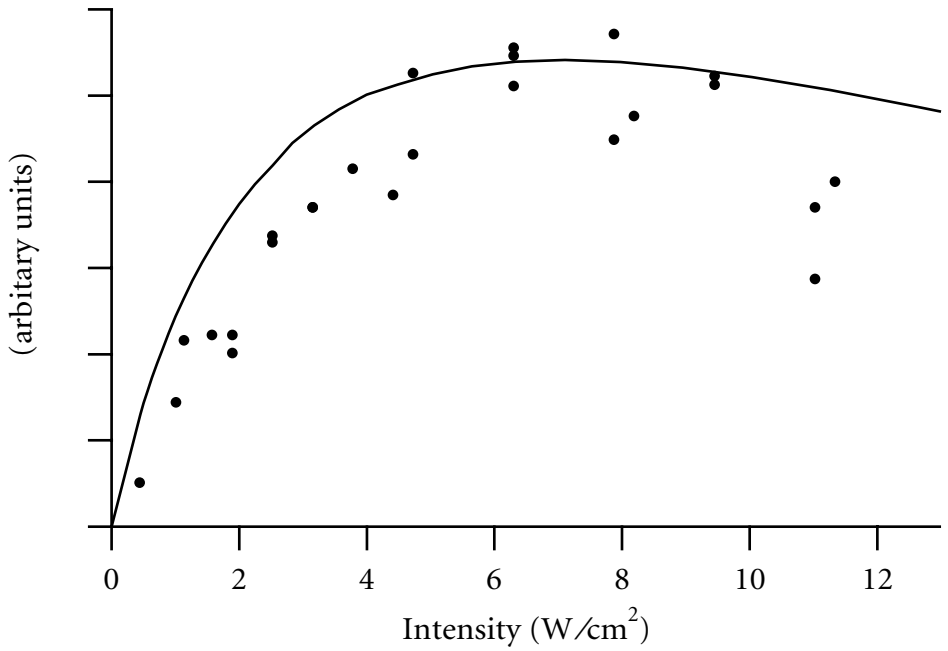

Figure 5.3: Intensity dependence of repulsive ultra-cold collisions. The maximum in the intensity dependence of the loss rate β is a consequence of the Landau-Zener excitation mechanism. The catalysis laser was detuned 10 GHz to the blue of the $5^2S_{1/2}(F = 3) \rightarrow 5^2P_{3/2}$ transition.

catalysis laser was held fixed at 10 GHz from the rubidium $5^2S_{1/2} \rightarrow 5^2P_{3/2}$ transition. The catalysis laser was chopped with a chopper wheel as described above (see Sec. 5.1), at a duty cycle d. The duty cycle was varied to make up for any change in loss rate in order to maintain a constant number of atoms $N = L/(\Gamma_t + \langle \beta n \rangle d)$, where L is the loading rate, Γ_t the loss rate due to collisions other than those induced by the catalysis laser, and $\langle \beta n \rangle$ is the spatially averaged collision rated induced by the catalysis laser. Thus $\beta(I) \propto 1/d(I)$, with I being the catalysis laser intensity.

We compared the measurements with a quantitative estimate. This estimate takes a simplified approach to the multitude of excited-state potential curves involved. Including fine structure but neglecting hyperfine structure, since it is small compared to the detuning, there are

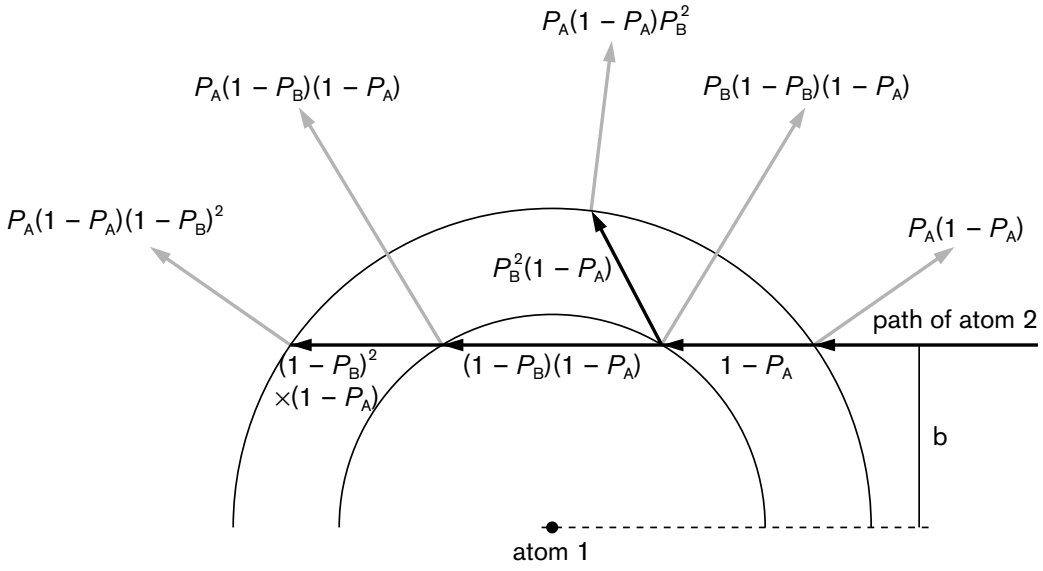

Figure 5.4: Trap-loss pathways for the case of two excited-state potentials, denoted "A" and "B." The partial circles represent interatomic separations where the laser is in resonance with the colliding atoms.Motion on ground-state curves is denoted by dark arrows, motion on excited-state curves by gray arrows. The relevant probabilities for each pathway are also shown.

only four molecular curves [0_g^+ (oscillator strength $f = 0.083$), 1_u (0.198), 2_g (0.5), and 1_g (0.365)] that are repulsive and have radiatively allowed dipole transitions to the ground state.[39] At the detunings used in this experiment the 0_g^+ and 1_u states are strongly mixed by the hyperfine interaction, so for simplicity we consider them as a single state with total oscillator strength equal to the sum of the individual oscillator strengths. We then have a model with the three excited-state potential curves shown in Fig. 5.2.

In the presence of multiple excited-state potentials there are a variety of collision pathways. To picture this, Fig. 5.4 uses an example of two excited-state potential curves. With a given detuning an atom 2 in the presence of atom 1 is resonant with the catalysis laser on two spherical surfaces, represented by the semicircles in the figure, centered on atom 1. The solid black lines show motion of atom 2 on the ground-state potential. The gray ones show repulsion on an excited-state potential. The expressions show the probability of each branch, calculated according to Eq. (5.2.2). In these, P_A is the probability of transfer to the outer potential curve,

and P_B is the probability of transfer to the inner potential curve. Summing all the possible branches we get the total trap-loss probability

$$P = \{P_{\mathrm{A}}[P_B^2 + (1 - P_B)] + 2P_B(1 - P_B)\}(1 - P_{\mathrm{A}}). \tag{5.3.1}$$

We see, since each branch's trap-loss probability contains a factor $1 - P_{\mathrm{A}}$, that the intensity dependence has to turn over and eventually reach zero as P_{A} increases.

Our estimate took into account the three excited-state potential curves mentioned above and was based on an integration over velocities v, as well as impact parameters b. The result is a curve with the overall scale as its only free parameter, which was adjusted to fit the data. It reproduces the data's peak at an intensity between 6 and 8 $\mathrm{W/cm^2}$.

As a further test, we have measured (Fig. 5.5) the positions $I_{\mathrm{m}}(\Delta)$ of the intensity maxima of curves like in Fig. 5.3 for various detunings. From Eq. (5.2.1), the detuning dependence should obey $I_{\mathrm{m}} \propto \Delta^{4/3}$, and the data is consistent with this prediction.

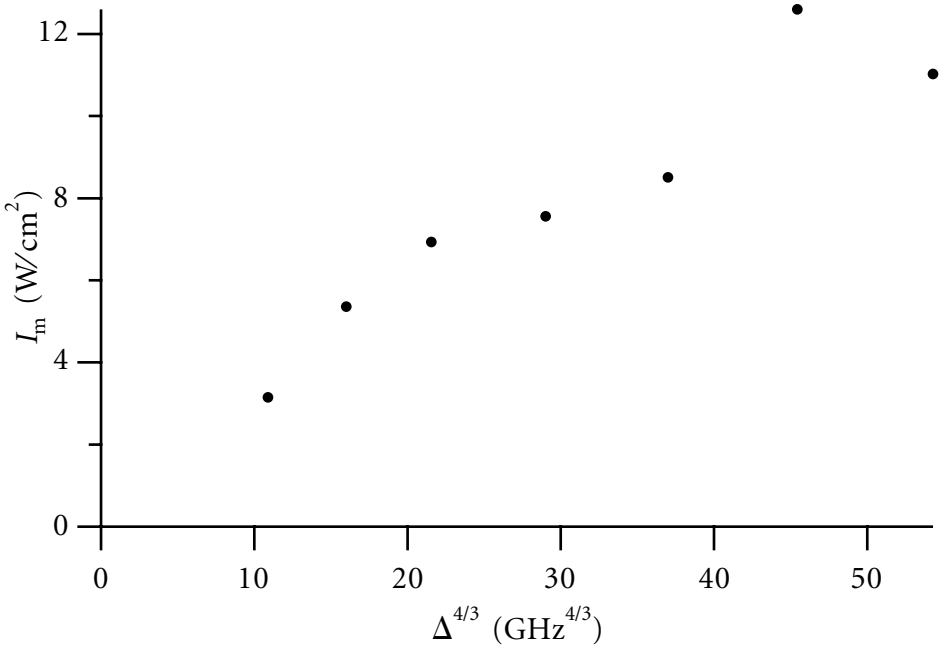

Figure 5.5: The detuning dependence of the maxima I_{m} of curves such as in Fig. 5.3 is linear in $\Delta^{4/3}$. This is the dependence expected from the Landau-Zener model.

5.4 Detuning dependence

The detuning dependence of repulsive excited-state collisions is expected to look quite similar to that of attractive collisions. In theory, both fall off like Δ^{-2} for larger detunings. There is an important difference, however. In attractive collisions the onset in the trap-loss spectrum is a result of spontaneous emission interrupting the collisions for detunings that are too small. This onset is around 50 MHz to the red of the asymptote. In repulsive collisions the onset is at a couple of tens of gigahertz. Here the process is very different. Spontaneous emission plays no role, because with detunings this large the dipole-dipole interaction is so strong that due to acceleration the duration of a collision is short compared to the exited-state lifetime. Instead, the onset is a result of the lower limit of detunings leading to trap loss imposed by the escape velocity of the trap.

Our measurements of repulsive trap-loss spectra in ^{85}Rb and ^{87}Rb are shown in Fig. 5.6.[9] The ^{85}Rb data exhibits the expected behavior. Above 20 GHz the loss rate falls off like Δ^{-2}. There also is a rapid onset around 15 GHz. From energy conservation we have that the kinetic energy of the atom pair when they are accelerated on the repulsive potential is $\frac{1}{2}h\Delta$ for each atom. If this is below a certain value, which is called the trap depth, the kinetic energy of the atoms is insufficient for leaving the trap. The trap depth is determined by the detuning of the trap laser, by the geometry of the trap laser beams,[25] as well as, weakly, by the magnitude of the magnetic field gradient. This escape velocity v_e is related to the trap depth by $\Delta_T = (1/2)mv_e^2/h$. While this evokes the image of a potential well, we have to be aware that the force field of a MOT is not conservative. Given that the excess energy of the blue-detuned photon from the catalysis laser has to be shared by both atoms, the position of the onset is in agreement with a trap depth Δ_T around 7.5 GHz.

Qualitatively our ^{87}Rb repulsive trap loss spectrum looks very similar. The data was taken with the same trap characteristics. However, we observe that at large detunings the ^{87}Rb data shows a falloff slower than Δ^{-2}. This deviation extends at least to detunings of 150 GHz. We address this problem in the following section.

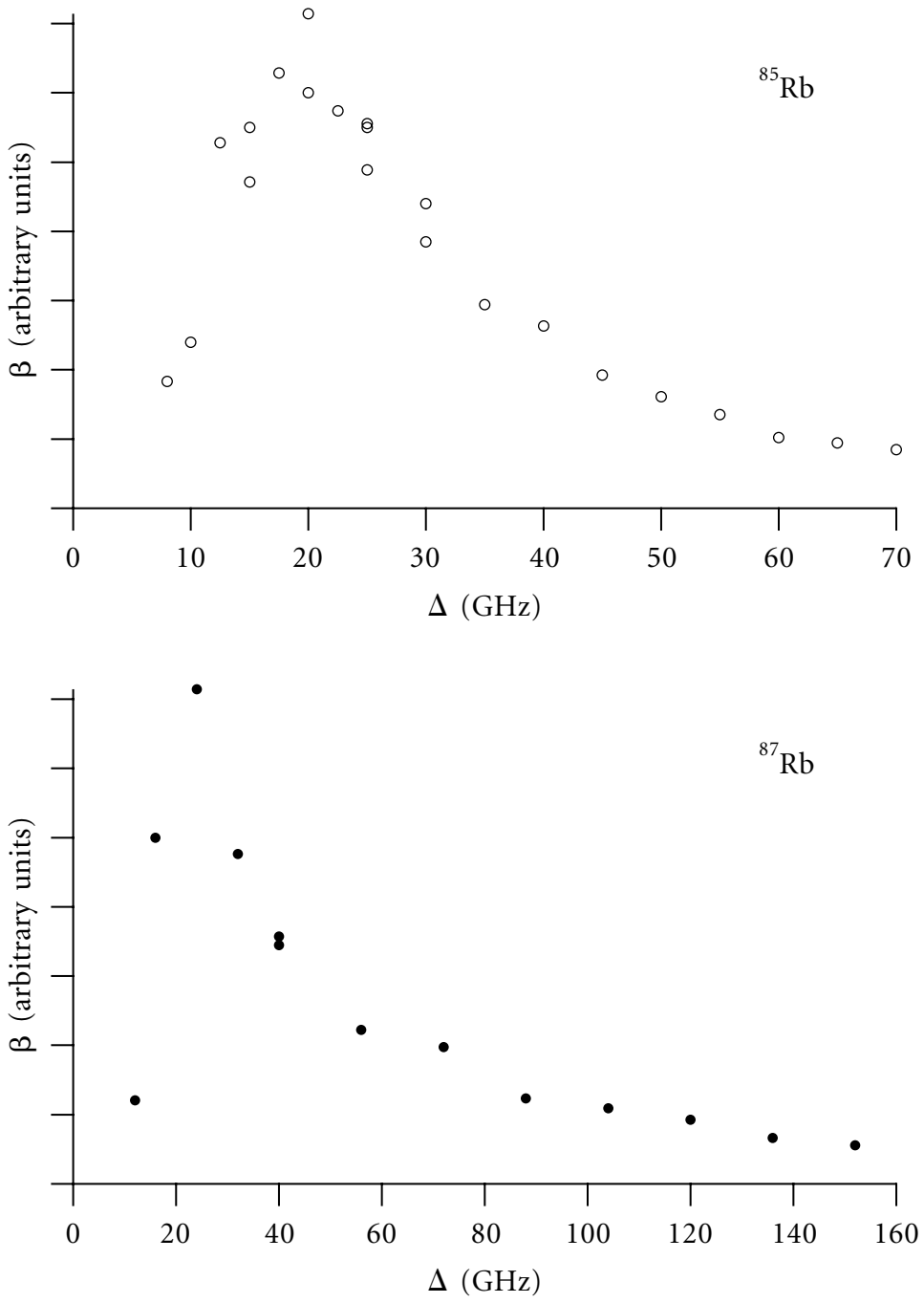

Figure 5.6: Measurements of repulsive trap loss rates β for rubidium MOTs as a function of catalysis-laser detuning Δ from the $5^2S_{1/2}(F = 3) \rightarrow 5^2P_{3/2}$ transition. The trap laser intensity, detuning, and beam diameter were 2.0 $\mathrm{mW/cm^2}$, –5 MHz, and 6.3 mm, respectively.

At any rate, the data shows no features that could be attributed to complications arising from the hyperfine structure of the repulsive excited-state potential curves. Therefore these types of collisions should be amenable to a comparison with theory.

5.5 Trap depth measurements using repulsive collisions

The trap depth has hitherto been an unaccessible parameter. The interpretation of several types of collision experiments can be improved by an accurate knowledge of this parameter. Weak cesium and rubidium have trap depths comparable to the ground-state hyperfine splitting, such that ground-state hyperfine-changing collisions can lead to trap loss.[32,15] Ritchie *et al.*[40] relied on a theoretical model for the trap depth of their study of radiative escape in lithium. A more reliable comparison between experiment and theory might have been facilitated by a direct knowledge of the trap depth. The trap depth is also related to the capture velocity in a background-vapor loaded trap.[15]

Dividing the data by the theoretical Δ^{-2} -detuning dependence arising from the R^{-3} -dependence of the excited-state potential curves, suggests a further interesting interpretation of the data. Fig. 5.7 shows $\beta\Delta^2$ for two different trap configurations with different trap laser intensities and detunings in ^{85}Rb.[9] More or less the data has the shape of a step function. We interpret this to be proportional to the escape probability of a trapped atom with kinetic energy E given by

$$P(E) = P(h\Delta/2) \propto \Delta^2\beta(\Delta) \,. \tag{5.5.1}$$

The limit $\Delta \to \infty$ gives the normalization, such that

$$\lim_{\Delta \to \infty} P(E) = 1 \,. \tag{5.5.2}$$

The fact that the data is not a step function is accounted for by a consideration of the trapping beam geometry. Because the MOT force field is not spherically symmetric, different directions have different escape velocities. This leads to a blurring of the transition from $P(E) = 0$ to $P(E) = 1$.

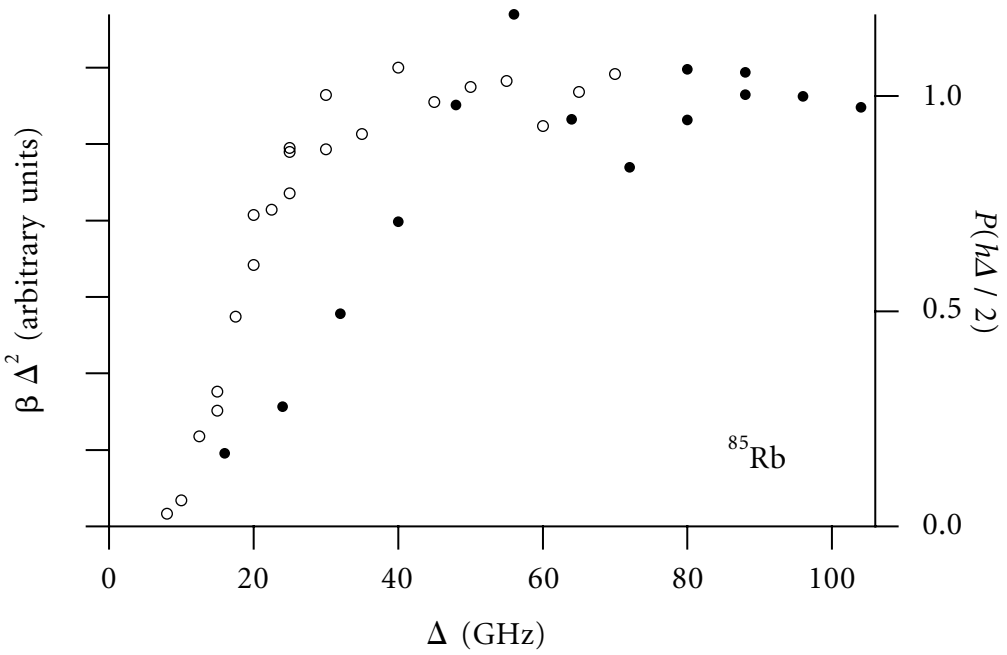

Figure 5.7: Measurement of $\beta\Delta^2$, which is proportional to the escape probability $P(h\Delta/2)$, as a function of Δ for ^{85}Rb MOTs. White circles: trap detuning and intensity of –5 MHz and 2.0 mW/cm²; black circles: –9.4 MHz and 3.2 mW/cm².

Also, in this picture the influence of different trap parameters, such as detuning and trap laser intensity is much more apparent. From this data it can be clearly seen that the escape probabilities at a given detuning decrease for deeper traps. Studies of several different sets of trap parameter show that deeper traps also have greater anisotropies.

With ^{87}Rb the situation is somewhat different. The falloff does not consistently have a Δ^{-2}-dependence. At detunings larger than 30 GHz the loss rate falls off like Δ^{-1}, instead. The reason for this may be that the larger ground-state hyperfine interaction may interfere with the dynamics of the excitation process. It is also possible that the oscillator strengths are affected in a detuning-dependent manner. Any such difference in the behavior of the two rubidium isotopes does not, however, show up in an intensity dependence such as in Fig. 5.3, where the maxima lie at very nearly the same intensities as for ^{85}Rb.

Thus a plot of $\beta\Delta^2$ is not meaningful for ^{87}Rb. Nevertheless, assuming a decay of the trap loss rate as $\Delta^{-1.3}$, we find consistency when plotting $P_{^{87}\mathrm{Rb}}(h\Delta/2) = \beta_{^{87}\mathrm{Rb}}\Delta^{1.3}$ and

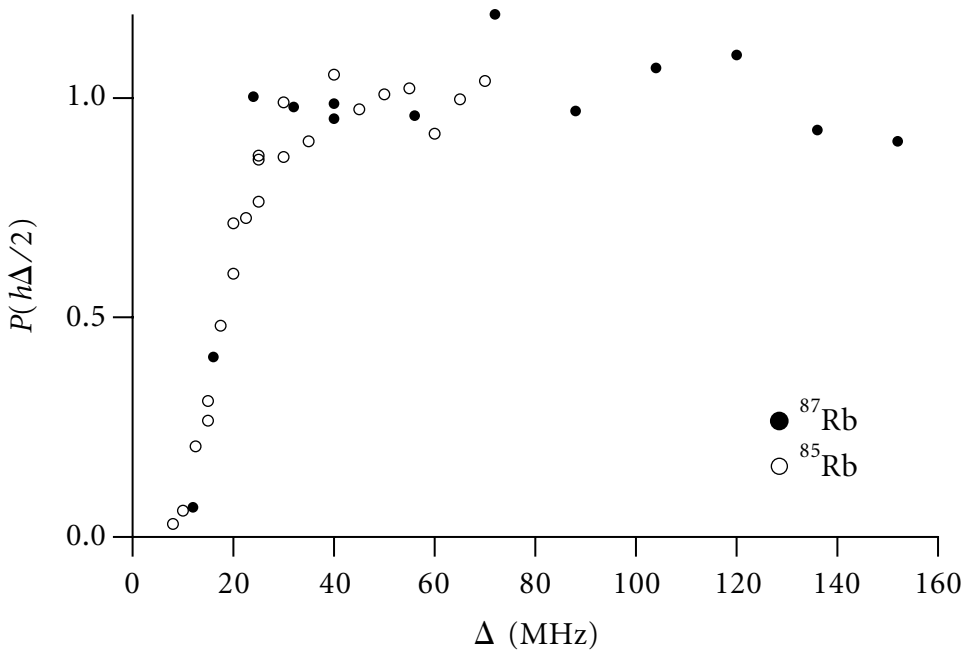

Figure 5.8: Escape probability as a function of Δ for rubidium MOTs. Trap parameters are a trap laser detuning of –5 MHz and an intensity of 2.0 mW/cm².

$P_{^{85}\mathrm{Rb}}(h\Delta/2) = \beta_{^{85}\mathrm{Rb}}\Delta^2$ on one graph (Fig. 5.8). As expected, $P_{^{87}\mathrm{Rb}}(h\Delta/2) = P_{^{85}\mathrm{Rb}}(h\Delta/2)$, with identical conditions for both traps of a trap laser detuning –5 MHz and an intensity of 2.0 mW/cm².[9]

In spite of this problem with ^{87}Rb, the trap depth can be deduced from repulsive trap-loss spectra. Should other atomic species exhibit deviations from the Δ^{-2}-falloff, as well, the data can be meaningful, if a power law for this falloff can be determined from the data. However, to this date no one has reported such measurements.

6 Two-photon collisions

The experiments that are the subject of this chapter build on the experience gained from those of both previous chapters. A two-step excitation of the colliding atoms involves the same $P_{1/2}$ states as in Ch. 4, and the models for describing the collision process use the Landau-Zener approach of Ch. 5 for the excitation mechanism. The collisions are detected by observing fluorescence from the colliding atoms. The data shows interesting new features that are not yet well understood. However, a further understanding of the results has to involve a detailed look at the hyperfine potential curves in the way prepared in Ch. 4.

Using two catalysis lasers to manipulate the colliding atoms gives us increased control over the collision process. One laser, red-detuned from the atomic resonance, excites the atom pair to an attractive potential curve in a manner similar to the other experiments in this dissertation. As before, the atoms are attracted toward each other. A second, blue-detuned laser terminates this attractive motion by exciting the atom pair to a doubly-excited potential curve (cf. Fig. 6.1). The blue-detuned excitation takes place at an intermediate interatomic separation where the atoms are still separated by a few tens of nanometers. If spontaneous emission in the near-infrared occurs after the second excitation, it may terminate the collision much like spontaneous emission in singly-excited collisions does, if the catalysis laser detuning is small. Because of side-effects like optical pumping and disturbance of the atoms' density distribution, the influence of those detunings is very difficult to observe quantitatively (Ch. 4). With these two-photon collisions, however, both catalysis lasers are tuned far enough from the atomic resonances so that none of the mentioned difficulties arise and spontaneous emission effects are still observable.

In addition, we observe these collisions directly,[10] instead of relying on trap loss, by detection of a violet photon that may be emitted by the atoms when they reach the chemical binding region ($R < 5$ Å) of the doubly-excited state potential curves. In the $R < 5$ Å region the overlap of the electron clouds breaks down the atomic dipole selection rules and allows the atoms to radiate directly to the molecular ground state. Because the photon is of a very different color compared to the laser photons we can separate out two-photon events from the other light

emitted by the atoms, most of which is near the frequency of the trap laser and the two catalysis lasers.

Others have done analogous experiments, involving two-step excitation. These experiments observe the collisions between ultracold sodium atoms by detecting the ions into which the Na_2 molecule can decay through autoionization.[35,41] Analogous processes are energetically forbidden for rubidium. This experiment constitutes an improvement in that it to a greater extent decouples the catalysis of collisions from trapping, by making both the initial, as well as the second excitation independent of the trap laser. It is also the first experiment that directly observes fluorescence generated during a collision.

6.1 Dynamics

It is the purpose of this experiment to explore the dynamics of the colliding atoms in such a way that all aspects of it — excitation, motion and termination of the collision by spontaneous emission — should be well represented by relatively simple collisional models. . The experiment involving excitations to the $5^2P_{1/2}$ term (see Sec. 4.2) already addressed the difficulty arising from excitation at small detunings to a regime where the atoms had to traverse a multitude of curve crossings and avoided curve crossings.[7,19] Our experiment with repulsive excited-state potential curves (see Ch. 5) also kept the colliding atoms from getting close enough to each other, where a treatment of the dynamics requires the knowledge of the interaction near zero-separation with a precision hard to obtain.[12] Neither experiment shows any effects of spontaneous emission interrupting the collision before it causes trap loss. The $P_{1/2}$ experiment does not, because it requires catalysis laser detunings so small that they exert a force on all trapped atoms. The repulsive trap loss experiment, on the other hand, does not, because the duration of the collisions is too short.

The two-photon experiment gets around these difficulties by exciting the atoms to an attractive potential in a regime charted by the $P_{1/2}$ experiment described in Sec. 4.2.[7] The detuning of the a catalysis laser (90 MHz to the red of the $5^2S_{1/2}(F = 3) \rightarrow 5^2P_{1/2}(F' = 2)$ transition) is chosen such that the lowest-lying attractive potential curves of the $5^2S_{1/2}(F = 3) + 5^2P_{1/2}$ manifold (see Fig. 6.1) are excited (step 1). These curves are all fully attractive over a range of a

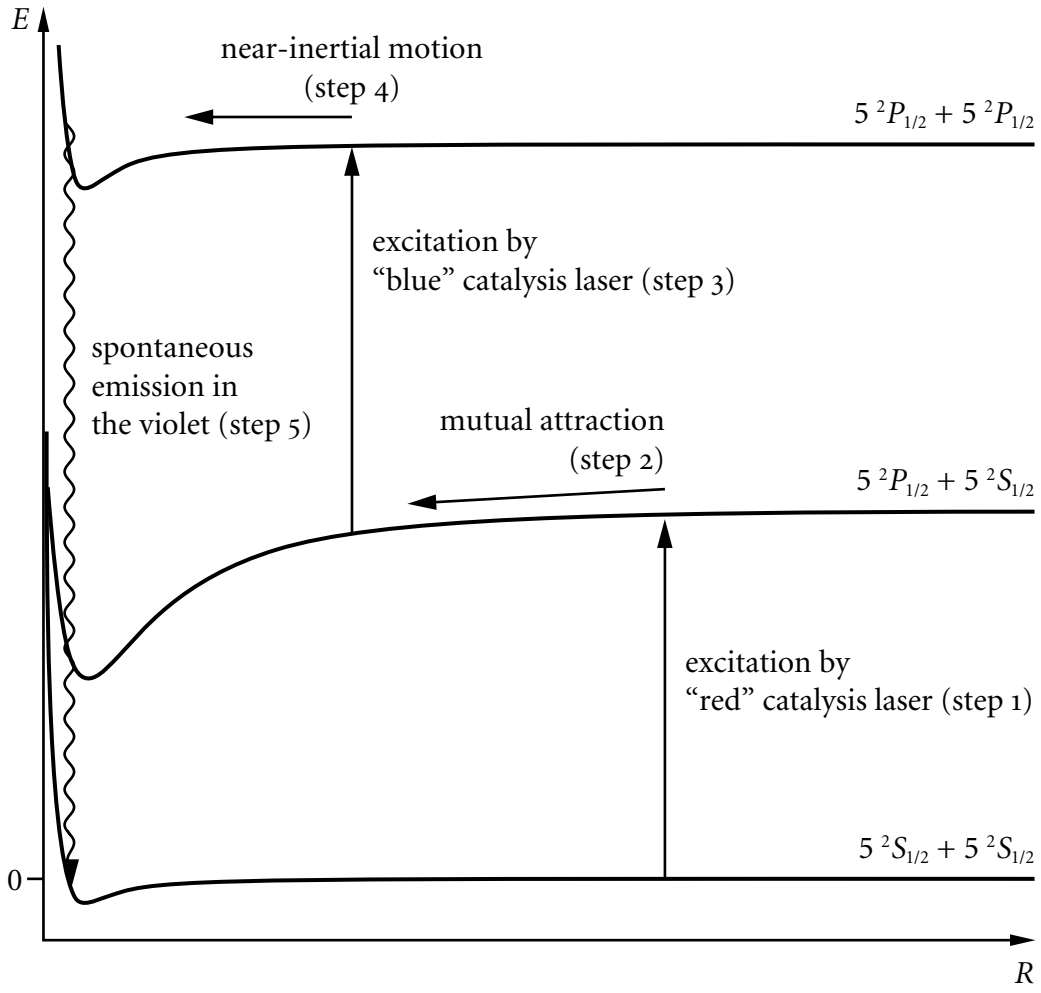

Figure 6.1: Sequence of a two-photon collision.

couple of gigahertz. Classical motion of the atoms toward each other under the influence of the dipole-dipole interaction follows (step 2). At a smaller separation, depending on the amount of blue detuning of a second catalysis laser, the atoms are excited to the $5^2P_{1/2} + 5^2P_{1/2}$ doubly-excited potential curve (step 3). After this second excitation they continue to approach each other (step 4) with the momentum gained in step 2. No appreciable acceleration occurs, because the dipole-dipole interaction is weak ($\propto R^{-5}$) compared to that on the singly-excited potential. As the atoms get so close that their electronic wavefunctions overlap, they may emit a single photon in the violet to the $5^2S_{1/2} + 5^2S_{1/2}$ state (step 5). In the

ground state the collision event ends as atoms then recede from each other, or chemically bind in $^1\Sigma$ or $^3\Sigma$ states.

As an alternative step 5, there is a possibility of energy pooling to the $6^2P + 5^2S_{1/2}$ state playing a role. Subsequent spontaneous emission at 422 nm ($6^2P_{1/2}$) or 420 nm ($6^2P_{3/2}$) would also be detected in this experiment. In order to distinguish this process the violet photons would have to be analyzed spectrally.

In these two-photon collisions spontaneous emission may occur during step 2 or 4. It would show up as an onset in the data showing the violet photon rate as a function of the detuning of the second catalysis laser (see Sec. 6.3). If the blue detuning for the second excitation is too small, the atoms have not been accelerated enough to be able to come close to each other within one molecular lifetime or so. As long as the atoms are still physically separated, spontaneous emission of two separate near-infrared photons is the only decay channel.

Taking into account the Landau-Zener model (see Eq. (5.2.1)), increasing the blue detuning reduces the probability of excitation by the second catalysis laser, because of the increased velocity of the atoms as they move through resonance. Therefore the detuning dependence should have a decay at larger detunings.

6.2 Apparatus

Setting up this experiment involved a number of fundamental changes from previous arrangements (see Ch. 2 and Sec. 5.1). The setup is shown in Fig. 6.2.

Hyperfine pumping is now achieved by directly modulating the current of the laser diode in the trap laser at microwave frequencies[42,43] to create sidebands in the output spectrum of the trap laser at the hyperfine pumping frequency.

We tune a voltage controlled oscillator (VCO) to 2.915 GHz $-\,\Delta$, where Δ is the detuning of the trap laser from the $5^2S_{1/2}(F = 3) \rightarrow 5^2P_{3/2}(F' = 4)$ trapping transition of ^{85}Rb. The signal is amplified by an RF amplifier to the 20 dBm level and capacitatively coupled to the laser diode's anode. Thus the low sideband created in the diode laser spectrum is resonant with the $5^2S_{1/2}(F = 2) \rightarrow 5^2P_{3/2}(F' = 3)$ transition and removes atoms from the $5^2S_{1/2}(F = 2)$ state,

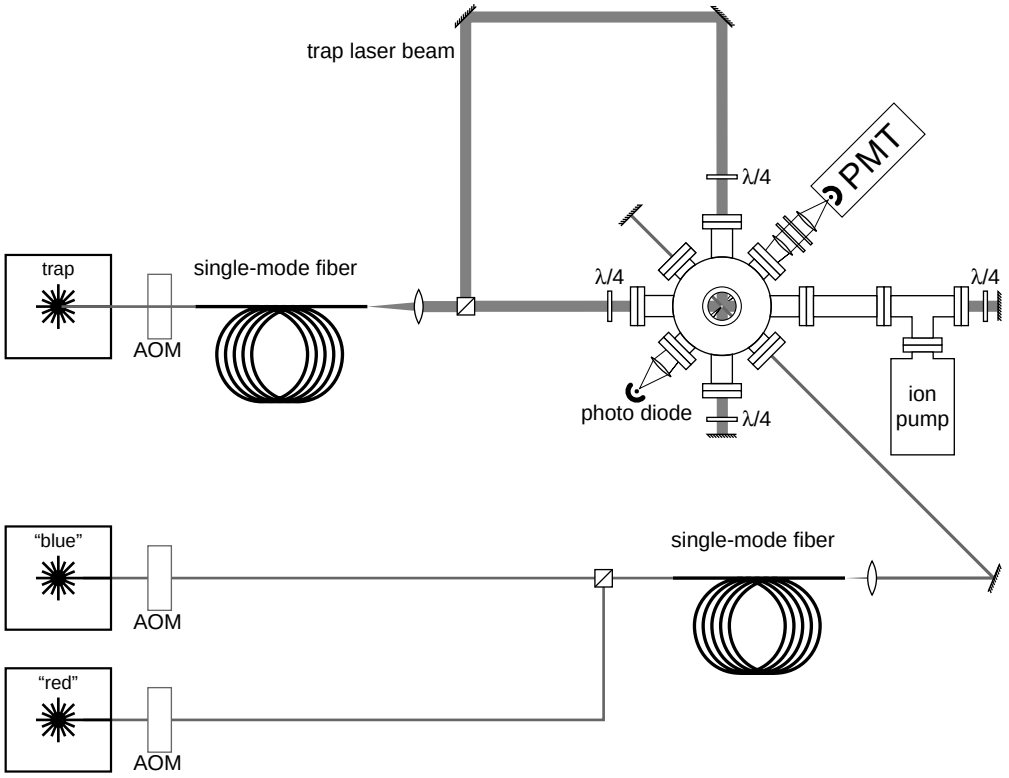

Figure 6.2: Apparatus for two-photon collisions. The trap laser light is conveyed by a single-mode fiber into a UHV chamber to form a MOT. To ensure perfect overlap, the "blue" and "red" catalysis lasers are combined in a single-mode whose output is sent through a set of viewports to overlap with the trapped atoms. The output from all three lasers is switched on and off by AOMs to allow control of the timing sequence (Fig. 6.4).

which is dark to the trap laser. The other sideband is detuned by the same amount to the blue of the trapping transition and has no effect on the operation of the trap. Each of the sidebands carry between 1½ and 2% of the total power of the laser's output. The coupling efficiency of the microwaves into the laser diode appears to strongly depend on the stability of the lasing mode. Near a mode hop the sidebands were up to three times as strong as elsewhere in the mode. Since small fluctuations in the diode laser's operating temperature affect the operating position within the mode this can lead to large changes in the number of atoms the MOT is able

to trap. To make up of the mode drifts we can adjust the operating current of the laser to ensure maximum hyperfine pumping.

The detuning of the trap laser was chosen to be $\Delta = 2\Gamma = 11.8$ MHz. The reason for this detuning being somewhat larger than in our earlier experiments is that it reduces radiation trapping and thereby permits higher trap densities. This in turn leads to a higher rate of excitation to the excited-state potential curve, which improves the violet-photon rate.

We upgraded the laser diode used in the trap laser to a Spectra Diode Labs SDL-5411-G1, nominally rated at 100 mW output power. This was necessary as the acousto-optic modulator used to switch the trapping light on and off at megahertz rates (see below), has relatively poor transmission efficiency (60%). Combined with the low transmission efficiency (50%) of the single-mode optical fiber in the trapping optics and the low output coupling of the feedback grating inside the laser itself, this still produces no more than 10 mW of light available for trapping.

The single-mode fiber was used to decouple the trapping optics from the laser optics. This allows changes made to the alignment of the feedback grating to leave the alignment of the trapping optics past the output of the fiber unaffected. Occasionally such grating adjustments are necessary to keep the laser operating at the trapping frequency when some of the operating parameters, especially the temperature, has drifted over the space of a few days.

In this experiment two catalysis lasers excite the colliding atoms. One, which we call the "red" laser, is detuned 90 MHz to the red of $5^2S_{1/2}(F = 3) \rightarrow 5^2P_{1/2}(F' = 2)$ transition. It provides the initial excitation to the attractive potential curve. After acceleration toward each other, the "blue" laser, detuned between 90 MHz and 2.4 GHz to the blue of the $5^2S_{1/2}(F = 3) \rightarrow 5^2P_{1/2}(F' = 3)$ transition may pick up the atoms and excite them to the doubly-excited potential curve.

One weakness of the experiment involving doubly-excited collisions of sodium by Bagnato *et al.*[35] is that the initial excitation is provided by the trap laser, so that the atoms have to traverse multiple avoided curve crossings before they get to interatomic separations, where they can be excited to a doubly-excited potential curve. Furthermore, more than two frequencies are

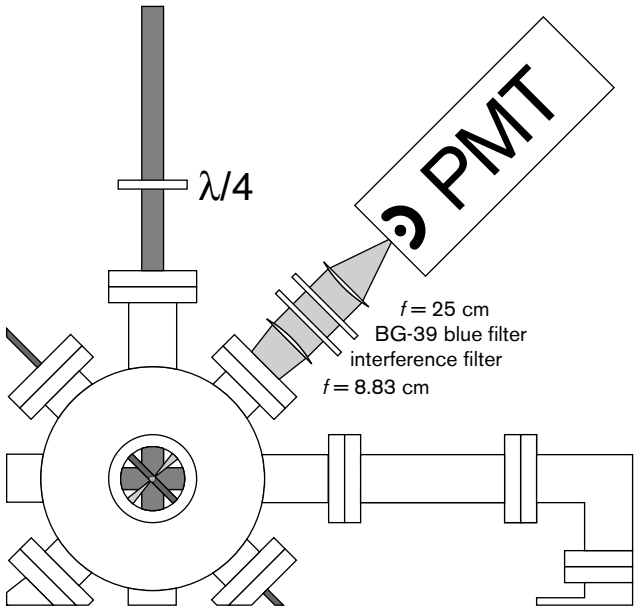

Figure 6.3: Violet photon collection and detection optics.

present and can influence the collisions. This makes the data more difficult to interpret, as multiple two-step excitation processes are possible concurrently.

We avoid this complication by alternating trapping and catalysis by the "red" and "blue" lasers (see Fig. 6.4 for timing). To this end, the beams from the three lasers are passed through separate acousto-optical modulators (AOM) before they reach the atoms in the vacuum chamber. On top of that, the switching has to occur at a rate of at least about 10 kHz, so that the "red" catalysis laser does not have enough time to pump the atoms into the dark $F = 3$ state. We use the first-order diffracted beams on the output side of the AOMs, because they have a high extinction ratio when the AOM is off, as opposed to the zeroth-order beams. Because the frequency of the 1st order beams is shifted by the AOM frequency, we have to lock the trap and "red" catalysis lasers to saturated-absorption features appropriately offset in the opposite direction. The "blue" catalysis laser is left free running. Its detuning is measured with a confocal optical spectrum analyzer with a free spectral range of 1.5 GHz. Light from the "red" catalysis laser is fed into the spectrum analyzer, as well, and provides an absolute frequency reference.

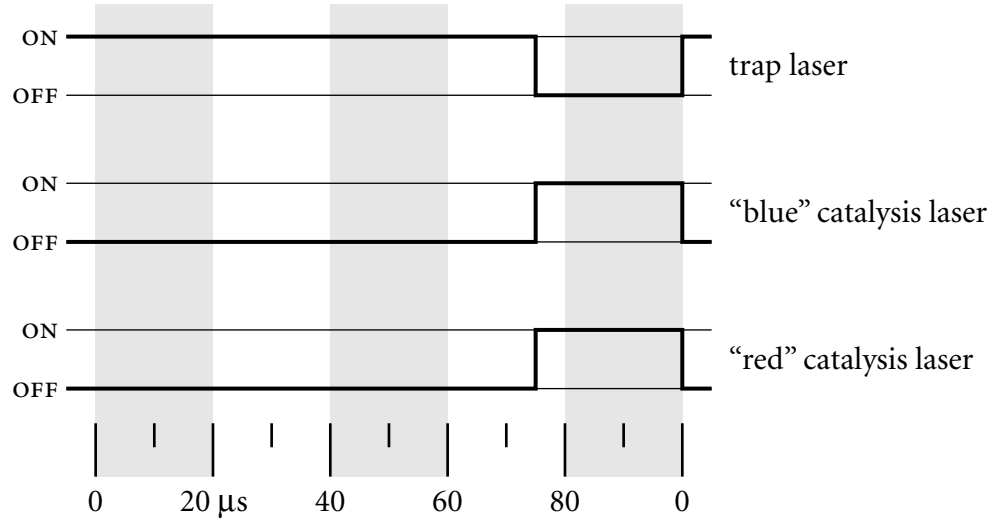

Figure 6.4: Timing of trap laser, “blue” and “red” catalysis lasers. Shown is one period of 100 µs duration. The trap laser is turned off, when the “blue” and “red” catalysis lasers are turned on to induce two-photon collisions. This prohibits any involvement of the trap laser in the collision process. The optimal trap laser duty cycle is 75%.

The beams of both catalysis lasers are combined in a polarizing beam splitter, where $\lambda/2$ plates allow us to adjust the intensity of each beam. To ensure perfect overlap as the catalysis light overlaps the trap atoms they are run through a single-mode fiber. As a result, at the fiber output both beams have the same geometrical properties. A microscope objective reduces the divergence of the light and before entering the vacuum chamber through one of the off-axis viewports sends it to a lens that produces a 1 mm waist at the position of the atom trap. After passing through the trap and the vacuum chamber the light passes through a second lens that brings the light to a waist on in the plane of a mirror. There the catalysis light has a plane wavefront, such that the mirror folds the beam geometry back on itself. Optimal retroreflection of the catalysis light is checked by maximizing the throughput through the fiber of the retroreflected light. The maximum single-pass peak intensity of the “red” catalysis light is 30 $\mathrm{mW/cm^2}$, and 220 $\mathrm{mW/cm^2}$ for the “blue” light.

The viewport on the vacuum chamber through which we observe the violet photons is uncoated. The coatings we have on the other viewports have very poor transmission in the blue to violet range. The light from the viewport is roughly collimated by a 8.83 cm plano-

convex lens passed through an interference filter, whose reflective side faces the trapped atoms, through one 1 mm and another 2 mm thick blue-glass filter (Schott BG-39) and is focused on the active region of the PMT by a 25 cm plano-convex lens (see Fig. 6.3). The interference filter has a 55% transmission centered at 405 nm and a 40 nm bandwidth. Together with the BG-39 filters it provides a 10^{-12} rejection of near infrared photons at 780 nm over violet ones.

The violet photons generated in the collisions are detected by a photo-multiplier tube (PMT) that has a quantum efficiency of roughly 10%. The electronic pulses from the PMT are passed through a discriminator and a series of two amplifiers. The signal is in ECL logic levels and we convert it to TTL. We then AND the signal with the timing pulses going to the AOMs in order to be able to restrict photon counting to specific phases in the timing diagram (see Fig. 6.4). The TTL counters used can be preset to count for a specific duration. In our experiment this was 10 — 15 min, in order to have reasonable counting statistics.

6.3 Detuning dependence

We measured the detuning dependence of the emission rate of violet photons generated in a two-photon ultra-cold collision.[10] This constitutes the first experiment that directly observes fluorescence from excited-state collisions. Fig. 6.5 shows our measurements. As expected, for small relative detunings the collision rate increases, suggestive of spontaneous emission. At large detunings, however, some unexpected behavior occurs.

In developing a qualitative understanding we progress from simple approaches to ones that acquire more complexity as more effects are included. The simplest approach to the problem neglects spontaneous emission from the singly-excited-state potential curve. For simplicity, hyperfine interaction is also neglected. Our violet photon detuning dependence was taken with fixed parameters in the initial excitation. This excitation takes place, when a photon from the "red" catalysis laser is absorbed, which has a detuning of 90 MHz to the red of the $5^2S_{1/2}(F = 3) \rightarrow 5^2P_{1/2}(F' = 2)$ transition and an intensity of 30 $\mathrm{mW/cm^2}$. The excitation rate is fixed and only affects the scaling of the detuning dependence. This is justified in that there are other factors that determine the overall scaling of the spectrum that are very hard to

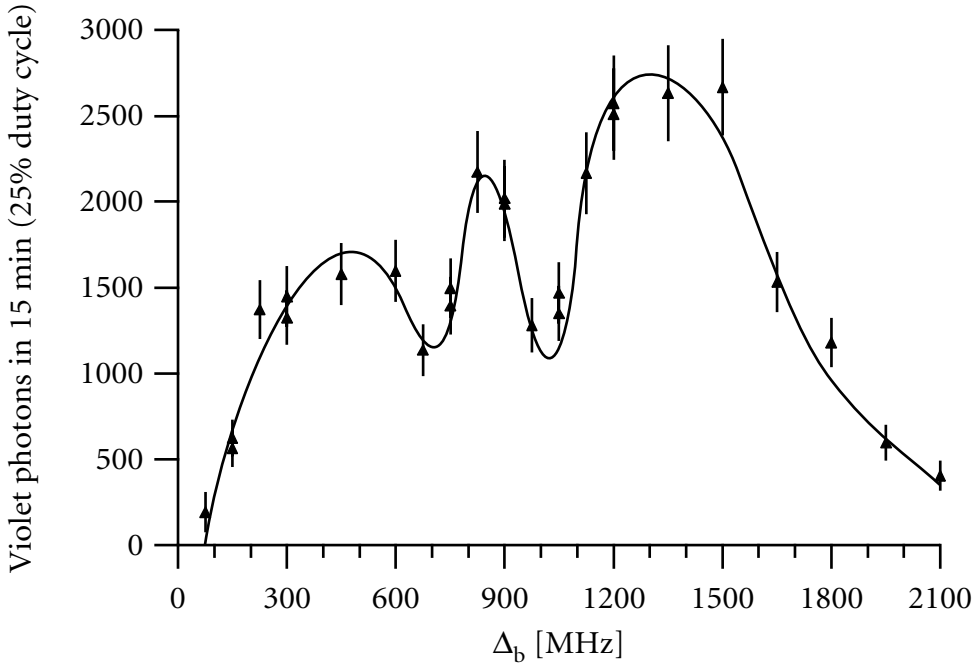

Figure 6.5: Measurement of the emission rate of violet photons as a function of the detuning of the "blue" catalysis laser. The multi-peaked structure cannot be explained with a simple picture of the potential curves involved. The line is drawn to guide the eye.

determine, for example, the violet-photon decay rate. Thus, we concentrate on the spectral shape of the violet photon emission data.

After excitation, attractive motion follows. We treat this classically, as spontaneous emission is negligible. This is shown by our $P_{1/2}$ collision data, where –90 MHz is well to the red of the trap loss spectrums onset, which is the detuning region where spontaneous emission interrupts the collision. Multiple orbits in the excited-state potential are also not important, as suggested by the same $P_{1/2}$ trap loss spectrum. At a detuning of –90 MHz the model calculations for motion with and without orbits shows no difference (see Fig. 4.7).The excitation by the "blue" laser to the doubly-excited state is treated using the Landau-Zener mechanism in the same manner as in Sec. 5.2.

With these assumptions the the violet photon rate is proportional to the excitation rate $\mathfrak{R}$ from the "blue" catalysis laser and the survival rate

$$\exp(-t(\Delta_b)/\tau_M) \tag{6.3.1}$$

on the doubly excited-state potential to $R = 0$ that is given by spontaneous emission:

$$\eta \propto \mathfrak{R}(\Delta_b)\exp(-t(\Delta_b)/\tau_M)\ , \tag{6.3.2}$$

where Δ_b is the detuning of the "blue" catalysis laser and τ_M is the lifetime of the atoms on the doubly-excited potential curve.

In the Landau-Zener model[33] the excitation probability is given by the velocity at which the transition region is traversed, by the relative curvature of lower and upper state, and by the intensity. The Landau-Zener transition probability is (Eq. (5.2.1)):

$$P = 1 - \exp\left(-\frac{8\pi\varepsilon C_3^{1/3}}{3v_r(\hbar\Delta_b)^{4/3}}\right). \tag{6.3.3}$$

Since the violet photon rate in the range of intensities accessible to us ($I_b \leq 220\ \mathrm{mW/cm^2}$) is linear in the intensity of the "blue" catalysis laser, we may assume that the argument of the exponential function is small such that

$$P = \frac{8\pi\varepsilon C_3^{1/3}}{3v_r(\hbar\Delta_b)^{4/3}}\,. \tag{6.3.4}$$

The excitation rate by the "blue" catalysis laser is the product of the arrival rate of atoms on the singly-excited potential, which is given by intensity and detuning of the "red" catalysis laser, and the excitation probability. It is therefore

$$\mathfrak{R} \propto \frac{1}{v_r\Delta_b^{4/3}}\,. \tag{6.3.5}$$

Considering, for simplicity, only radial motion, the relative velocity of the atoms at the point of exciation by the "blue" catalysis laser is determined by conservation of energy. If the thermal energy of the atoms when they are excited by the "red" catalysis laser is negligible, then

$$v = v_r = \sqrt{(2h/\mu)(\Delta_b + \Delta_r)}\,, \tag{6.3.6}$$

where μ is the reduced mass of the atoms and the detunings relate to the singly-excited potential through the relation $h\Delta \equiv V(R) = -C_3/R^3$, as described in Sec. 1.1. The rate of excitation by the "blue" catalysis laser is therefore

$$\Re \propto \frac{1}{\Delta_b^{4/3}\sqrt{(\Delta_b + \Delta_r)}}\,. \tag{6.3.7}$$

The survival rate on the doubly-excited potential depends on the time spent to get from the excitation separation of the atoms to $R = 0$. The doubly-excited potential asymptotically connects to the $5^2P_{1/2} + 5^2P_{1/2}$ state of the infinitely-separated atoms. In that case, the dipole-dipole interaction vanishes, leaving the interaction between the atoms' quadrupole moments as the highest contributing term. This interaction has a R^{-5} dependence, which, for the purpose of this calculation, is considered to be independent of the atoms' separation. The atoms therefore move toward each other with the nearly uniform velocity v. Thus, the time it takes to get to $R = 0$ is

$$t(\Delta_b) = \frac{R(\Delta_b)}{v} = \frac{(C_3/h\Delta_b)^{1/3}}{\sqrt{(2h/\mu)(\Delta_b + \Delta_r)}}\,. \tag{6.3.8}$$

Substituting Eqs. (6.3.7) and (6.3.8) into Eq. (6.3.2) we then get

$$\eta \propto \exp\left[-(1/\tau_M)\frac{(C_3/h\Delta_b)^{1/3}}{\sqrt{(2h/\mu)(\Delta_b + \Delta_r)}}\right]/(\Delta_b^{4/3}\sqrt{(\Delta_b + \Delta_r)})\,, \tag{6.3.9}$$

which is plotted in Fig. 6.6. The width is considerably narrower than what we observed. The calculation contains nothing to accomodate a multipeaked structure like in the data.

When looking at a picture of the potential $P_{1/2}$ curves for ^{85}Rb (Fig. 6.7), a quite different interpretation emerges. As the dipole-dipole interaction of the atoms becomes strong enough,

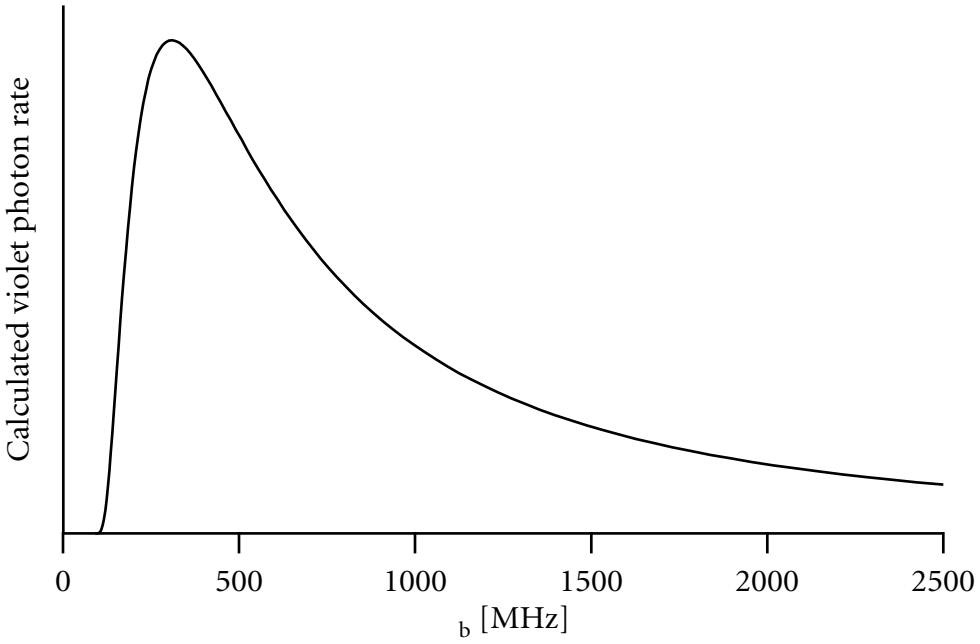

Figure 6.6: Theoretical spectrum of the violet photon emission rate. The onset is at 90 MHz, corresponding to the detuning of the "red" catalysis laser. The fall-off is noticeably sharper than observed in the data (Fig. 6.5). The calculation assumes a molecular lifetime in the $5^2P_{1/2} + 5^2P_{1/2}$ state of $\tau_M = 13$ ns.

it mixes the two ground-state hyperfine levels. The curves emerging from the $(F = 3) + (F' = 2')$ and $3 + 3'$ asymptote are strongly mixing with those of the $2 + 2'$ and $2 + 3'$ asymptotes around half the ground-state hyperfine splitting below the $3 + 2'$ and $3 + 3'$ levels. Furthermore, the potential curves have nearly no dependence on the atoms' separation.

Since only a very small portion of the curves behave like $-C_3/R^3$, the considerations leading to a theoretical violet photon spectrum like in Eq. (6.3.9) have to be modified extensively. We could simplify the description of the collision dynamics by picking a characteristic potential curve going from $3 + 2'$ level to the flat manifold. The excitation rate would then be determined by the density of states to which all the other curves contribute.

Because of the lack of acceleration on most of these potential curves, motion on them toward $R = 0$ can last several hundred nanoseconds. This is enough time for spontaneous emission

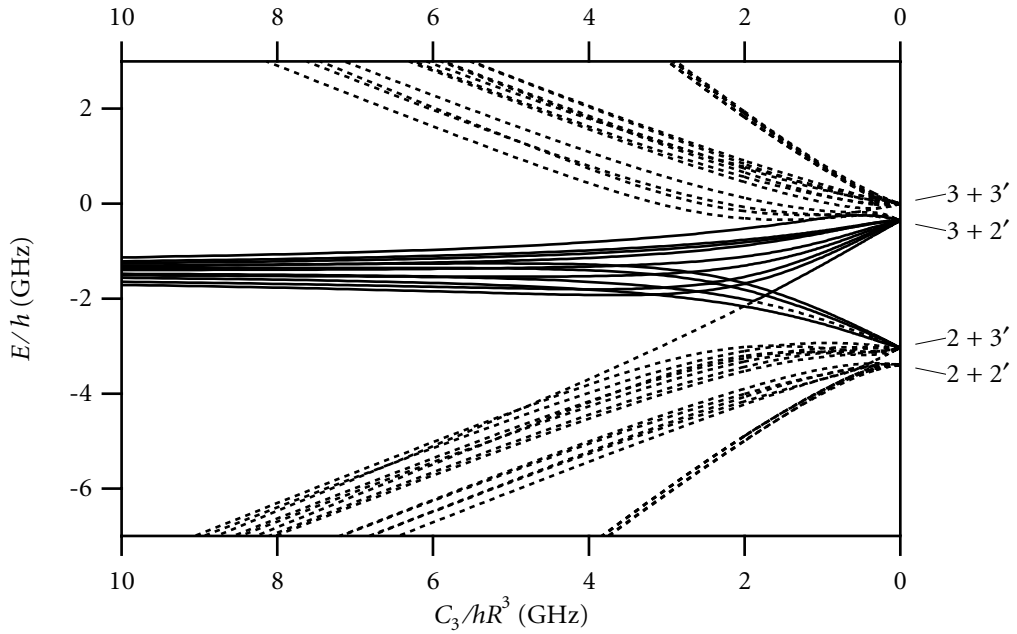

Figure 6.7: Selected potential curves corresponding to the $5^2S_{1/2} + 5^2P_{1/2}$ asymptote in ^{85}Rb. Shown are the 1^g, 2^g and 3^g symmetries. Around –1.5 GHz there are a large number of curves (solid lines) with $dE/dR \approx 0$ that are resonant with the "blue" catalysis laser over a large range of interatomic separations R. This greatly enhances the excitation rate around that detuning.

to significantly limit the interaction time of the "blue" catalysis laser with the colliding atoms. An accurate treatment of spontaneous emission from the singly-excited potential involves numerical integration of the potential curves, as their dependence on the interatomic separation is not simple.

Another question is, how valid the Landau-Zener picture is in this case. The term $\left|(d/dR)(\varepsilon_2 - \varepsilon_1)\right|_{R = R_x}$ in Eq. (4.1.5), which is implicit in Eq. (6.3.3) with the assumption of a $-C_3/R^3$ potential, goes to zero. The excitation probability would therefore automatically go to one, without taking the duration of the atoms' interaction with the "blue" catalysis laser into account. It is likely that a quasistatic approach to this excitation is more appropriate.

In spite of these difficulties a few qualitative observations can be made. The broader onset observed in the data (Fig. 6.5) may very well be explained by the longer duration of the singly-

excited dynamics. Here there is a survival term like in expression (6.3.1) that is responsible for the onset. The main difference is that is the time between the excitations by the "red" and "blue" catalysis lasers. The steepness of the onset is given by the ratio $[t(\Delta_b)/\tau_M]\exp(-t(\Delta_b)/\tau_M)$. Thus, the longer $t(\Delta_b)$ is, the more gradual do we expect the onset of the violet photon rate to be. Further broadening is expected to result from the different dynamics on the different potential curves. As can be seen from Fig. 6.7, some of the potential curves have a minimum near $-C_3/R^3 = 2\ \text{GHz}$, which produces different times $t(\Delta_b)$.

One explanation for the multi-peaked structure in the data is excitation to the multiplet of doubly-excited-state potentials having asymptotic quantum numbers $2' + 2'$, $3' + 2'$ and $3' + 3'$. The potential curves associated with these states are offset from each other by the $P_{1/2}$ hyperfine splitting of 362 MHz. Thus, for each given interatomic separation R, the "blue" catalysis laser will be resonant with an excitation to the doubly-excited potential curve manifold at three detunings, about 360 MHz apart from each other (see Fig. 6.8).

More calculations are needed to account for these effects quantitatively.

The comparison with a violet photon spectrum from collisions starting from $2 + 2'$ excited-state potentials should give further insight into these collisions. This requires that the atoms be optically pumped to the lower ground-state hyperfine state, before catalysis begins. The benefit of this type of collision is that all of the attractive potential curves emerging from that asymptotic state remain so over the entire range of interatomic separations that is of interest. This greatly increases the validity of the simple model. We expect the spectrum to be considerably sharper.

6.4 "Saturation"

Another, as yet unexplained phenomenon is what appears to be saturation of the violet-photon signal that results from the "red" catalysis laser. In testing the dependence on the intensity of the "red" catalysis laser intensity, the violet-photon rate decreased less than linearly. In addition, blocking the retro-reflection of the catalysis laser beams resulted in a reduction of the sig-

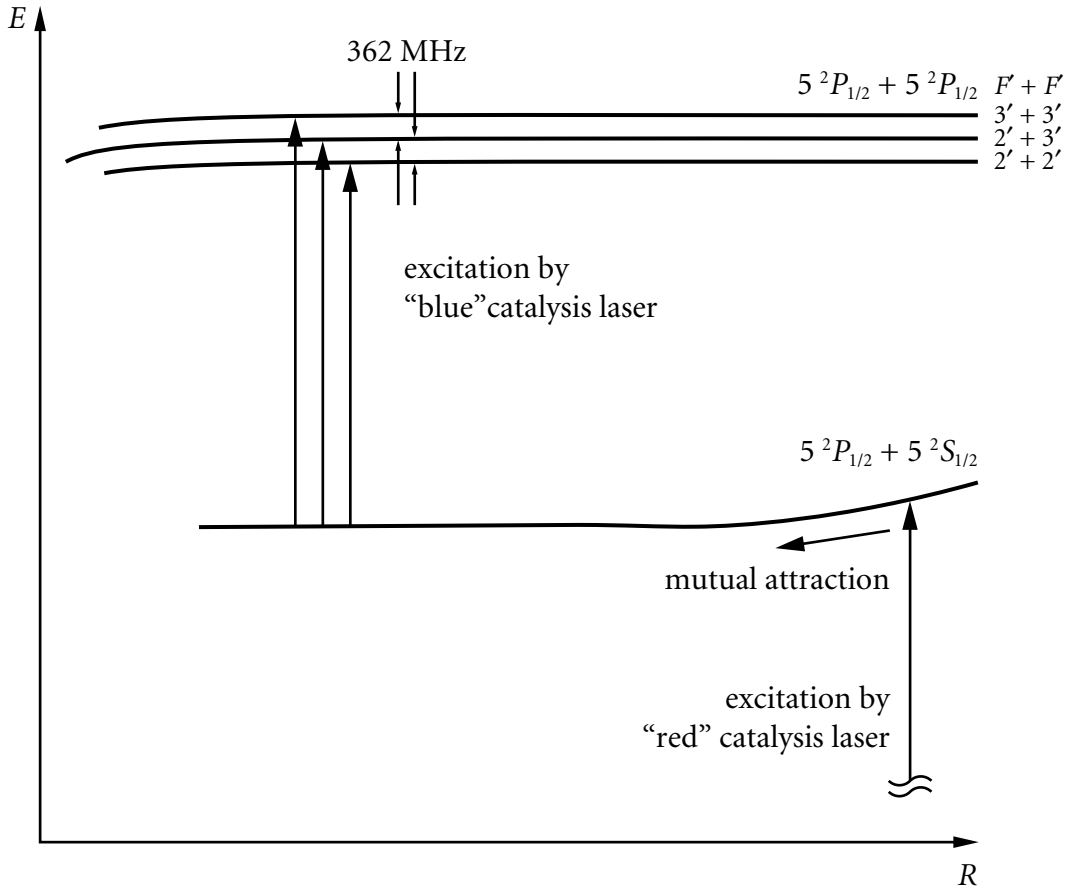

Figure 6.8: Because of the doubly-excited-state hyperfine splitting of 362 MHz, the “blue” catalysis laser is resonant with a transition from the singly- to the double-excited potential curves at three detunings, separated by this hyperfine splitting from each other. The singly-excited potential curve shown belongs to the manifold for which $dE/dR \approx 0$ for smaller R.

nal of only a factor of two, instead of four, as expected, if the rate depends linearly on each of the intensities of the “red” and “blue” catalysis laser. The measurements are shown in Fig. 6.9.

The data is fit to a saturation function of the form

$$f(I) = A\frac{I/I_s}{1 + I/I_s}, \tag{6.4.1}$$

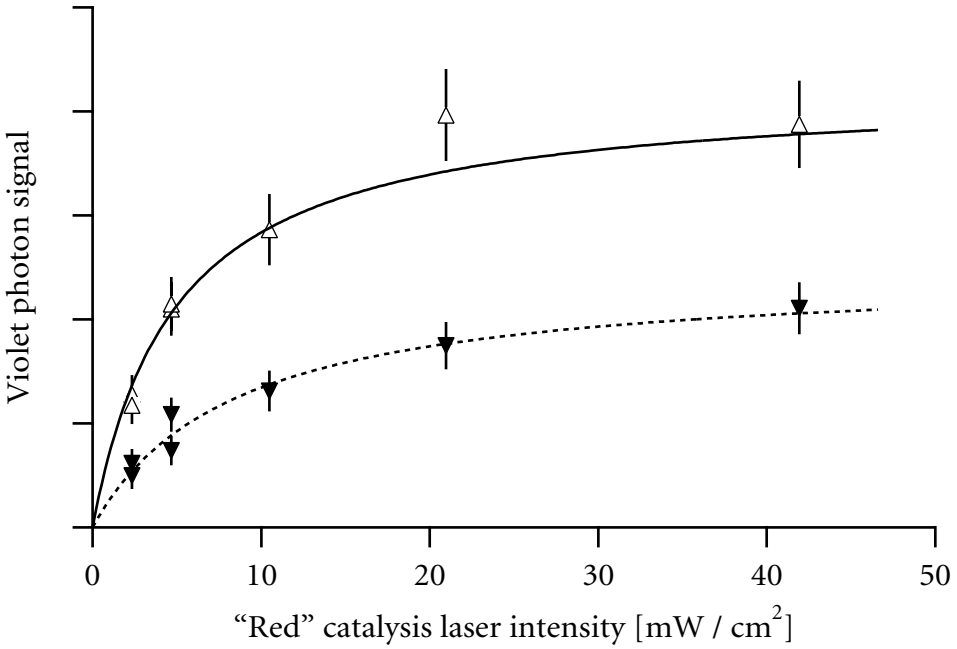

Figure 6.9: "Saturation" of the violet-photon rate as a function of the intensity of the "red" catalysis laser. The solid triangles show the data taken with blocked retro-reflection. The outline-triangles represent the data with retro-reflection. The lines are fits of the form $f(I) = A(I/I_s)/(1 + I/I_s)$, where A allows for overall scaling and I_s can be interpreted as the saturation intensity. The fits give a saturation intensity of 8.4 $\mathbf{mW/cm^2}$. The intensity of the "blue" catalysis laser was 220 $\mathbf{mW/cm^2}$.

in the case of the blocked retro-reflection, where A allows for overall scaling, and

$$f(I) = A\eta\frac{(\eta I)/I_s}{1 + (\eta I)/I_s}, \tag{6.4.2}$$

in the case of the presence of the retro-reflection of the catalysis laser beam, where η accounts for the increased intensity in the "blue" and "red" catalysis lasers resulting from it. The fit determines η to be 1.8, which we attribute to the losses in the retro-reflection optics on one hand and a decrease of intensity due to widening of the catalysis laser beams on the other.

We measured this intensity dependence several times, but the "saturation intensity" determined from the fits to the data varied by up to a factor of three. In part this may have to do with the large errors in the measurement, which results from the counting statistics. While the trap was sufficiently stable while taking data, it did not provided identical conditions from day

to day. Largely because of less than optimal hyperfine-pumping the equilibrium number of atoms in the absence of the catalysis lasers varied by as much as a factor of four. The sensitivity of the "saturation" data may therefore be closely connected to the density of the trapped atoms or their temperature.

This measurement, as well as the violet-photon spectrum, has to be repeated in the case where the atoms start in the $2 + 2$ ground state. If a difference in the behavior shows up, it will provide important clues to understanding the data presented here.

Obviously, considerable additional work is to be done on this experiment, which is beyond the scope of this dissertation. Further investigations are hoped to shed light on the nature of the "saturation" phenomenon, as well as the quantitative shape of the violet-photon spectrum.

7 Conclusion and outlook

In retrospect, the experiments described in this dissertation fit into the historical context of the development of the field of ultra-cold collisions in the following way. The comparison between the $P_{3/2}$ data of ^{85}Rb and ^{87}Rb led to an understanding of the importance of hyperfine interaction in the description of the collision. Up to that point none of the models took it into account.

The $P_{1/2}$ experiment was the first one that exhibited quantitative agreement with the dynamics of the Gallagher-Pritchard model. This was the first quantitative confirmation of any aspect of an ultra-cold collisions model. Furthermore, it shed additional light on how hyperfine and dipole-dipole interaction together influence the collision dynamics. In this experiment we observed evidence of multiple collision orbits, which had not been seen before. Further development of this by others led to new sensitive forms of molecular spectroscopy.

In the meantime theories had been proposed that involved various ideas for the process of the initial excitation by the catalysis laser. Our experiment on repulsive trap loss provided the first direct test of one of these, the Landau-Zener excitation mechanism, in that the intensity dependence of the trap loss rate showed a maximum.

Finally, the two-photon experiment presented new challenges. It became clear that an understanding of the results involves the details of the hyperfine potential curves of the two interacting atoms. A further investigation of the non-linear dependence of the violet-photon generation rate upon the intensity of the light inducing the first excitation potentially might lead to interesting insights into the physics of ultra-cold collisions as a whole. In addition, the two-photon experiment is the first one that directly measures fluorescence generated in spontaneous emission from colliding excited-state atoms.

We hope to gain a better understanding of the two-photon collision dynamics by letting the colliding atoms begin in the lower hyperfine ground state. The attractive potential curves belonging to this state do not exhibit any avoided crossings with other hyperfine potential curves. The comparison of the violet-photon emission spectra from the two collision processes should provide valuable clues for understanding the challenges posed by the existing data.

Two ongoing investigations in our research group also concern ultra-cold collisions. One looks at the collision rate between spin-polarized atoms. If the atoms are spin-polarized, the number of potential curves involved in the collision is greatly reduced. This could considerably alter the shape of the loss rate spectrum, especially at catalysis laser detunings between hyperfine levels.

The other will let ultra-cold atoms from a MOT drop onto a glass surface with an evanescent wave. In addition to their repulsion with the light from the evanescent wave, the atoms interact with their images. The evanescent wave is necessary to prevent atoms from colliding with the surface, because the interaction between atom and image is always attractive. This is a consequence of the perfect correlation between the dipole moment of the atom and its image. This correlation is also responsible for a vastly simplified dipole-dipole interaction. Thus, it is hoped that ultra-cold collisions models can be tested for this case particularly well.

The experiments described in this dissertation have spurred the development of theories and have helped establish the catalysis laser method and the interplay between experiment and theory has led to significant improvements in our understanding of ultra-cold collisions. In summary it can be said, that the experiments reported in this dissertation have been an important contribution to the field of ultra-cold excited-state collisions.

Bibliography

1. E. L. Raab, M. Prentiss, A. Cable, S. Chu, and D. E. Pritchard, Phys. Rev. Lett. **59**, 2631 (1987).
2. M. Prentiss, A. Cable, J. E. Bjorkholm, S. Chu, E. L. Raab, and D. E. Pritchard, Opt. Lett. **13**, 452 (1988).
3. E. Tiesinga, A. J. Moerdijk, B. J. Verhaar, and H. T. C. Stoof, Phys. Rev. A **46**, R1167 (1992); C. R. Monroe, E. A. Cornell, C. A. Sackett, E. J. Myatt, and C. E. Wieman, Phys. Rev. Lett. **70**, 414 (1993).
4. K. Gibble and S. Chu, Metrologia **29**, 201 (1992).
5. D. Hoffmann, P. Feng, R. S. Williamson III, and T. Walker, Phys. Rev. Lett. **69**, 753 (1992).
6. P. Feng, D. Hoffmann, and T. Walker, Phys. Rev. A **47**, R3495 (1993).
7. M. G. Peters, D. Hoffmann, J. D. Tobiason, and T. Walker, Phys. Rev. A **50**, R906 (1994).
8. S. Bali, D. Hoffmann, and T. Walker, Europhys. Lett. **27**, 273 (1994).
9. D. Hoffmann, S. Bali, and T. Walker (to be published).
10. C. Sukenik, D. Hoffmann, S. Bali, and T. Walker (to be published).
11. A. Gallagher and D. E. Pritchard, Phys. Rev. Lett. **63**, 957 (1989).
12. O. Dulieu, P. Julienne, and J. Weiner, Phys. Rev. A **49**, 607 (1994).
13. T. Walker, D. Sesko, C. Monroe, and C. Wieman, in *Proceedings of the Sixteenth International Conference on the Physics of Electronic and Atomic Collisions*, edited by A. Dalgarna, R. Freund, P. Koch, M. Lubell, and T. Lucatorto (AIP, New York, 1989).
14. P. S. Julienne and J. Vigué, Phys. Rev. A **44**, 4464 (1991).
15. D. Sesko, T. Walker, C. Monroe, A. Gallagher, and C. Wieman, Phys. Rev. Lett. **63**, 961 (1989).
16. Y. B. Band and P. S. Julienne, Phys. Rev. A **46**, 330 (1992).
17. H. M. J. M. Boesten and B. J. Verhaar, Phys. Rev. A **49**, 4240 (1994).
18. K.-A. Suominen, M. J. Holland, K. Burnett, and P. S. Julienne, Phys. Rev. A **49**, 3897 (1994)
19. T. Walker and D. Pritchard, Laser Physics **4**, 1085 (1994).
20. C. Monroe, W. Swann, H. Robinson, and C. Wieman, Phys. Rev. Lett. **65**, 1571 (1990)
21. C. Adams, M. Sigel, and J. Mlynek, Phys. Rep. **240**, 143 (1994).

22. A. Lambrecht, J.M. Courty, S. Reynaud, and E. Giacobino, Appl. Phys. B **60**, 129 (1995).

23. M. H. Anderson, J. R. Ensher, M. R. Matthews, C. E. Wieman, E. A. Cornell, Science **269**, 198 (1995); C. Bradley *et al.*, Phys. Rev. Lett., **75**, 1687 (1995).

24. R. S. Schappe, P. Feng, L. W. Anderson, C. C. Lin, and T. Walker, Europhys. Lett. **29**, 439 (1995).

25. K. Lindquist, M. Stephens, and C. Wieman, Phys. Rev. A **46**, 4082 (1992).

26. C. E. Wieman and L. Hollberg, Rev. Sci. Instrum. **62**, 1 (1991).

27. D. Sesko, T. Walker, and C. Wieman, J. Opt. Soc. Am. B **8**, 946 (1991).

28. J. W. R. Tabosa, G. Chen, Z. Hu, R. B. Lee, and H. J. Kimble, Phys. Rev. Lett. **66**, 3245 (1991).

29. D. Grison, B. Lounis, C. Salomon, J.Y. Courtois, and G. Grynberg, Europhys. Lett. **15**, 149 (1991).

30. P. D. Lett, K. Mølmer, S. D. Gensemer, K. Y. N. Tan, A. Kumarakrishnan, C. D. Wallace, and P. L. Gould, J. Phys. B **28**, 65 (1995).

31. M. O'Callaghan, A. Gallagher, and T. Holstein, Phys. Rev. A **32**, 2754 (1985).

32. C. Wallace, T. Dinneen, K. Tan, and P. Gould, Phys. Rev. Lett. **69**, 897 (1992).

33. L. D. Landau, Phys. Z. Sowjet Union **2**, 46 (1932); C. Zener, Proc. R. Soc. London, Ser. A **137**, 696 (1932).

34. J. D. Miller, R. A. Cline, and D. J. Heinzen, Phys. Rev. Lett. **71**, 2204 (1993); R. A. Cline, J. D. Miller and D. J. Heinzen, Phys. Rev. Lett. **73**, 632 (1994).

35. V. Bagnato L. Marcassa, C. Tsao, Y. Wang, and J. Wiener, Phys. Rev. Lett. **70**, 3225 (1993).

36. P. S. Julienne, A. M. Smith, and K. Burnett, in *Advances in Atomic, Molecular, and Optical Physics*, edited by Bederson and H. Walther (Academic Press, San Diego, 1992)

37. P. S. Julienne, K.-A. Suominen, Y. B. Band, Phys. Rev. A 49, 3890 (1994).

38. M. J. Holland, K.-A. Suominen, and K. Burnett, Phys. Ref. A **50**, 1513 (1994).

39. M. Movre and G. Pichler, J. Phys. B **10**, 2631 (1977); M. Movre and G. Pichler, J. Phys. B **13**, 697 (1980).

40. N. Ritchie, E. Abraham, and R. Hulet, Laser Physics **4**, 1066 (1994).

41. M. E. Wagshul, K. Helmerson, P. D. Lett, S. L. Rolston, W. D. Phillips, R. Heather, and P. S. Julienne, Phys. Rev. Lett **70**, 2074 (1993).

42. C. J. Myatt, N. R. Newbury, and C. E. Wieman, Opt. Lett. **18**, 649 (1993).

43. P. Feng and T. Walker, Am. J. Phys. **63**, 905 (1995).

Acknowledgments

Many are to thank for in some way or other helping me complete this six-year project. It is impossible to mention everyone who did.

I would like to thank my adviser Professor Thad Walker for guiding me through the research I have done while at the University of Wisconsin. Thanks goes to him for the encouragement or "kick in the butt" he gave me when I was low on motivation to carry on with this project. I thank him for all that he taught me and for giving me the opportunity to learn on my own, as well.

The other members of our research group have helped in various ways by either building equipment, running the experiments, or giving advice in helpful discussions. The graduate students are Paul Feng and Rob Williamson, who came to the University of Wisconsin the same year I did, Renée Nesnidal and Steve Kadlecek. Their help and contributions are too numerous to mention individually. Krista Mullman built a diode laser currently in use on my experiment, before joining another atomic physics group in the department. Our post-docs Joe Tobiason, Samir Bali and Charles Sukenik have helped with everything from building electronics, taking data to writing papers. There have been similar contributions from our European exchange students Stefan König from Germany and Michiel Peters from the Netherlands. José Siman worked in our lab on his Senior thesis and researched optical fibers before they became a standard part of our trapping optics.

None of the work in a research lab is possible without the backup from a staff, both clerical and technical. Thank you, Ed Slotten, for making it easy for us to buy the "toys" for our experiments by shielding us from the bureaucracy of the Petersen Building! Thanks also to Karen Fiene, Luise Olbrantz, Jean LeBeck and Jesse Prochaska who have been Ed's assistants over the years. Thank you, Pat Cady, for making sure we get our pay checks and for your help with health insurance and visa matters! Thank you, Melody Schneeberger and Barb Schutz, for making sure we have our course requirements in and all the other things that are necessary for academic progress. Thank you Jean Michael, Marian Schmidt and Jennifer Etheridge in the Atomic and Solid State Physics Office for letting me know when an important fax arrived and for arranging for travel expense reimbursements. Thank you, Dave Lockman, and, yes, Ron

Harrington, for seeing to it that I got my mail. Thanks to Art Fritsche and Walt Wigglesworth for helping making parts in the Student Machine Shop. I learned a great deal from you both. Thanks to Lee Potratz, Norbert Meier, Bill Foster, Mike Gerber, and Dave Guitzkow for machining done for the experiments described in this dissertation. The people of the Electronics Shop, Mike Murray, Jerry Glowacki and Art Webb, were a huge help by giving very valuable advice in building electronics. Thank you also for the equipment you built for our research group!

Were it not for my many friends I made here in Madison, I don't know whether I would have retained my sanity during my stay here. Thank you very much for your friendship!

I am also very indebted to my dear parents, Leonhard and Ursula Hoffmann, who supported me financially, emotionally and spirtually throughout my graduate school career. Thank you very much!

I especially thank the almighty God, Father, Son and Holy Spirit, who is the Creator and Mover of all things, and this includes the Physics that I studied. There is nothing I am or was able to do without His cooperation. I thank Him for giving me this opportunity to learn so much about his Creation and for sending me to beautiful Madison.